U.S. DEPARTMENT OF ENERGY

PNNL-18745

Prepared for the U.S. Department of Energy
under Contract DE-AC05-76RL01830

Effect of Concrete Waste Form Properties on Radionuclide Migration

SV Mattigod
DM Wellman
EA Cordova
CC Bovaird
DJ Skinner
MI Wood

September 2009

Pacific Northwest
NATIONAL LABORATORY

Proudly Operated by Battelle *Since 1965*

DISCLAIMER

PACIFIC NORTHWEST NATIONAL LABORATORY
operated by
BATTELLE
for the
UNITED STATES DEPARTMENT OF ENERGY
under Contract DE-AC05-76RL01830

Printed in the United States of America

Available to DOE and DOE contractors from the
Office of Scientific and Technical Information,
P.O. Box 62, Oak Ridge, TN 37831-0062;
ph: (865) 576-8401
fax: (865) 576-5728
email: reports@adonis.osti.gov

Available to the public from the National Technical Information Service,
U.S. Department of Commerce, 5285 Port Royal Rd., Springfield, VA 22161
ph: (800) 553-6847
fax: (703) 605-6900
email: orders@ntis.fedworld.gov
online ordering: http://www.ntis.gov/ordering.htm

This document was printed on recycled paper.
(9/2003)

PNNL-18745

Effect of Concrete Waste Form Properties on Radionuclide Migration

SV Mattigod
DM Wellman
EA Cordova
CC Bovaird
DJ Skinner
MI Wood

September 2009

Prepared for
The U.S. Department of Energy
Under Contract DE-AC05-76RL01830

Pacific Northwest National Laboratory
Richland, Washington 99352

Summary

Assessing long-term performance of Category 3 waste cement grouts for radionuclide encasement requires knowledge of the radionuclide-cement interactions and mechanisms of retention (i.e., sorption or precipitation); the mechanism of contaminant release; the significance of contaminant release pathways; how waste form performance is affected by the full range of environmental conditions within the disposal facility; the process of waste form aging under conditions that are representative of processes occurring in response to changing environmental conditions within the disposal facility; the effect of waste form aging on chemical, physical, and radiological properties; and the associated impact on contaminant release. This knowledge will enable accurate prediction of radionuclide fate when the waste forms come in contact with groundwater. Numerous sets of tests were initiated in fiscal years (FY) 2006 through2009 to evaluate 1) diffusion of iodine (I) and technetium (Tc) from concrete into uncontaminated soil after 1 and 2 years, 2) I and rhenium (Re) diffusion from contaminated soil into fractured concrete, 3) I and Re (set 1) and Tc (set 2) diffusion from fractured concrete into uncontaminated soil, 4) the moisture distribution profile within the sediment half-cell, 5) the reactivity and speciation of uranium (VI) [U(VI)] compounds in concrete porewaters, 6) the rate of dissolution of concrete monoliths, and 7) the diffusion of simulated tank waste into concrete.

In FY 2008, concrete-soil half-cells initiated during FY 2007 using fractured concrete prepared with and without metallic iron, half of which were carbonated, were sectioned to evaluate the diffusion of I and Re in the concrete part of the half-cell. Probit plots were constructed from this data set.

A second set of diffusion experiments, which had been initiated during FY 2007 using concrete-soil half-cells containing Tc, was sectioned in FY 2008 to measure the diffusion profile in the soil half-cell. These half-cells were prepared with and without metallic iron (Fe) and set up under unsaturated conditions (4%, 7%, and 15% moisture content by weight). Probit plots were constructed from this data set. In FY 2008, a set of concrete-soil half-cells were initiated. The half-cells were sectioned in FY 2009 to measure the diffusion profile in the concrete half-cell. Concentration and probit analysis was performed on the half-cells.

A study was initiated during FY 2004 to better understand the reactivity of limited solubility U(VI)-bearing compounds in Portland cement grout specimens. The U(VI) nitrate-spiked specimens were aged for various time spans ranging from 2 weeks to 1 year. The uranium phases in these specimens were identified to be soddyite, becquerelite, uranophane, and autunite. Reliable thermochemical data are not available for these phases under conditions present in concrete waste forms. Therefore, to gather such data, synthetic routes were developed for the precipitation of pure uranium phases. From FY 2007 to FY 2008, the solubility measurements of these U-solid phases were completed under concrete porewater conditions. Preliminary results had suggested the formation of 1) a calcium-uranium oxide from the reaction of becquerelite, 2) uranophane group minerals from the reaction of soddyite, and 3) mixed sodium-calcium uranium phosphate secondary phases from the reaction of autunite in simulated Portland cement-equilibrated porewater. During FY 2009 analytical analyses were completed to quantify aqueous cations and anions. This information was used with geochemical thermodynamic modeling to further understand the stability and long-term control of uranium in concrete waste forms. It is suggested here that 1) the release of uranium from the degradation of uranium oxyhydroxides will be controlled by the formation of secondary uranium oxides, 2) regardless of the replacement of soddyite by uranophane, uranyl-silicate phases will persist within concrete waste forms, and 3) the release of uranium from the

degradation of uranium-phosphate phases will be controlled by the formation of secondary uranyl-phosphate phases.

A set of concrete monolith single-pass flow-through (SPFT) experiments were initiated in FY 2009. Preliminary results indicate that the release mechanism of calcium (Ca) is different for that of the other major elemental species (magnesium [Mg], silicon [Si], phosphorus [P], and aluminum [Al]). It is postulated that Ca release is controlled by ion exchange. Secondary phases, which could influence the dissolution rate, were not observed with scanning electron microscopy (SEM). In FY 2010, further analysis of concrete monolith SPFT tests will provide a better understanding of the release mechanisms of the major elemental species, which influences long term stability of concrete.

Two sets of simulated tank waste-concrete half-cells were prepared in FY 2006 and FY 2008 with and without technetium, respectively. In FY 2010, the half-cells will be sectioned to measure the diffusion of simulated tank waste into concrete. Concentration and probit analysis will be performed.

Acknowledgments

Funding for this project was provided by CHPRC (Marc Wood). The authors thank Kent Parker for preparing concrete-sediment half-cell tests; Sara Rither, Steven Baum, John Nelson, and Danielle Saunders for sectioning the concrete monoliths and conducting water extractions; and Steven Baum and Eric Clayton for conducting inductively coupled plasma optical emission spectrometry (ICP-OES) and ICP-mass spectrometry (ICP-MS) analyses, respectively.

Acronyms and Abbreviations

Al	aluminum
BFS	blast furnace slag
Ca	calcium
EDS	energy dispersive spectrometer
EXAFS	extended absorption X-ray fine structure
Fe	iron
FY	fiscal year(s)
I	iodine
ICP-MS	inductively coupled plasma-mass spectrometry
ICP-OES	inductively coupled plasma-optical emission spectrometry
IEX	ion exchange
L	limestone
MC	moisture content
Mg	magnesium
OPC	ordinary Portland cement
P	phosphorus
PVC	polyvinyl chloride
Re	rhenium
Se	selenium
SEM	scanning electron microscopy
Si	silicon
SPFT	single-pass flow-through
SRPC	sulfate-resistant Portland cement
Tc	technetium
THAM	tris hydroxymethyl aminomethane buffer
U(VI)	uranium (VI)
wt	weight

Contents

Figures

Tables

1.0 Introduction

1.1 Background

One of the methods being considered for safely disposing of Category 3 low-level radioactive wastes is to encase the waste in concrete. Concrete encasement would contain and isolate the waste packages from the hydrologic environment and would act as an intrusion barrier. The current plan for waste isolation consists of stacking low-level waste packages on a trench floor, surrounding the stacks with reinforced steel, and encasing these packages in concrete. These concrete-encased waste stacks are expected to vary in size with maximum dimensions of 6.4 m long, 2.7 m wide, and 4 m high. The waste stacks are expected to have a surrounding minimum thickness of 15 cm of concrete encasement. These concrete-encased waste packages are expected to withstand environmental exposure (solar radiation, temperature variations, and precipitation) until an interim soil cover or permanent closure cover is installed and to remain largely intact thereafter. Any failure of concrete encasement may result in water intrusion and consequent mobilization of radionuclides from the waste packages.

Key contaminants within low activity and secondary wastes from treatment of the Hanford tank wastes include 129I, 75Se, 99Tc, and 238U (Mann et al. 2001, Wood et al. 1995). The geochemistry of porefluids in contact with cementitious materials is characterized by highly alkaline pH values. Because of their anionic nature in aqueous solutions, 129I, 75Se, 99Tc, and carbonate-complexed 238U may readily leach into the subsurface environment (Serne et al. 1989, 1992, 1993, and 1995) by mass flow and/or diffusion and move into the surrounding subsurface environment. Thus, it is critical to understand the: 1) speciation and interaction of the radionuclides within the concrete waste form, 2) diffusion of radionuclide species when contacted with vadose zone porewater or groundwater, and 3) long-term durability and weathering of concrete waste forms under environmental conditions relevant to the depository.

Although significant research has been conducted on the design and performance of cementitious waste forms, the current protocol conducted to assess radionuclide stability within these waste forms has been limited to the Toxicity Characteristic Leaching Procedure, Method 1311 Federal Registry and ANSI/ANS-16.1 leach test (ANSI 1986). These tests evaluate the performance under water-saturated conditions and do not evaluate the performance of cementitious waste forms within the context of waste depositories that are located in hydraulically unsaturated environments. Moreover, these tests assess only the diffusion of radionuclides from concrete waste forms and neglect evaluating the mechanisms of retention, stability of the waste form, and formation of secondary phases during weathering, which may serve as long-term secondary hosts for immobilization of radionuclides.

The results of recent investigations conducted under arid and semi-arid conditions provide valuable information suggesting structural and chemical changes to concrete waste forms which may affect contaminant containment and waste form performance (Al-Khayat et al. 2002, Garrabrants and Kosson 2003, Garrabrants et al. 2002 and 2004, Gervais et al. 2004, and Sanchez et al. 2002 and 2003). A recent review conducted by the National Academies of Science recognized the efficacy of cementitious materials for waste isolation, but further noted the significant short-comings in our current understanding and testing protocol for evaluating the performance of various formulations (National Research Council 2009). Continued research is necessary to understand:

- the mechanism of contaminant release, the significance of contaminant release pathways,
- how waste form performance is affected by the full range of environmental conditions within the disposal facility,
- the process of waste form aging under conditions that are representative of processes occurring in response to changing environmental conditions within the disposal facility, and
- the effect of waste form aging on chemical, physical, and radiological properties and the associated impact on contaminant release.

1.2 Purpose and Scope

The objective of the investigation reported here is to demonstrate a testing protocol designed to understand the speciation of radionuclides within concrete waste forms, quantify the diffusion of highly mobile radionuclides, and evaluate the long-term stability of concrete waste forms. The results present the progress for annual concrete-sediment half-cell diffusion tests initiated in FY 2008 to 1) quantify the diffusion of I and Tc from concrete into uncontaminated soil after 1 and 2 years, 2) quantify I and Re (set 1) and Tc (set 2) diffusion from fractured concrete into uncontaminated soil, and 3) evaluate the moisture distribution profile within the sediment half-cell. The 1-year half-cells were sectioned in FY 2009, and the 2-year samples will be sectioned in FY 2010. Probit analysis results are presented that complete the data sets for concrete-sediment half-cell tests initiated in FY 2007 for 1) concrete-soil half-cells using fractured concrete, prepared with and without metallic iron, and of which half were carbonated and 2) data from concrete-soil half-cells containing Tc were analyzed to measure the diffusion profile in the soil half-cell unsaturated conditions (4%, 7%, and 15% moisture content by weight). Geochemical modeling results are presented to further elucidate the chemical speciation and controlling phases for uranium in concrete waste forms and porefluids. Finally, preliminary results are presented for a new SPFTtesting protocol initiated in FY 2009 to understand the rate limiting mechanisms controlling the chemical stability of concrete waste forms and radionuclide immobilization.

1.3 Report Contents and Organization

The ensuing sections of this report present the results of the concrete-soil half-cell tests, modeling of uranium (VI) solubility in concrete porewaters, single-pass flow-through tests on cementitious waste forms, and preparation of simulated tank waste concrete half-cell tests.

- Section 2.0, describes the procedures for preparing concrete-soil half-cells
- Section 3.0 describes the diffusion experiments initiated during FY 2007 and FY 2008 to determine the effects of concrete carbonation and colloidal iron on the diffusion of technetium using carbonated concrete-soil half-cells prepared with and without metallic iron, half of which were carbonated using carbonate solution.
- Section 4.0 describes the diffusion experiments initiated during FY 2007 using fractured concrete-soil half-cells to determine the diffusion of I and Re into fractured concrete.
- Section 5.0 describes the diffusion experiments initiated during FY 2008 using fractured concrete-soil half-cells to determine the diffusion of I, Re, and Tc from fractured concrete into soil.

- Section 6.0 describes the set of experiments initiated during FY 2008 to determine the moisture gradient within concrete-soil half-cells.
- Section 7.0 describes continued analysis of the reactivity of limited solubility U(VI)-bearing compounds in concrete.
- Section 8.0 describes the preliminary analysis of Portland cement coupons using the SPFT test.
- Section 9.0 describes the FY 2006 preparation of simulated tank waste-soil half-cell diffusion experiments.

2.0 Materials and Methods

2.1 Specified Concrete Composition for Encasement

Table 2.1. Material Specifications and Composition

Material	Specifications	Specified Field Mix	Normalized Specification Design
Cement	Portland Type I or Type I/II sulfate-resistant cement	381 kg/m^3	0.27
Fly Ash	Class F fly ash; nominal 15% of cement by volume	54 kg/m^3	0.04
Coarse Aggregate	No. 676 or equivalent (3/4″ nominal size)	55% by volume	0.04
Fine Aggregate	Sand	45% by volume	0.51
Water	Nominal water:cement ratio: 0.4	399 kg/m^3	0.10
Steel Fiber	Deformed Type I, nominal length 2.5–3.8 cm (1–1.5″)	59 kg/m^3	0.04
Air Content		6.0±1.5%	

The concrete composition for the burial encasement was specified in *Specification for Concrete Encasement for Contact-Handled Category 3 Waste*. ("Specification for Concrete Encasement for Contact-Handled Category 3 Waste," 1998) [(a)] This specification was used as the basis to prepare a concrete for fabrication of test specimens. The composition includes sulfate-resistant Portland Type I or Type II cement, a pozzolanic material (Class F fly ash), fine and coarse aggregates, and steel fiber. Additional specifications include a water-to-cement ratio of 0.4 and an air content 6.0 ± 1.5%. The nominal proportions and material specifications based on this initial design are listed in Table 2.1.

2.1.1 Materials and Laboratory-Scale Mixture Design

A laboratory-scale concrete mixture (Table 2.2) was prepared based on specifications shown in Table 2.1. Because of the required small dimensions of laboratory test specimens, the size of the coarse aggregate and the dimensions of the steel fiber specified in Table 2.1 were proportionately reduced. This was accomplished by decreasing the 2-cm (~0.75 in.) coarse aggregate size in the original specification to a particle size ranging from 2.83 mm to 2 mm in the laboratory mix. Aggregate passing a 7-mesh sieve and retained on a 10-mesh sieve met this particle size specification. Iron particles were used in the laboratory mix in place of the steel fibers. Based on these modifications, a concrete mix was prepared that consisted of Portland Cement (Type I and II, American Society for Testing and Materials C-150 compliant), Class F fly ash, scaled-down coarse aggregate, fine aggregate, iron particles, and a water-entraining agent (Polyheed 997). The water-entraining agent was included in the mix to facilitate the workability of the concrete. The volumes of the Polyheed 997 and the air-entraining agent, MB AE 90, were not included in the normalization calculations because of their negligible contribution to the overall mix volume. The material specification and composition for the laboratory-scale concrete mixture is given in Table 2.2.

Table 2.2. Laboratory-scale Material Specification and Composition

Material	Material Specifications for Field Mix	Normalized Laboratory Design	Material Specifications Used in Revised Laboratory Mix Comparison
Cement	Portland Type I or Type I/II sulfate-resistant cement	0.27	Portland Type I & II
Fly Ash	Class F fly ash; nominal 15% of cement by volume	0.04	Class F fly ash; nominal 20% of cement by volume
Coarse Aggregate	No. 676 or equivalent (3/4-in. nominal size)	0.04	Sieve size +7 to -10 (2.83–2 mm size)
Fine Aggregate	Sand	0.51	Sand -10 sieve size (< 2 mm)
Water	Nominal water:cement ratio: 0.4	0.10	Water-to-cement ratio: 0.5
Iron Powder	Iron particles	0.04	-200 mesh
Polyheed 997		0.00375	Water-entraining agent
Air Content	6.0±1.5%	6.0±1.5%	--

2.2 Concrete Mix and Specimen Preparation

In general, concrete monoliths were prepared with mix components added in the order: water, steel (if applicable), coarse aggregate, fine aggregate, fly ash, cement, Polyheed 997, and MB AE 90. The concrete was mixed on medium speed using a Hobart three-speed, bench-top mixer in a 4 L steel bowl. The concrete molds for casting specimens were fabricated from Schedule 40 polyvinyl chloride (PVC) piping material. Gaskets were glued to the bottom of the molds and leak tested before use. The PVC molds were filled in the vertical position. After filling, the molds were lightly tapped on the laboratory bench until a significant decrease in the release of air bubbles was observed. The forms were stored in a humidity chamber for 28 days to provide moisture while the concrete set. The concrete monoliths were subsequently removed from the molds and the respective monoliths were carbonated by soaking for 7 days in a saturated sodium-bicarbonate solution. Specific treatments for concrete monoliths (e.g., carbonation, iron content, contaminant content) used in concrete-sediment half-cell experiments are discussed below within the context of the respective half-cell preparation.

2.2.1 Solid and Fractured Concrete-Sediment Half-Cells Spiked with Iodine and Rhenium

Concrete monoliths were prepared in two separate batches based on the laboratory-scale specifications for the concrete (Table 2.2). One batch contained iron particles; the other batch did not contain any added iron. Within the two batches of concrete, with and without iron, half the monoliths were carbonated by submersion in a saturated sodium bicarbonate solution for 7 days. The resulting compositions consisted of four concrete specimens: 1) no iron, carbonated; 2) no iron, uncarbonated; 3) iron, carbonated; and 4) iron, uncarbonated.

In order to assess the effect of fractures within the concrete monolith on the diffusion of iodine and rhenium, concrete monoliths were encased in shrink-wrap and struck with a hammer to prevent the formation of rubble. Each fractured core possessed a single fracture extending the length of the core, perpendicular to the concrete-sediment interface.

2.2.2 Solid Concrete-Sediment Half-Cells Spiked with Technetium

The concrete half-cells were prepared using the preparation detailed in section 2.2. Two separate batches, one with and one without iron particles, were prepared based on the laboratory-scale specifications for the concrete (Table 2.2). None of the concrete monoliths were subjected to carbonation because the process of carbonating the cores via submersion in a saturated sodium bicarbonate solution would result in leaching of Tc prior to half-cell testing. The resulting compositions consisted of two concrete specimens: 1) no iron, uncarbonated and 2) iron, not carbonated.

2.3 Half-Cell Preparation, Testing, and Analysis

Diffusion tests were conducted to assess the effects of carbonation and the inclusion of colloidal iron on the rate of diffusion of key, long-lived, mobile contaminants (I, Re, and Tc), in unsaturated Hanford sediments (~4%, 7%, and 15% moisture content by weight). The experiments were conducted using a sediment half-cell ~4 cm in diameter and 20-cm long in contact with a concrete monolith ~4 cm in diameter and ~4-cm long. One concrete core of each composition was encased in a Schedule 40, 24-cm long, PVC pipe. The remaining volume of each pipe was filled with Hanford Site sediment, spiked with stable I and Re or Tc added to the water component prior to mixing with the sediment, at the respective moisture content. Medium coarse sand obtained from the sidewall of the W-5 burial ground located on the Hanford Site in southeastern Washington state was used for the sediment half-cell. The physical, chemical, and mineralogical properties of this sediment have been previously characterized by Serne et al. (1993). The ends of each pipe were machined and fit with o-ring gaskets to confirm the test cells were sealed. The diffusion tests were allowed to set horizontally and undisturbed for the test duration, nominally 1 or 2 years, with periodic rotation of the cell by 90 degrees.

At the conclusion of the test period, the end caps of the cells were removed and the sediment was extruded at approximately 1 cm intervals along the length of the half-cell (Figure 2.1). The moisture content of each section was quantified and found to be uniform throughout the length of the half-cell and consistent with the starting moisture content. The sediment samples were weighed and extracted with deionized water. One-to-one water extracts were done on sediment fractions. The concentrations of iodine, rhenium, and technetium were measured via ICP-MS.

Concrete half-cells were sectioned parallel to the concrete-sediment interface using a Buehler slow-speed saw fitted with a diamond blade. During the process, cutting was done without water cooling to prevent the leaching of soluble I, Re, and Tc. The concrete slices were then ground using an agate mortar and pestle. Two-to-one extracts (due to small sample size) were performed on concrete fractions. The concentrations of I, Re, and Tc were measured via ICP-MS in sediment and concrete thin slices.

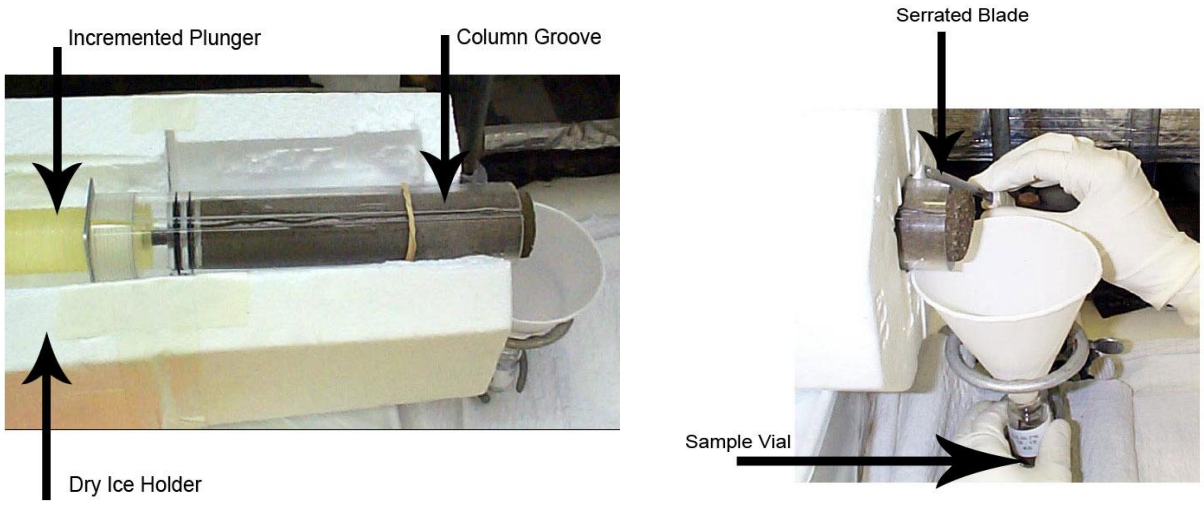

Figure 2.1. Mechanism for Sediment Sampling from a Concrete-Sediment Diffusion Half-cell (left) and Sediment Sampling from a Diffusion Half-Cell (right)

2.4 Effective Diffusion Coefficient Calculations

The diffusivities in the soil were reduced using the probit analysis approach previously presented by Mattigod et al. (2001). The details of the probit analysis are provided in Finney (1971). This technique allows the transformation of a sigmoid curve of concentrations, normalized with respect to the initial concentration (C/C_0), as a function of diffusion distance produced in a half-cell diffusion experiment to a linear plot. The slope (b) of this plot is then used to calculate the diffusivity (D) as $D = 1/(2b^2t)$, where t is the sampling time. This approach has been used previously to determine diffusivity in half-cell diffusion experiments such as those conducted by Brown et al. (1964) and Lamar (1989)..

In a diffusion test where one boundary can be represented by a constant concentration, the concentration profile that develops is one-half of the normal sigmoid curve produced in the half-cell diffusion experiment. Thus, to apply the probit transformation, the concentrations are normalized by dividing by 2* C_i, where C_i is the concentration at the constant concentration interface. This approach has been used to model diffusion from a non-depleting reservoir into asphalt (Martin et al. 1994).

The configuration of concrete-soil experiments had the soil in a half-cell arrangement with a dissimilar material (hardened concrete) containing the radionuclide spike. In the case of diffusion occurring between two dissimilar media, one of which is spiked and both of which are semi-infinite in dimension from the interface, the concentration at the interface will quickly reach and remain at a constant concentration as the diffusion proceeds. For an explanation of why this occurs, refer to Crank (1975). Because of this result, the problem is mathematically the same as the case where a boundary is held at a constant concentration and the data can be normalized by dividing by 2*C_i, where C_i is the concentration at the interface. However, because the concentration C_i at the interface of the two dissimilar materials is not known, the concentration in the soil slice nearest the interface is used to approximate this value. This approximation introduces some bias in the calculated diffusivity because the concentration profile averaged over the first soil slice is systematically lower than the concentration at the

interface of the first soil slice with the spiked concrete. The extent of the error is estimated to be about 12% from one of Crane et al. (1992) concentration profiles. We assumed the relative errors for the other tests were similar. This error magnitude is considered acceptable relative to the variance in the diffusivity values for all the tests.

For purposes of data reduction, the radionuclide diffusivity is defined by the equation:

$$J = - D_w \, dC_w/dx \tag{1}$$

where J = flux of radionuclide at a given point

D_w = the diffusivity of water-based radionuclide concentration

C_w = the radionuclide concentration in the porewater

Using this definition, and acknowledging that in the case of a two-phase system (water and soil) there will be insignificant amounts of radionuclides within the air phase of the unsaturated sediment, a mass balance can be performed over a small volume leading to the equation

$$dC_w/dt = D_w/\theta * (d^2C_w/dx^2) \tag{2}$$

where θ = the volume pore water per total pore volume

However, the slope on the probit plot provides the diffusivity that solves the equation for diffusion in a homogeneous single phase medium:

$$dC/dt = D * (d^2C/dx^2) \tag{3}$$

The diffusion coefficient, D_w, was calculated from D obtained from the probit plot based on concentrations in the porewater that must then be multiplied by θ. From concrete-soil experiments, the diffusivity coefficients in concrete were calculated using soil diffusivity coefficients derived from probit plots.

3.0 Concrete-Soil Half-Cell Experiments to Determine the Effects of Concrete Carbonation and Colloidal Iron on the Diffusion of Technetium

Two sets of diffusion experiments were initiated during FY 2008 using carbonated concrete-soil half-cells. Soil half-cell specimens were spiked with I and Tc to achieve a measurable diffusion profile in the concrete part of the half-cell. The general preparation of the half-cells is described above in section 2.1. The characteristics of the FY 2009 and FY 2010 concrete half-cells are listed in Table 3.1. For the FY 2009 half-cells, concentration data and probit plots and the diffusion coefficients for these contaminants are presented below. We will correlate the calculated diffusion coefficients with the degree of microcracking in the cement specimens used in the half-cell experiments. The FY 2010 half-cells still are in progress.

Table 3.1. Characteristics of Concrete Specimens Used in Concrete-Soil Half-Cells

Core ID	Length (cm)	Diameter (cm)	r^2	Surface Area (cm^2)	Volume (cm^3)	Weight (g)	Density (g/cm^3)	Colloidal Iron (%)	Carbonated	Moisture
FY 2009 Diffusion Tests										
C-08-3-0-325	4.09	4.33	4.68	84.97	60.10	131.44	2.19	0	N	4
C-08-3-0-329	4.32	4.33	4.68	88.13	63.53	139.50	2.20	0	N	7
C-08-3-0-330	3.85	4.33	4.68	81.77	56.65	123.50	2.18	0	N	15
C-08-3-0-332	4.33	4.32	4.67	88.09	63.48	139.65	2.20	0	Y	4
C-08-3-0-333	4.35	4.33	4.68	88.57	64.00	140.79	2.20	0	Y	7
C-08-3-0-334	4.07	4.32	4.67	84.56	59.67	130.55	2.19	0	Y	15
C-08-3-4-350	3.84	4.32	4.67	81.43	56.28	127.25	2.26	4	N	4
C-08-3-4-351	4.00	4.33	4.69	83.92	58.96	132.78	2.25	4	N	7
C-08-3-4-353	4.01	4.33	4.68	83.99	59.04	133.38	2.26	4	N	15
C-08-3-4-357	3.90	4.32	4.66	82.19	57.11	128.77	2.25	4	Y	4
C-08-3-4-359	3.83	4.32	4.67	81.25	56.09	126.50	2.26	4	Y	7
C-08-3-4-360	4.11	4.33	4.69	85.47	60.64	136.11	2.24	4	Y	15
C-08-3-8-401	4.07	4.32	4.66	84.40	59.50	135.91	2.28	8	N	4
C-08-3-8-402	3.81	4.32	4.67	81.02	55.84	127.31	2.28	8	N	7
C-08-3-8-403	4.00	4.33	4.69	83.87	58.91	133.35	2.26	8	N	15
C-08-3-8-404	4.05	4.33	4.69	84.61	59.71	133.69	2.24	8	Y	4
C-08-3-8-405	3.86	4.33	4.68	81.77	56.65	126.96	2.24	8	Y	7
C-08-3-8-406	3.94	4.33	4.69	83.08	58.05	130.61	2.25	8	Y	15
C-08-3-12-425	4.33	4.27	4.68	87.54	62.88	143.44	2.28	12	N	4
C-08-3-12-426	4.33	4.33	4.69	88.35	63.76	145.77	2.29	12	N	7
C-08-3-12-427	4.33	4.22	4.70	86.94	62.23	141.71	2.28	12	N	15
C-08-3-12-432	4.02	4.32	4.67	83.83	58.88	134.09	2.28	12	Y	4
C-08-3-12-433	4.15	4.33	4.68	85.81	61.01	139.80	2.29	12	Y	7
C-08-3-12-435	3.88	4.33	4.69	82.22	57.12	130.04	2.28	12	Y	15

Table 3.1. (contd)

Core ID	Length (cm)	Diameter (cm)	r^2	Surface Area (cm^2)	Volume (cm^3)	Weight (g)	Density (g/cm^3)	Colloidal Iron (%)	Carbonated		Moisture
FY 2010 Diffusion Tests											
C-08-3-0-326	4.15		4.34	4.70	86.13	61.35	136.30	2.22	0	N	4
C-08-3-0-327	4.02		4.32	4.67	84.01	59.06	131.30	2.22	0	N	7
C-08-3-0-328	4.11		4.33	4.68	85.24	60.39	134.10	2.22	0	N	15
C-08-3-0-325	4.09		4.33	4.68	84.97	60.10	131.44	2.19	0	Y	4
C-08-3-0-337	4.20		4.32	4.66	86.28	61.52	135.86	2.21	0	Y	7
C-08-3-0-338	4.19		4.33	4.69	86.54	61.80	135.91	2.20	0	Y	15
C-08-3-4-352	4.14		4.32	4.67	85.56	60.74	136.22	2.24	4	N	4
C-08-3-4-354	4.08		4.33	4.69	84.99	60.12	134.63	2.24	4	N	7
C-08-3-4-355	4.06		4.33	4.68	84.60	59.70	134.13	2.25	4	N	15
C-08-3-4-361	3.91		4.33	4.68	82.48	57.41	131.18	2.28	4	Y	4
C-08-3-4-362	4.11		4.32	4.67	85.12	60.27	135.96	2.26	4	Y	7
C-08-3-4-363	4.09		4.32	4.66	84.70	59.82	135.08	2.26	4	Y	15
C-08-3-8-404	4.05		4.33	4.69	84.61	59.71	133.69	2.24	8	N	4
C-08-3-8-405	3.86		4.33	4.68	81.77	56.65	126.96	2.24	8	N	7
C-08-3-8-406	3.94		4.33	4.69	83.08	58.05	130.61	2.25	8	N	15
C-08-3-8-408	4.49		4.33	4.70	90.60	66.19	148.87	2.25	8	Y	4
C-08-3-8-411	4.26		4.33	4.68	87.32	62.64	140.64	2.25	8	Y	7
C-08-3-8-412	4.31		4.33	4.69	88.09	63.48	142.26	2.24	8	Y	15
C-08-3-12-428	4.21		4.33	4.69	86.65	61.92	143.22	2.31	12	N	4
C-08-3-12-429	4.11		4.33	4.69	85.43	60.59	140.25	2.31	12	N	7
C-08-3-12-430	3.84		4.31	4.65	81.30	56.16	129.75	2.31	12	N	15
C-08-3-12-434	4.13		4.32	4.66	85.25	60.41	138.49	2.29	12	Y	4
C-08-3-12-436	3.90		4.32	4.66	82.17	57.09	131.15	2.30	12	Y	7
C-08-3-12-437	4.21		4.32	4.67	86.57	61.84	142.39	2.30	12	Y	15

3.1 Concentration Profile Results and Discussion

The diffusion profiles of soil half-cells spiked with I and Tc are shown in Figures 3.1 through 3.3, and the concrete half-cells are shown in Figures 3.4 through 3.6. Except very near the interfaces, no distinctive concentration gradients were observed in any of the soil half-cells. Therefore, on average, the relatively constant concentrations throughout the soil half-cells reflected the spike concentrations of I and Tc, respectively.

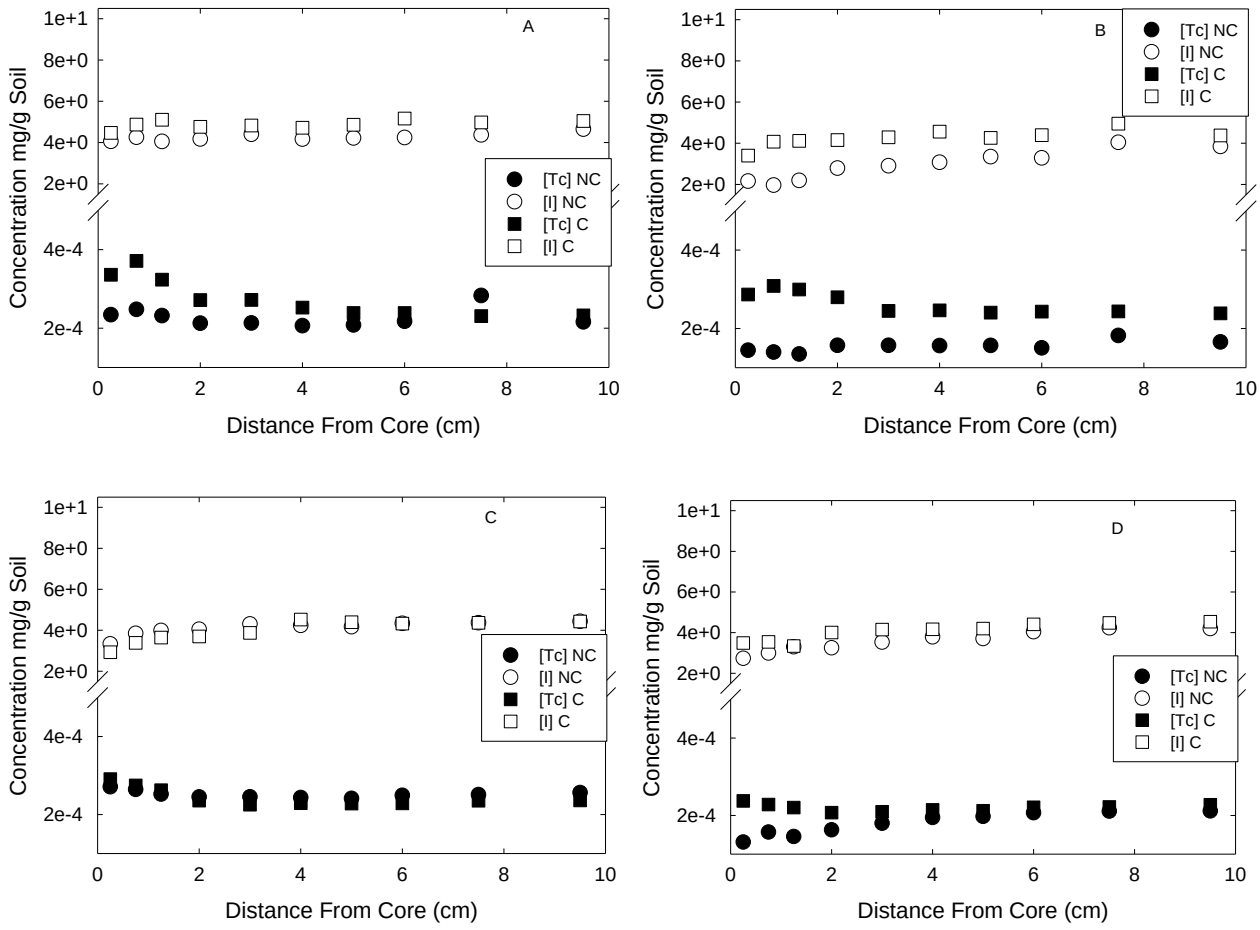

Figure 3.1. Tc and I Soil Concentration Profiles
A) 4% soil moisture, 0% Fe, B) 4% soil moisture, 4% Fe,
C) 4% soil moisture, 8% Fe, D) 4% soil moisture, 12% Fe

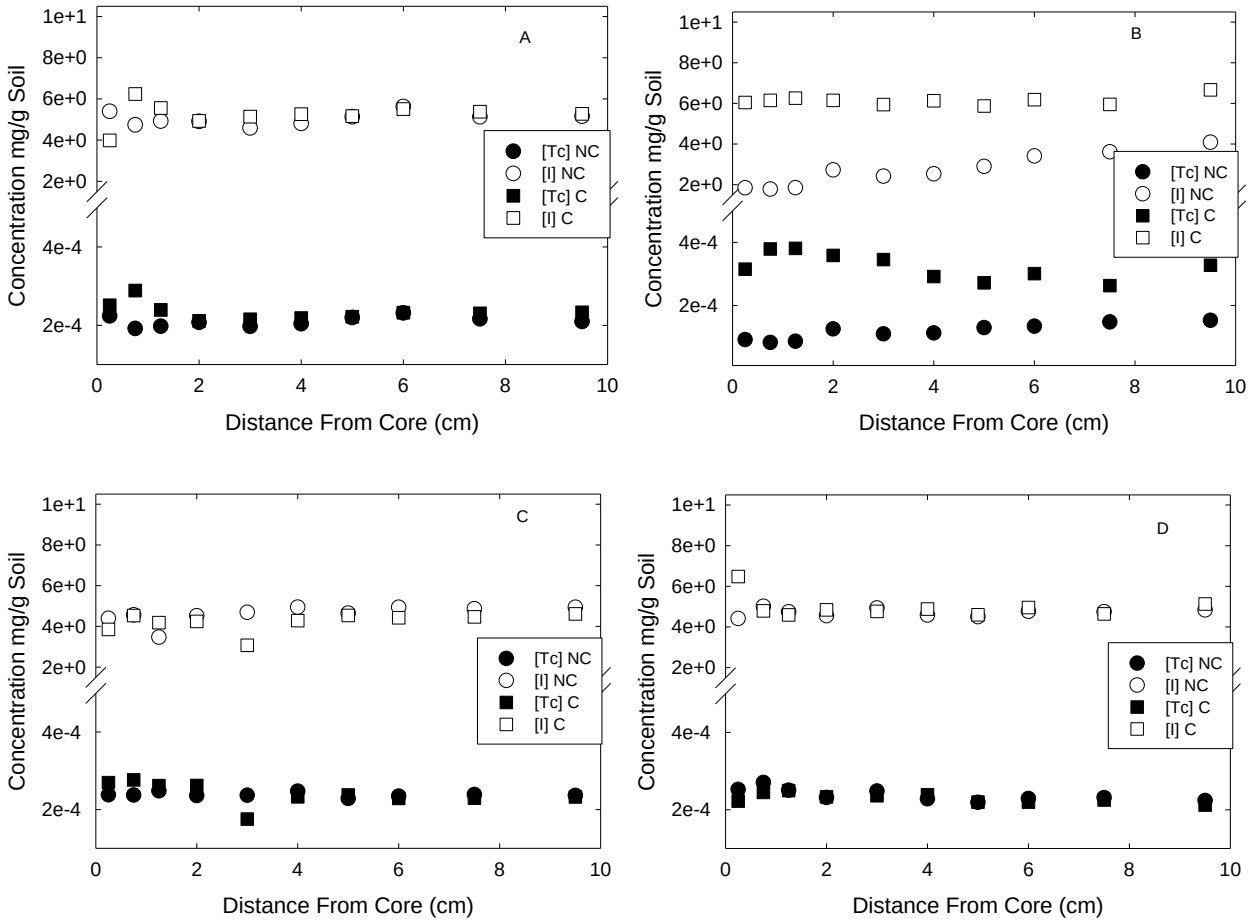

Figure 3.2. Tc and I Soil Concentration Profile
A) 7% soil moisture, 0% Fe, B) 7% soil moisture, 4% Fe,
C) 7% soil moisture, 8% Fe, D) 7% soil moisture, 12% Fe

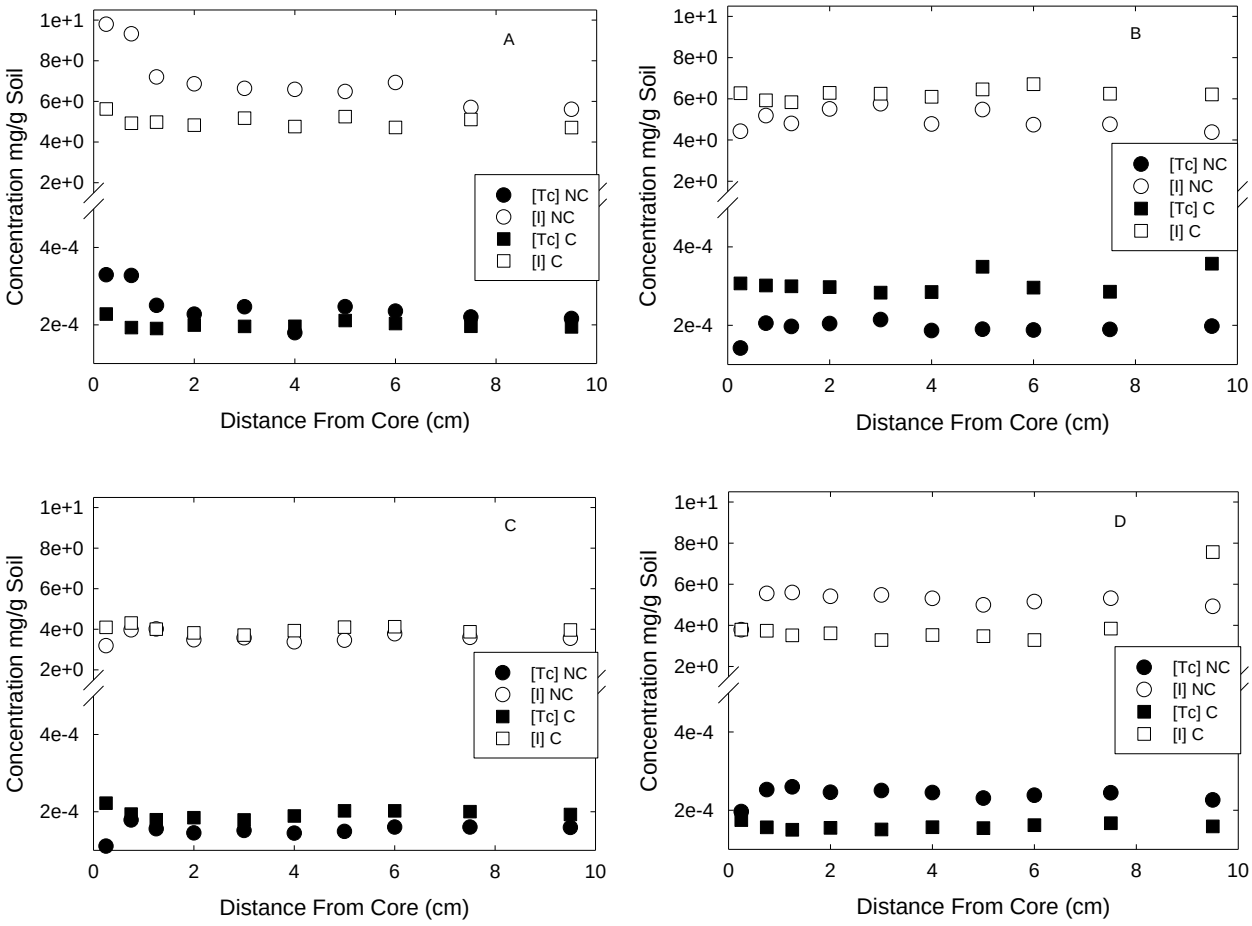

Figure 3.3. Tc and I Soil Concentration Profile
A) 15% soil moisture, 0% Fe, B) 15% soil moisture, 4% Fe,
C) 15% soil moisture, 8% Fe, D) 15% soil moisture, 12% Fe

Table 3.2. Tc and I Soil Concentration Profile

Distance From Core, cm	Tc, mg/g	I, mg/g	Distance From Core, cm	Tc, mg/g	I, mg/g	Distance From Core, cm	Tc, mg/g	I, mg/g	Distance From Core, cm	Tc, mg/g	I, mg/g
4% Soil--NC 0% Iron			4% Soil--NC 4% Iron			4% Soil--C 0% Iron			4% Soil--C-4% Iron		
9.5	2.16E-04	4.65	9.5	1.66E-04	3.85	9.5	2.32E-04	5.05	9.5	2.39E-04	4.38
7.5	2.83E-04	4.37	7.5	1.82E-04	4.04	7.5	2.31E-04	4.98	7.5	2.44E-04	4.95
6	2.17E-04	4.24	6	1.50E-04	3.29	6	2.39E-04	5.17	6	2.43E-04	4.39
5	2.08E-04	4.22	5	1.56E-04	3.35	5	2.39E-04	4.86	5	2.40E-04	4.26
4	2.06E-04	4.16	4	1.56E-04	3.07	4	2.52E-04	4.72	4	2.46E-04	4.56
3	2.13E-04	4.40	3	1.57E-04	2.90	3	2.72E-04	4.83	3	2.45E-04	4.29
2	2.12E-04	4.17	2	1.57E-04	2.79	2	2.71E-04	4.76	2	2.80E-04	4.16
1.25	2.32E-04	4.05	1.25	1.35E-04	2.19	1.25	3.23E-04	5.11	1.25	3.00E-04	4.11
0.75	2.48E-04	4.26	0.75	1.40E-04	1.96	0.75	3.71E-04	4.87	0.75	3.09E-04	4.08
0.25	2.34E-04	4.05	0.25	1.44E-04	2.16	0.25	3.36E-04	4.47	0.25	2.87E-04	3.40
4% Soil--NC 8% Iron			4% Soil--NC 12% Iron			4% Soil--C 8% Iron			4% Soil--C-12% Iron		
9.5	2.56E-04	4.44	9.5	2.11E-04	4.20	9.5	2.36E-04	4.43	9.5	2.28E-04	4.54
7.5	2.51E-04	4.36	7.5	2.11E-04	4.24	7.5	2.35E-04	4.37	7.5	2.22E-04	4.48
6	2.49E-04	4.34	6	2.07E-04	4.04	6	2.29E-04	4.32	6	2.21E-04	4.41
5	2.41E-04	4.17	5	1.97E-04	3.71	5	2.28E-04	4.39	5	2.12E-04	4.20
4	2.43E-04	4.24	4	1.95E-04	3.79	4	2.29E-04	4.53	4	2.14E-04	4.17
3	2.45E-04	4.30	3	1.80E-04	3.53	3	2.25E-04	3.87	3	2.10E-04	4.15
2	2.45E-04	4.05	2	1.63E-04	3.25	2	2.36E-04	3.70	2	2.07E-04	4.01
1.25	2.52E-04	3.99	1.25	1.45E-04	3.30	1.25	2.62E-04	3.65	1.25	2.20E-04	3.34
0.75	2.64E-04	3.85	0.75	1.57E-04	2.99	0.75	2.75E-04	3.38	0.75	2.28E-04	3.54
0.25	2.71E-04	3.33	0.25	1.31E-04	2.74	0.25	2.91E-04	2.93	0.25	2.38E-04	3.49

Table 3.2. (contd)

Distance From Core, cm	Tc, mg/g	I, mg/g	Distance From Core, cm	Tc, mg/g	I, mg/g	Distance From Core, cm	Tc, mg/g	I, mg/g	Distance From Core, cm	Tc, mg/g	I, mg/g
7% Soil--NC 0% Iron			7% Soil--NC 4% Iron			7% Soil--C 0% Iron			7% Soil--C-4% Iron		
9.5	2.09E-04	5.16	9.5	1.53E-04	4.08	9.5	2.33E-04	5.28	9.5	3.28E-04	6.66
7.5	2.16E-04	5.13	7.5	1.48E-04	3.62	7.5	2.30E-04	5.38	7.5	2.63E-04	5.95
6	2.32E-04	5.63	6	1.34E-04	3.41	6	2.32E-04	5.51	6	3.01E-04	6.18
5	2.20E-04	5.13	5	1.30E-04	2.90	5	2.22E-04	5.17	5	2.72E-04	5.87
4	2.04E-04	4.80	4	1.13E-04	2.53	4	2.19E-04	5.26	4	2.92E-04	6.13
3	1.97E-04	4.59	3	1.10E-04	2.42	3	2.15E-04	5.14	3	3.45E-04	5.94
2	2.08E-04	4.91	2	1.26E-04	2.72	2	2.11E-04	4.93	2	3.59E-04	6.15
1.25	1.98E-04	4.92	1.25	8.65E-05	1.85	1.25	2.39E-04	5.56	1.25	3.81E-04	6.26
0.75	1.92E-04	4.74	0.75	8.27E-05	1.78	0.75	2.89E-04	6.24	0.75	3.79E-04	6.15
0.25	2.24E-04	5.39	0.25	9.16E-05	1.84	0.25	2.51E-04	3.99	0.25	3.15E-04	6.05
7% Soil--NC 8% Iron			7% Soil--NC 12% Iron			7% Soil--C 8% Iron			7% Soil--C-12% Iron		
9.5	2.36E-04	4.93	9.5	2.24E-04	4.84	9.5	2.33E-04	4.61	9.5	2.12E-04	5.13
7.5	2.39E-04	4.86	7.5	2.31E-04	4.75	7.5	2.30E-04	4.47	7.5	2.25E-04	4.64
6	2.34E-04	4.94	6	2.29E-04	4.77	6	2.29E-04	4.42	6	2.20E-04	4.96
5	2.28E-04	4.65	5	2.19E-04	4.50	5	2.37E-04	4.54	5	2.20E-04	4.60
4	2.47E-04	4.94	4	2.28E-04	4.59	4	2.33E-04	4.28	4	2.39E-04	4.88
3	2.37E-04	4.69	3	2.48E-04	4.93	3	1.75E-04	3.07	3	2.36E-04	4.77
2	2.36E-04	4.52	2	2.32E-04	4.55	2	2.62E-04	4.25	2	2.33E-04	4.84
1.25	2.48E-04	3.47	1.25	2.50E-04	4.74	1.25	2.62E-04	4.19	1.25	2.50E-04	4.59
0.75	2.37E-04	4.56	0.75	2.70E-04	5.02	0.75	2.76E-04	4.53	0.75	2.45E-04	4.79
0.25	2.38E-04	4.39	0.25	2.53E-04	4.42	0.25	2.69E-04	3.85	0.25	2.22E-04	6.48

Table 3.2. (contd)

Distance From Core, cm	Tc, mg/g	I, mg/g	Distance From Core, cm	Tc, mg/g	I, mg/g	Distance From Core, cm	Tc, mg/g	I, mg/g	Distance From Core, cm	Tc, mg/g	I, mg/g
15% Soil--NC 0% Iron			15% Soil--NC 4% Iron			15% Soil--C 0% Iron			15% Soil--C-4% Iron		
9.5	2.16E-04	5.61	9.5	1.98E-04	4.38	9.5	1.95E-04	4.71	9.5	3.57E-04	6.21
7.5	2.20E-04	5.70	7.5	1.89E-04	4.76	7.5	1.96E-04	5.11	7.5	2.86E-04	6.25
6	2.35E-04	6.92	6	1.88E-04	4.74	6	2.03E-04	4.72	6	2.96E-04	6.71
5	2.47E-04	6.48	5	1.90E-04	5.48	5	2.11E-04	5.25	5	3.49E-04	6.46
4	1.79E-04	6.59	4	1.86E-04	4.77	4	1.96E-04	4.76	4	2.85E-04	6.10
3	2.47E-04	6.64	3	2.14E-04	5.76	3	1.96E-04	5.17	3	2.83E-04	6.25
2	2.27E-04	6.86	2	2.04E-04	5.50	2	1.99E-04	4.83	2	2.97E-04	6.29
1.25	2.50E-04	7.20	1.25	1.97E-04	4.80	1.25	1.91E-04	4.98	1.25	2.99E-04	5.84
0.75	3.27E-04	9.32	0.75	2.05E-04	5.18	0.75	1.93E-04	4.92	0.75	3.01E-04	5.92
0.25	3.29E-04	9.79	0.25	1.42E-04	4.42	0.25	2.28E-04	5.63	0.25	3.07E-04	6.28
15% Soil--NC 8% Iron			15% Soil--NC 12% Iron			15% Soil--C 8% Iron			15% Soil--C-12% Iron		
9.5	1.59E-04	3.55	9.5	2.26E-04	4.92	9.5	1.93E-04	3.97	9.5	1.59E-04	7.57
7.5	1.60E-04	3.60	7.5	2.44E-04	5.31	7.5	2.00E-04	3.88	7.5	1.67E-04	3.84
6	1.60E-04	3.77	6	2.38E-04	5.15	6	2.02E-04	4.12	6	1.62E-04	3.29
5	1.49E-04	3.46	5	2.31E-04	4.99	5	2.02E-04	4.11	5	1.54E-04	3.48
4	1.44E-04	3.38	4	2.45E-04	5.31	4	1.89E-04	3.93	4	1.57E-04	3.53
3	1.51E-04	3.57	3	2.50E-04	5.47	3	1.79E-04	3.71	3	1.51E-04	3.29
2	1.45E-04	3.48	2	2.46E-04	5.41	2	1.85E-04	3.82	2	1.55E-04	3.62
1.25	1.55E-04	4.01	1.25	2.60E-04	5.59	1.25	1.79E-04	4.01	1.25	1.50E-04	3.52
0.75	1.78E-04	3.97	0.75	2.53E-04	5.55	0.75	1.94E-04	4.31	0.75	1.56E-04	3.74
0.25	1.11E-04	3.19	0.25	1.96E-04	3.78	0.25	2.22E-04	4.09	0.25	1.75E-04	3.79

Contrastingly, well-developed I and Tc concentration gradients from interface were observed in concrete half-cells. Therefore, these concentration gradients were linearized by probit analyses to allow calculation of diffusion coefficients. In concrete half-cells in contact with spiked soil-cells at 4% moisture content, the carbonation of concrete treatment seemed to significantly reduce the diffusivity of both I and Tc (Figure 3.4). Both Tc and I diffusivities in both the uncarbonated and carbonated half-cells seem to be noticeably attenuated by the presence of Fe particles.

In concrete half-cells in contact with soil at 7% moisture content, reduction of diffusivity of both Tc and I were also observed in carbonated specimens (Figure 3.5). Additionally, in most cases, the presence of Fe seemed to exert a more pronounced influence in attenuating the diffusion of Tc and I in concrete. While such attenuation of Tc diffusivity can be ascribed to probable Tc reduction by metallic Fe, it is unclear how the metallic Fe may be contributing towards reduction in iodide mobility.

In carbonated concrete specimens in contact with high moisture content (15%) soils, similar reductions in Tc and I were also observed (Figure 3.6). In both uncarbonated and carbonated concrete specimens, the presence of metallic Fe significantly reduced the diffusivity of both Tc and I.

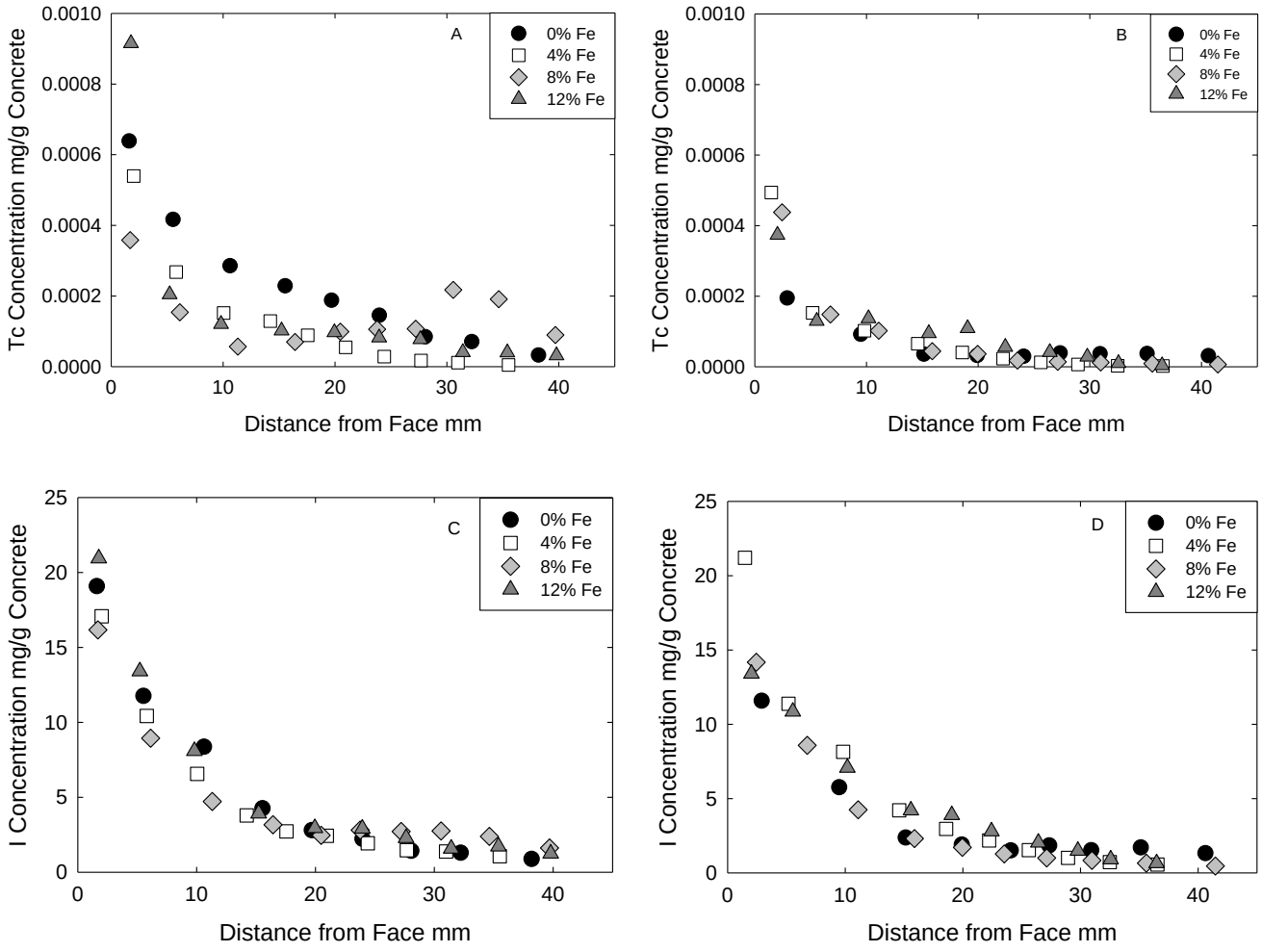

Figure 3.4. Concrete Half-Cell Concentration Profiles as a Function of Iron Content
A) Tc concentration for uncarbonated concrete at 4% soil moisture,
B) Tc concentration for carbonated concrete at 4% soil moisture,
C) I concentration for uncarbonated concrete at 4% soil moisture,
D) I concentration for carbonated concrete at 4% soil moisture

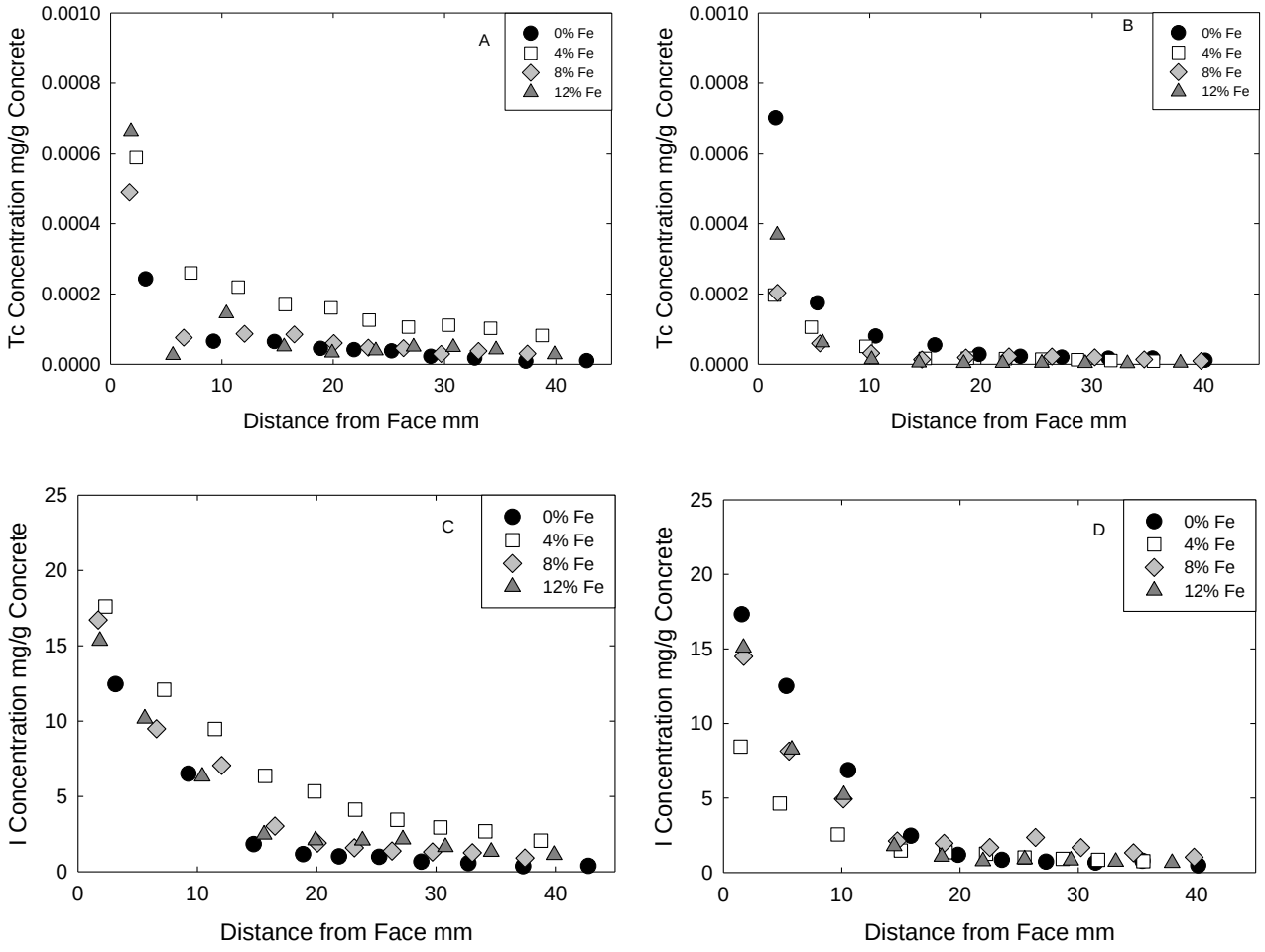

Figure 3.5. Concrete Half-Cell Concentration Profiles as a Function of Iron Content
A) Tc concentration for uncarbonated concrete at 7% soil moisture,
B) Tc concentration for carbonated concrete at 7% soil moisture,
C) I concentration for uncarbonated concrete at 7% soil moisture,
D) I concentration for carbonated concrete at 7% soil moisture

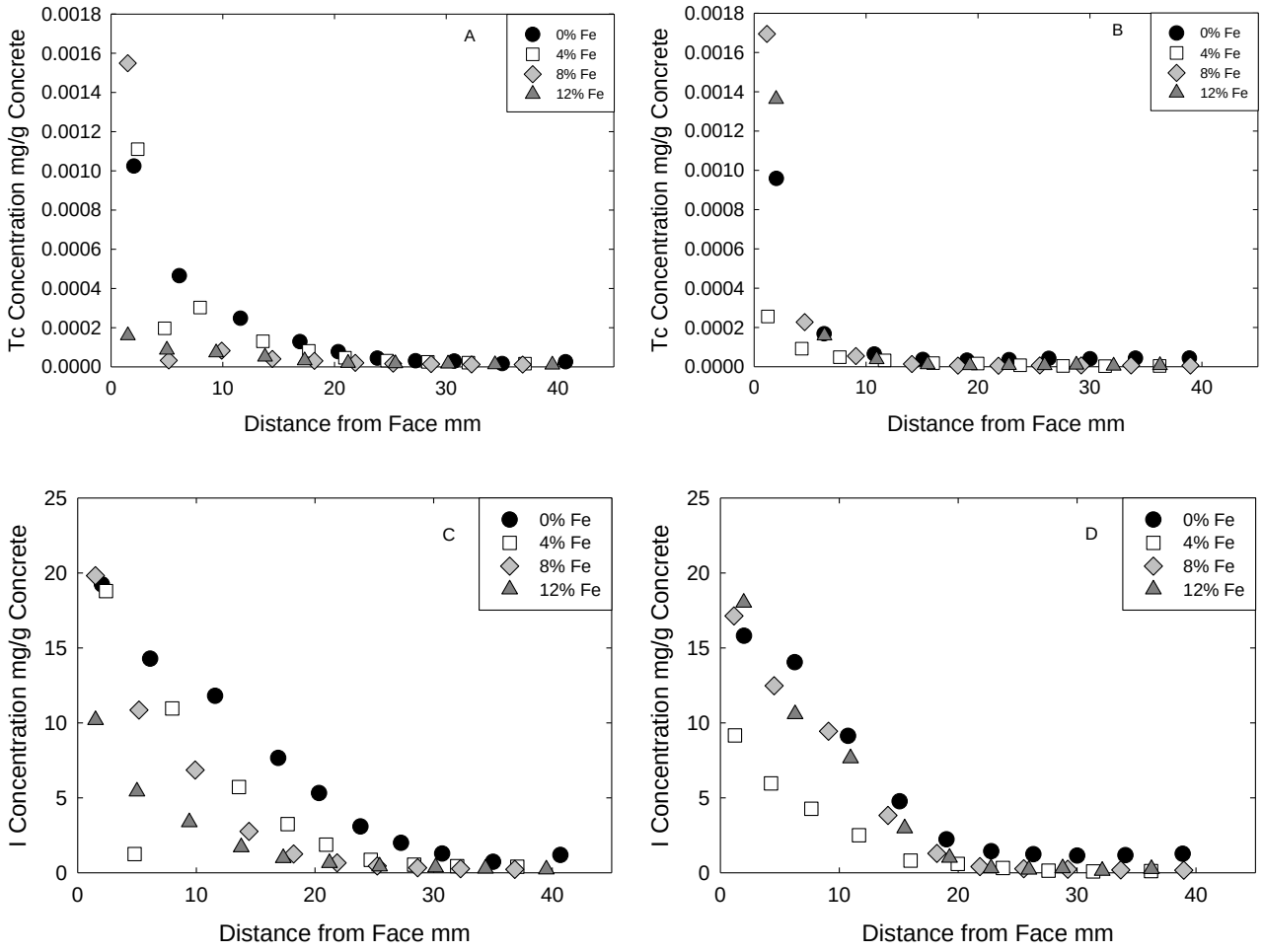

Figure 3.6. Concrete Half-Cell Concentration Profiles as a Function of Iron Content
A) Tc concentration for uncarbonated concrete at 15% soil moisture,
B) Tc concentration for carbonated concrete at 15% soil moisture,
C) I concentration for uncarbonated concrete at 15% soil moisture,
D) I concentration for carbonated concrete at 15% soil moisture

Table 3.3. Concentration Profile for Tc and I Concrete Half-Cells

Center of slice to face, mm	I, mg/g	Tc, mg/g	Center of slice to face, mm	I, mg/g	Tc, mg/g	Center of slice to face, mm	I, mg/g	Tc, mg/g	Center of slice to face, mm	I, mg/g	Tc, mg/g
4% Soil--NC 0% Iron			4% Soil--NC 4% Iron			4% Soil--C 0% Iron			4% Soil--C-4% Iron		
1.61	19.08	6.39E-04	2.02	17.07	5.40E-04	2.91	11.58	1.95E-04	1.48	21.20	4.94E-04
5.53	11.76	4.17E-04	5.81	10.43	2.68E-04	9.49	5.76	9.18E-05	5.18	11.38	1.53E-04
10.63	8.37	2.86E-04	10.05	6.56	1.52E-04	15.14	2.38	3.57E-05	9.83	8.15	1.02E-04
15.55	4.26	2.29E-04	14.22	3.79	1.29E-04	19.91	1.90	3.18E-05	14.59	4.21	6.52E-05
19.70	2.80	1.88E-04	17.56	2.72	8.87E-05	24.08	1.51	2.95E-05	18.58	2.96	4.05E-05
23.97	2.22	1.45E-04	20.96	2.43	5.48E-05	27.35	1.85	3.91E-05	22.23	2.19	2.30E-05
28.07	1.42	8.48E-05	24.41	1.93	2.84E-05	30.92	1.52	3.67E-05	25.61	1.53	1.24E-05
32.22	1.30	7.09E-05	27.69	1.47	1.74E-05	35.13	1.71	3.74E-05	28.94	1.01	6.32E-06
38.20	0.88	3.26E-05	31.00	1.38	1.13E-05	40.62	1.33	3.13E-05	32.49	0.73	2.71E-06
			35.51	1.07	4.59E-06				36.55	0.56	2.16E-06
4% Soil--NC 8% Iron			4% Soil--NC 12% Iron			4% Soil--C 8% Iron			4% Soil--C-12% Iron		
1.70	16.17	3.58E-04	1.77	20.94	9.15E-04	2.44	14.18	4.38E-04	2.03	13.41	3.73E-04
6.13	8.94	1.54E-04	5.23	13.41	2.04E-04	6.77	8.58	1.48E-04	5.55	10.85	1.30E-04
11.32	4.72	5.68E-05	9.82	8.09	1.20E-04	11.10	4.25	1.02E-04	10.19	7.07	1.37E-04
16.43	3.17	7.00E-05	15.23	3.92	1.02E-04	15.89	2.31	4.42E-05	15.59	4.21	9.48E-05
20.48	2.46	9.91E-05	19.95	2.95	9.70E-05	19.96	1.72	3.63E-05	19.06	3.89	1.09E-04
23.77	2.81	1.06E-04	23.94	2.91	8.22E-05	23.52	1.28	1.74E-05	22.43	2.79	5.60E-05
27.21	2.72	1.07E-04	27.63	2.28	7.73E-05	27.13	1.01	1.38E-05	26.42	2.04	4.12E-05
30.57	2.75	2.17E-04	31.43	1.58	4.08E-05	30.97	0.84	1.22E-05	29.78	1.49	2.81E-05
34.64	2.39	1.91E-04	35.40	1.72	3.98E-05	35.60	0.65	9.04E-06	32.57	0.91	9.99E-06
39.70	1.62	8.94E-05	39.80	1.25	3.16E-05	41.47	0.46	6.49E-06	36.48	0.65	3.56E-06
7% Soil--NC 0% Iron			7% Soil--NC 4% Iron			7% Soil--C 0% Iron			7% Soil--C-4% Iron		

Table 3.3. (contd)

Center of slice to face, mm	I, mg/g	Tc, mg/g	Center of slice to face, mm	I, mg/g	Tc, mg/g	Center of slice to face, mm	I, mg/g	Tc, mg/g	Center of slice to face, mm	I, mg/g	Tc, mg/g
3.15	12.45	2.43E-04	2.30	17.60	5.90E-04	1.56	17.31	7.01E-04	1.46	8.44	1.97E-04
9.25	6.50	6.50E-05	7.22	12.08	2.60E-04	5.31	12.51	1.75E-04	4.76	4.63	1.05E-04
14.72	1.82	6.41E-05	11.47	9.47	2.19E-04	10.54	6.86	7.98E-05	9.67	2.55	5.08E-05
18.86	1.16	4.48E-05	15.68	6.36	1.70E-04	15.86	2.46	5.45E-05	14.99	1.47	1.63E-05
21.88	1.01	4.09E-05	19.82	5.33	1.60E-04	19.85	1.19	2.76E-05	18.79	1.36	1.71E-05
25.24	0.98	3.75E-05	23.24	4.12	1.26E-04	23.55	0.85	2.21E-05	22.21	1.26	1.60E-05
28.77	0.66	2.22E-05	26.75	3.45	1.05E-04	27.28	0.72	1.98E-05	25.46	1.01	1.45E-05
32.72	0.56	1.72E-05	30.36	2.94	1.11E-04	31.46	0.66	1.70E-05	28.68	0.92	1.28E-05
37.31	0.36	8.37E-06	34.14	2.68	1.02E-04	35.43	0.78	1.74E-05	31.68	0.86	1.05E-05
42.77	0.38	9.87E-06	38.77	2.06	8.16E-05	40.15	0.48	1.09E-05	35.50	0.76	8.69E-06
7% Soil--NC 8% Iron			7% Soil--NC 12% Iron			7% Soil--C 8% Iron			7% Soil--C-12% Iron		
1.70	16.71	4.88E-04	1.84	15.33	6.62E-04	1.71	14.49	2.03E-04	1.70	15.08	3.68E-04
6.57	9.49	7.55E-05	5.59	10.17	2.56E-05	5.54	8.14	5.91E-05	5.78	8.25	6.13E-05
12.04	7.05	8.65E-05	10.41	6.32	1.44E-04	10.14	4.93	3.12E-05	10.18	5.20	1.36E-05
16.51	3.02	8.46E-05	15.58	2.47	4.99E-05	14.71	2.12	1.33E-05	14.43	1.77	4.25E-06
20.06	1.90	6.01E-05	19.91	2.09	3.25E-05	18.66	1.96	1.89E-05	18.46	1.06	2.75E-06
23.16	1.59	4.69E-05	23.84	2.08	3.85E-05	22.53	1.68	2.22E-05	21.95	0.76	3.07E-06
26.31	1.38	4.55E-05	27.22	2.15	4.92E-05	26.38	2.36	2.19E-05	25.47	0.89	3.31E-06
29.71	1.31	2.92E-05	30.78	1.64	4.80E-05	30.23	1.68	1.96E-05	29.38	0.81	2.63E-06
33.05	1.26	3.75E-05	34.64	1.32	4.13E-05	34.68	1.33	1.35E-05	33.17	0.72	2.22E-06
37.45	0.91	3.02E-05	39.88	1.12	2.75E-05	39.80	1.03	9.38E-06	37.93	0.64	3.59E-06
15% Soil--NC 0% Iron			15% Soil--NC 4% Iron			15% Soil--C 0% Iron			15% Soil--C-4% Iron		
2.05	19.23	1.02E-03	2.39	18.79	1.11E-03	1.99	15.80	9.59E-04	1.23	9.16	2.56E-04

Table 3.3. (contd)

Center of slice to face, mm	I, mg/g	Tc, mg/g	Center of slice to face, mm	I, mg/g	Tc, mg/g	Center of slice to face, mm	I, mg/g	Tc, mg/g	Center of slice to face, mm	I, mg/g	Tc, mg/g
6.12	14.28	4.65E-04	7.97	10.96	3.03E-04	6.26	14.04	1.68E-04	4.27	5.96	9.19E-05
11.59	11.79	2.48E-04	13.59	5.72	1.31E-04	10.75	9.13	6.41E-05	7.65	4.27	4.87E-05
16.91	7.66	1.29E-04	17.70	3.25	8.15E-05	15.08	4.76	3.64E-05	11.66	2.51	3.20E-05
20.35	5.31	7.70E-05	20.94	1.88	4.64E-05	19.02	2.23	3.25E-05	16.00	0.81	1.81E-05
23.84	3.09	4.39E-05	24.70	0.86	3.15E-05	22.79	1.43	3.52E-05	19.97	0.59	1.64E-05
27.26	1.99	3.04E-05	28.35	0.54	2.55E-05	26.33	1.23	4.21E-05	23.77	0.32	7.65E-06
30.72	1.27	2.92E-05	31.98	0.44	2.13E-05	30.01	1.14	4.00E-05	27.60	0.14	4.00E-06
35.02	0.73	1.62E-05	37.05	0.40	1.62E-05	34.07	1.17	4.32E-05	31.36	0.09	3.06E-06
40.69	1.18	2.55E-05				38.89	1.26	4.33E-05	36.22	0.11	4.10E-06
15% Soil--NC 8% Iron			15% Soil--NC 12% Iron			15% Soil--C 8% Iron			15% Soil--C-12% Iron		
1.50	19.81	1.55E-03	1.51	10.19	1.60E-04	1.15	17.13	1.69E-03	1.97	18.02	1.36E-03
5.17	10.86	3.25E-05	5.00	5.42	8.67E-05	4.52	12.48	2.27E-04	6.29	10.58	1.58E-04
9.90	6.85	8.27E-05	9.41	3.38	7.29E-05	9.10	9.44	5.44E-05	10.95	7.64	3.74E-05
14.44	2.76	4.01E-05	13.79	1.71	5.11E-05	14.10	3.83	1.35E-05	15.50	2.97	1.16E-05
18.21	1.25	3.08E-05	17.33	0.98	3.22E-05	18.22	1.29	5.56E-06	19.28	1.01	7.07E-06
21.87	0.66	2.05E-05	21.22	0.65	1.91E-05	21.83	0.41	4.88E-06	22.77	0.30	7.43E-06
25.25	0.45	1.61E-05	25.45	0.43	1.72E-05	25.52	0.27	6.64E-06	25.95	0.21	6.71E-06
28.66	0.33	1.43E-05	30.16	0.36	1.59E-05	29.22	0.23	6.36E-06	28.79	0.31	9.61E-06
32.27	0.27	1.19E-05	34.37	0.28	1.23E-05	33.67	0.19	6.44E-06	32.12	0.13	4.29E-06
36.84	0.22	1.14E-05	39.50	0.22	1.05E-05	38.97	0.16	5.74E-06	36.26	0.26	7.12E-06

3.2 Probit Analysis Results and Discussion

Probit analysis of the set of diffusion experiments detailed in section 3.1 are presented. The preparation method, previously discussed, is found in section 2.1. Soil half-cell specimens were spiked with Tc to achieve a measurable diffusion profile in the soil part of the half-cell. The characteristics of the specimens used are listed in Table 3.1.

Figure 3.12, and the resulting diffusivities are tabulated (Table 3.4). Overall, the calculated diffusivities for Tc ranged from 1.9 x 10^{-9} to 1 x 10^{-10} cm^2/s, and I ranged from 2.3 x 10^{-9} to 3.1 x 10^{-10} cm^2/s. The highest Tc and I diffusivities were observed in all uncarbonated, Fe-free concrete cores contacting spiked soils at all three moisture contents (4%, 7%, and 15%). However, the diffusivities of both Tc and I (except in one case) were significantly attenuated in all carbonated concrete cores. The reduction of Tc diffusivities ranged from 55% to 72%. Meanwhile, I diffusivities were reduced by 61% at soil moisture content 4% and 58% at soil moisture content of 15%, respectively. However, I diffusivity showed an anomalous increase of ~38% in uncarbonated, Fe-free concrete core in contact with soil core containing 7% moisture content.

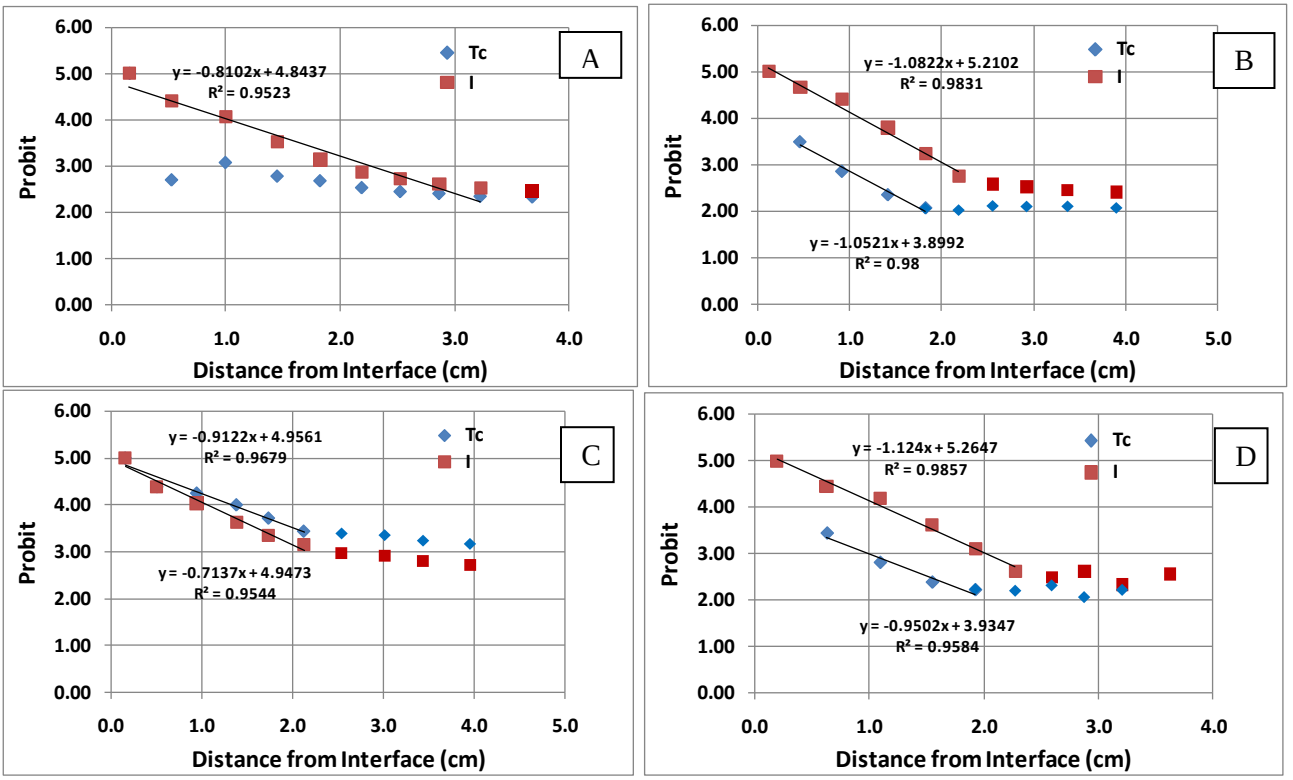

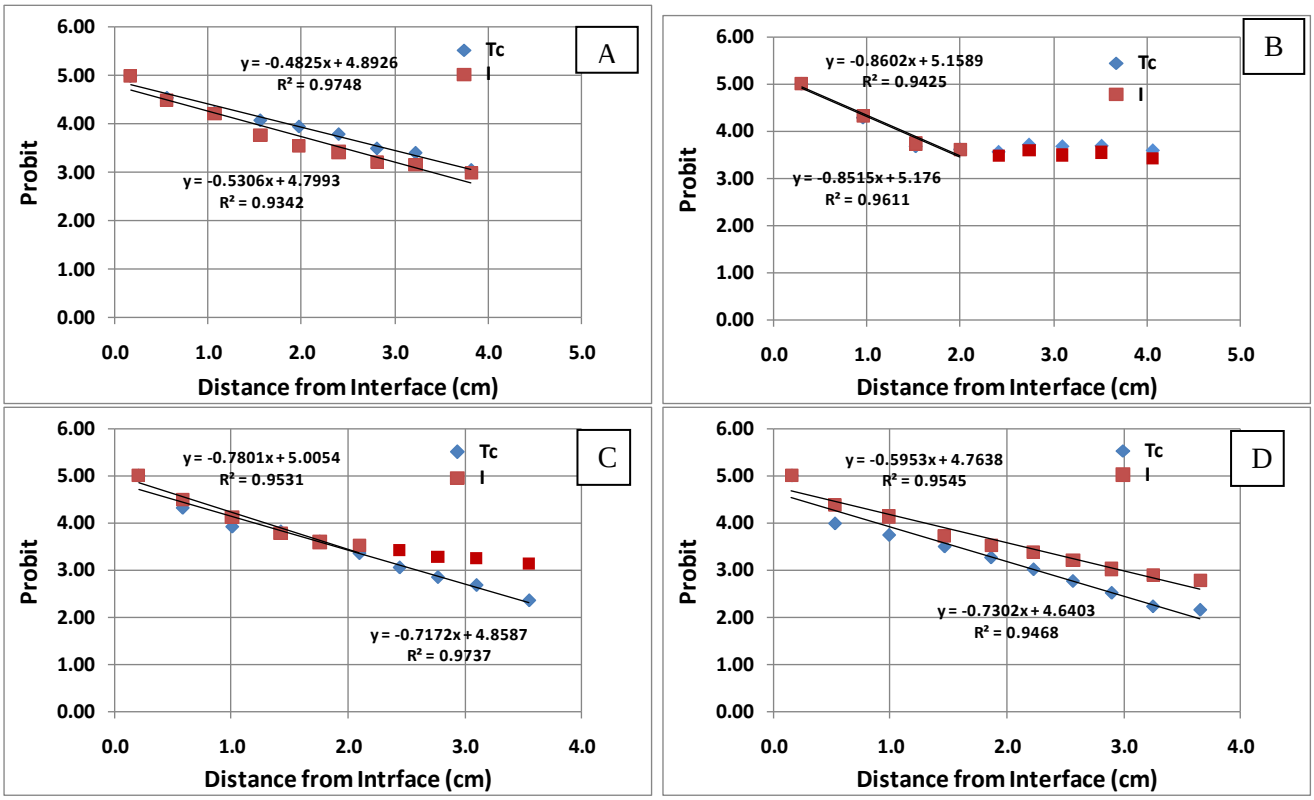

Figure 3.7. Probit Analysis of FY 2009 Tc Cores
A) Tc-C-08-3-0-325, B) Tc-C-08-3-0-332, C) Tc-C-08-3-4-350, D) Tc-C-08-3-4-357

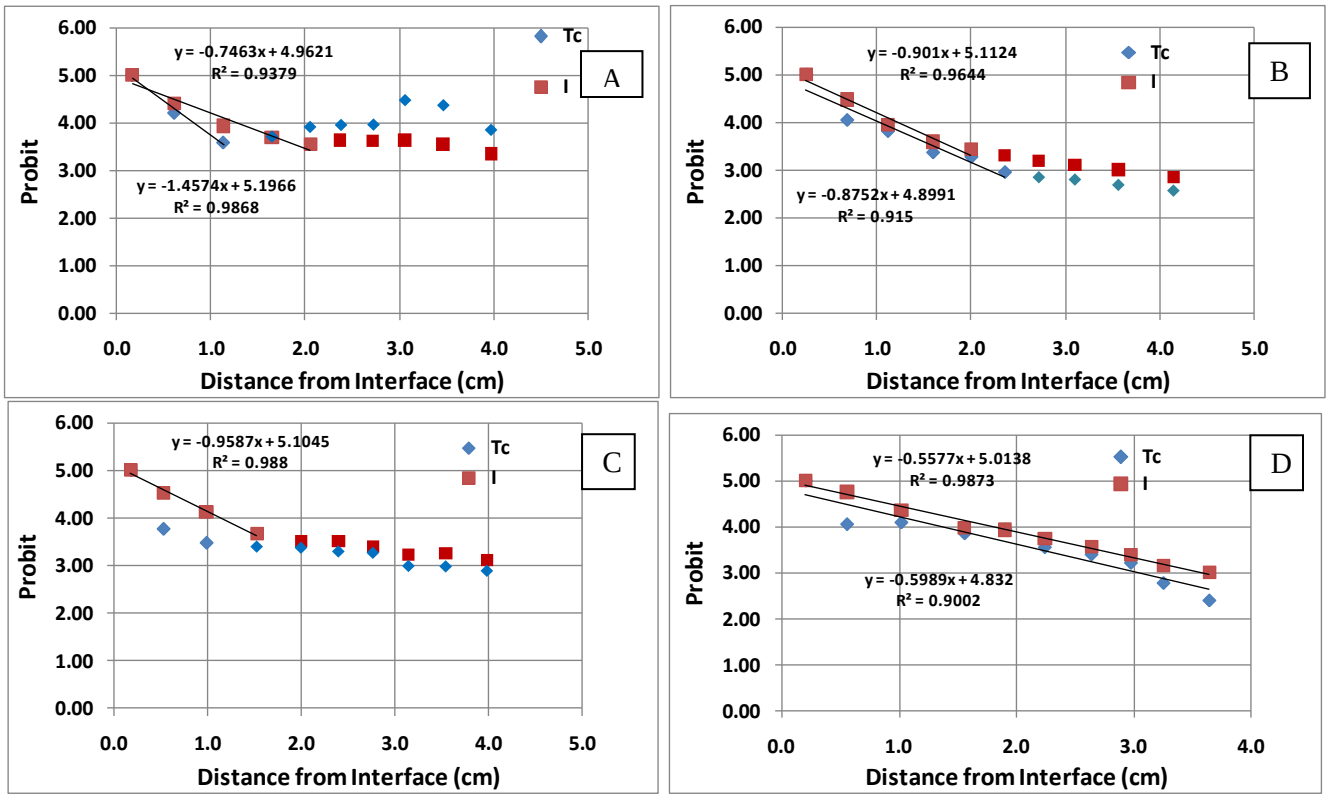

Figure 3.8. Probit Analysis of FY 2009 Tc Cores
A) Tc-C-08-3-8-401, B) Tc-C-08-3-8-407, C) Tc-C-08-3-12-425, D) Tc-C-08-3-12-432

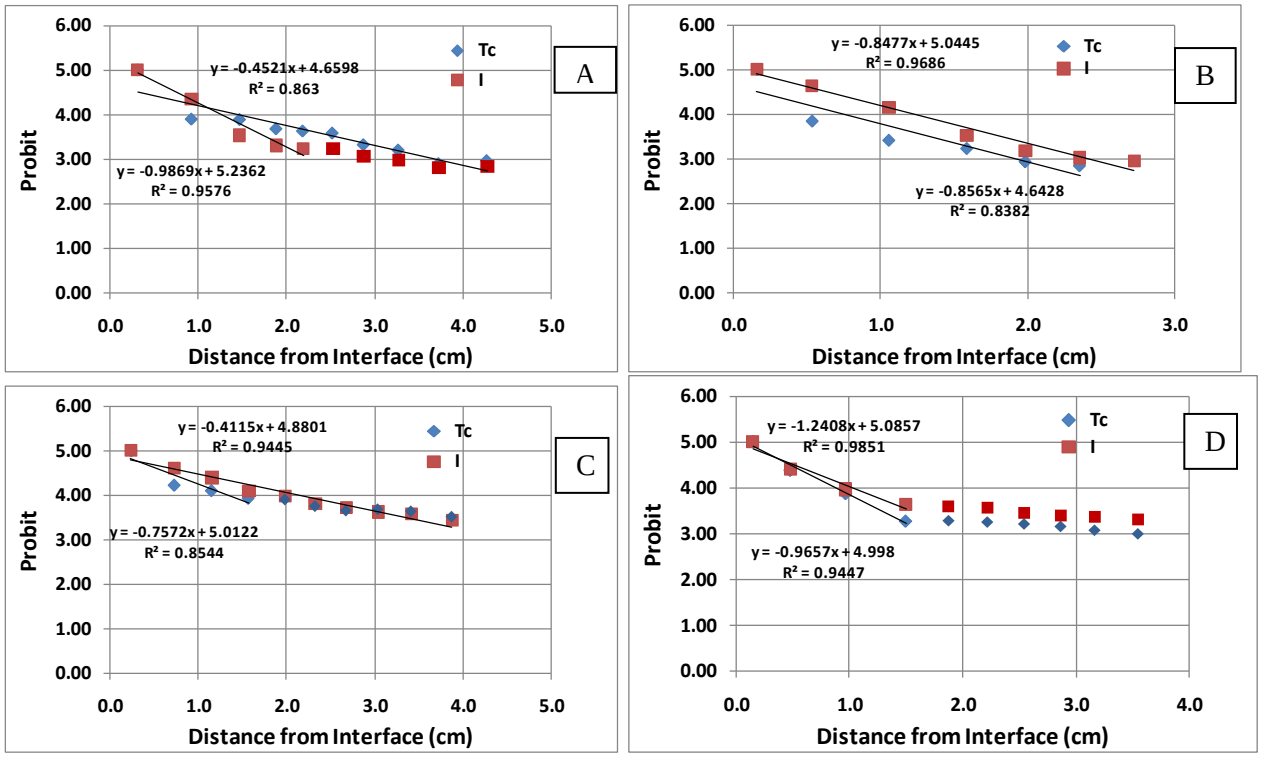

Figure 3.9. Probit Analysis of FY 2009 Tc Cores
A) Tc-C-08-3-0-329, B) Tc-C-08-3-0-333, C) Tc-C-08-3-4-351, D) Tc-C-08-3-4-359

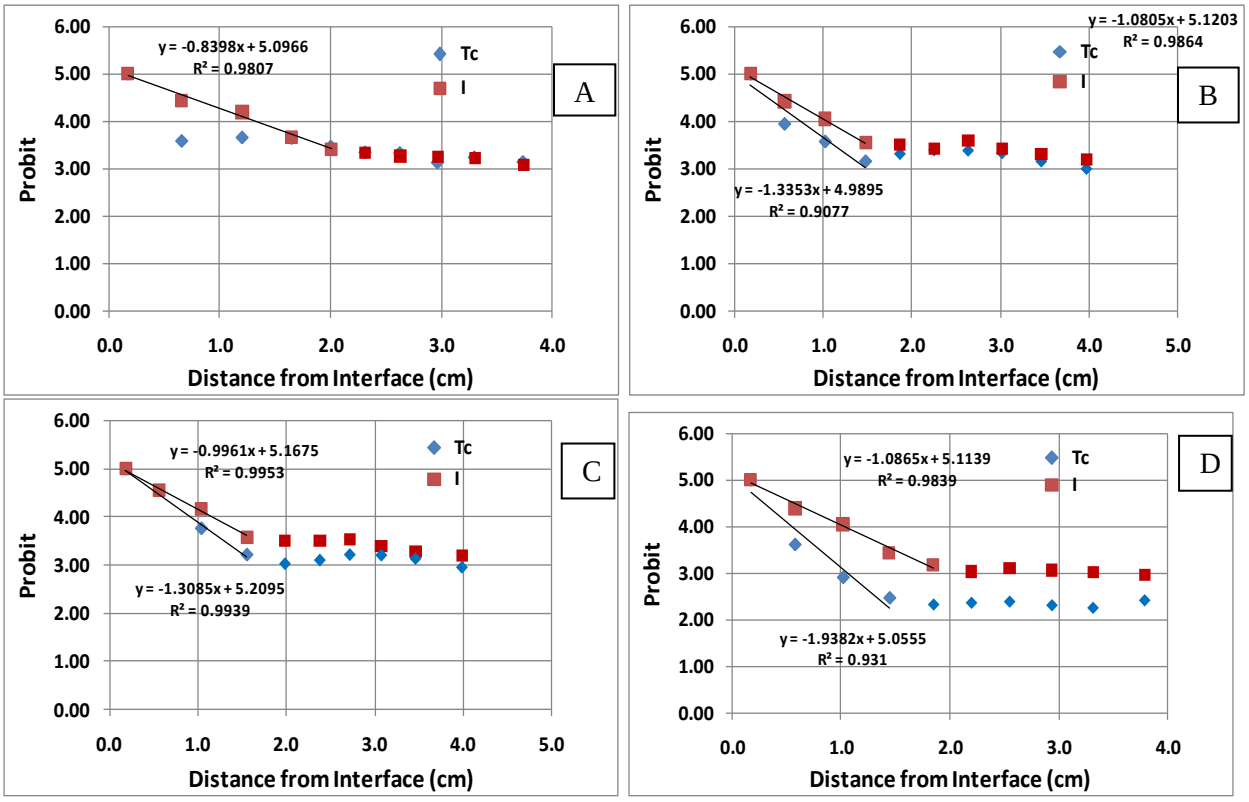

Figure 3.10. Probit Analysis of FY 2009 Tc Cores
A) Tc-C-08-3-8-402, B) Tc-C-08-3-8-409, C) Tc-C-08-3-12-426, D) Tc-C-08-3-12-433

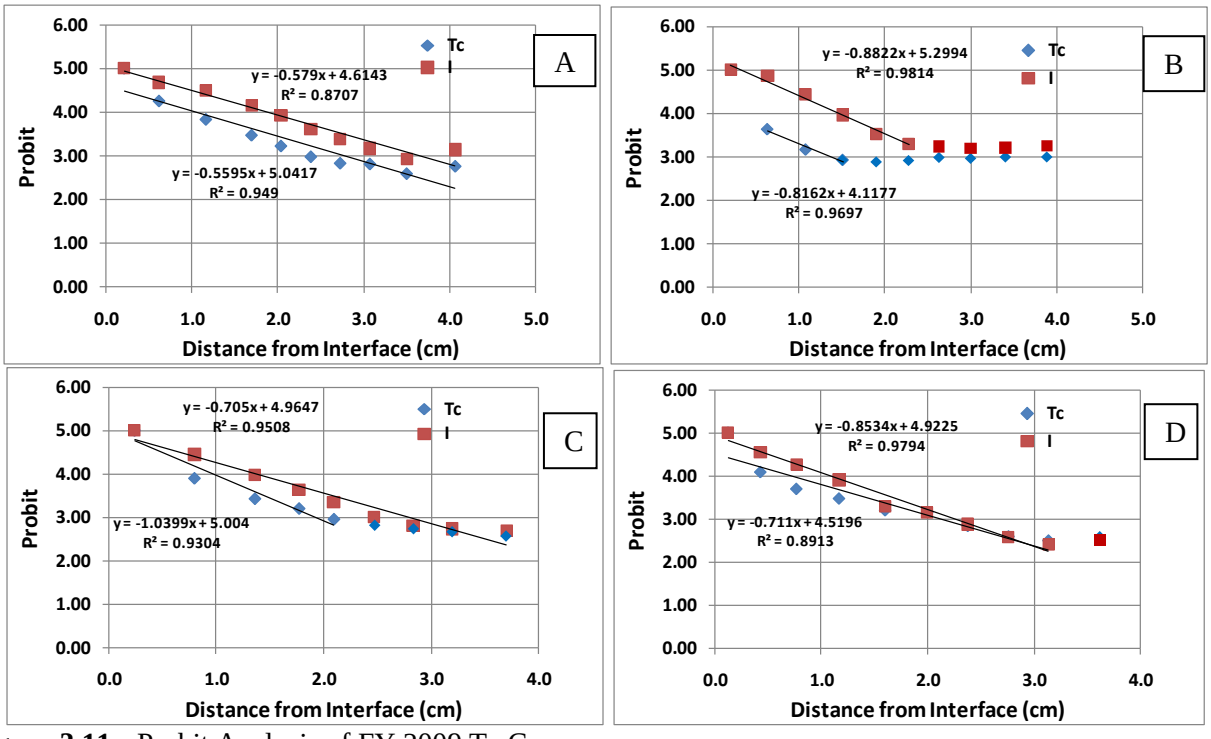

Figure 3.11. Probit Analysis of FY 2009 Tc Cores
A) Tc-C-08-3-0-330, B) Tc-C-08-3-0-334, C) Tc-C-08-3-4-353, D) Tc-C-08-3-4-360

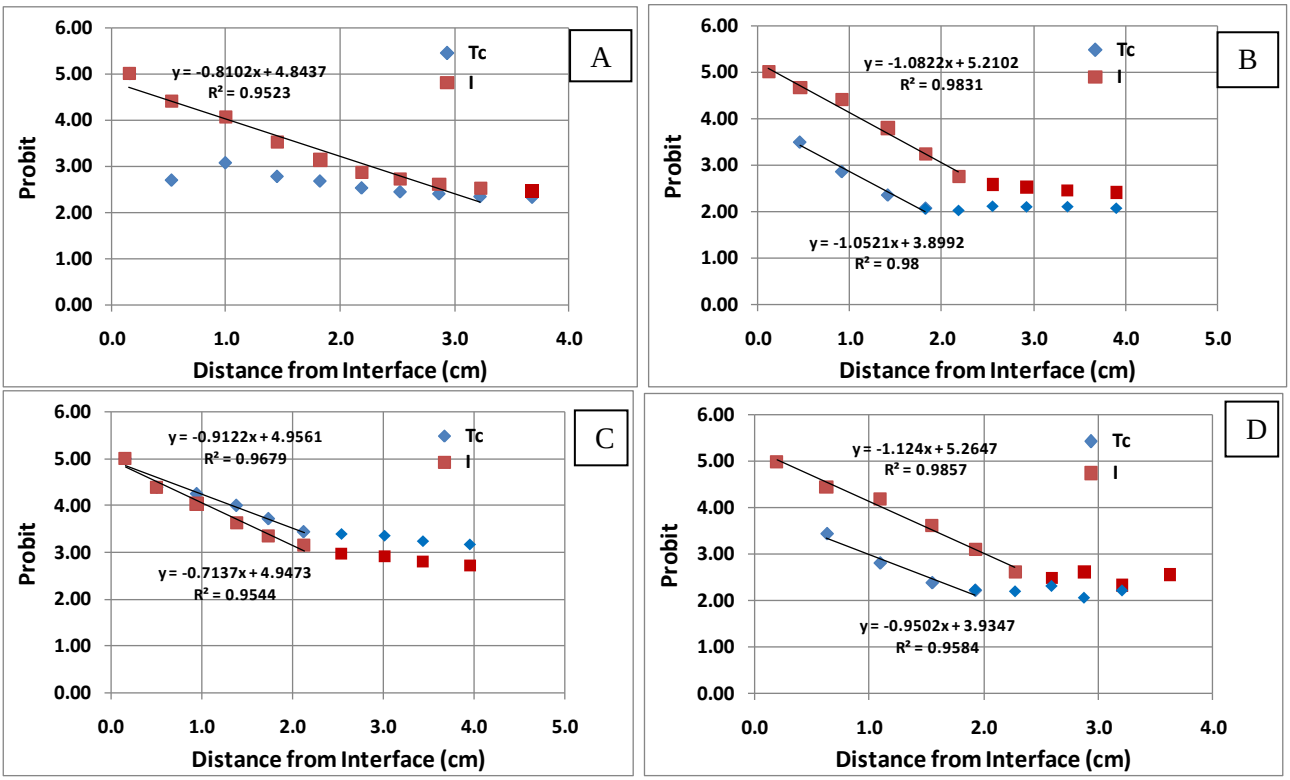

Figure 3.12. Probit Analysis of FY 2009 Tc Cores
A) Tc-C-08-3-8-403, B) Tc-C-08-3-8-410, C) Tc-C-08-3-12-427, D) Tc-C-08-3-12-435

In almost all cases, adding Fe to uncarbonated concrete half-cells resulted in significant reduction in Tc and I diffusivities. For instance, Tc diffusivities were reduced by 55% to 89% when Fe was present in concrete cores. Similarly, I diffusivities were attenuated by 34% to 54% in Fe-containing concrete cores, except anomalously enhanced diffusivities found in uncarbonated concrete cores in contact soil half-cells containing 7% moisture content.

Similar attenuation in Tc and I diffusivities were also observed in carbonated concrete half-cell containing various quantities of Fe. The diffusivities of Tc showed reduction typically ranging from 25% to 81%, except enhanced diffusivities (~40% to 30%) observed in two concrete cores containing 4% Fe and in contact with soil with 4% and 15% moisture contents, respectively. In these same cores, similar increases in I diffusivities were also observed (100% to 6%). However, all other Fe-containing carbonated concrete cores exhibited reduction in I diffusivities that ranged from 9% to 76%.

In summary, these data showed that:

- Carbonation of concrete results in substantial attenuation in Tc and I diffusivities.
- Generally, addition of Fe particles to both uncarbonated and carbonated concrete also results in significant reduction in Tc and I diffusivities.

- Based on previous studies, attenuation of Tc diffusivities upon Fe addition can be attributable to reduction of Tc(VII) to relatively insoluble Tc(IV) solid forms. Mechanisms of similar attenuation of I diffusivity upon Fe addition needs further investigation.

Table 3.4. Diffusivity Analysis of FY 2009 Tc Cores

Core ID	MC (wt %)	Carbonation	Fe (wt %)	Tc Diffusivity (cm^2/s)	I Diffusivity (cm^2/s)
Tc-C-08-3-0-325	4	N	0	1.7×10^{-09}	1.4×10^{-09}
Tc-C-08-3-0-329	7	N	0	1.9×10^{-09}	4.0×10^{-10}
Tc-C-08-3-0-330	15	N	0	1.3×10^{-09}	1.2×10^{-09}
Tc-C-08-3-0-332	4	Y	0	5.3×10^{-10}	5.4×10^{-10}
Tc-C-08-3-0-333	7	Y	0	5.4×10^{-10}	5.5×10^{-10}
Tc-C-08-3-0-334	15	Y	0	5.9×10^{-10}	5.1×10^{-10}
Tc-C-08-3-4-350	4	N	4	7.7×10^{-10}	6.5×10^{-10}
Tc-C-08-3-4-351	7	N	4	6.9×10^{-10}	2.3×10^{-09}
Tc-C-08-3-4-353	15	N	4	3.6×10^{-10}	7.9×10^{-10}
Tc-C-08-3-4-357	4	Y	4	7.4×10^{-10}	1.1×10^{-09}
Tc-C-08-3-4-359	7	Y	4	2.6×10^{-10}	4.2×10^{-10}
Tc-C-08-3-4-360	15	Y	4	7.8×10^{-10}	5.4×10^{-10}
Tc-C-08-3-8-401	4	N	8	1.9×10^{-10}	7.1×10^{-10}
Tc-C-08-3-8-402	7	N	8	NA	5.6×10^{-10}
Tc-C-08-3-8-403	15	N	8	NA	6.0×10^{-10}
Tc-C-08-3-8-407	4	Y	8	5.1×10^{-10}	4.9×10^{-10}
Tc-C-08-3-8-409	7	Y	8	2.2×10^{-10}	3.4×10^{-10}
Tc-C-08-3-8-410	15	Y	8	3.6×10^{-10}	3.4×10^{-10}
Tc-C-08-3-12-425	4	N	12	NA	4.3×10^{-10}
Tc-C-08-3-12-426	7	N	12	2.3×10^{-10}	4.0×10^{-10}
Tc-C-08-3-12-427	15	N	12	4.7×10^{-10}	7.7×10^{-10}
Tc-C-08-3-12-432	4	Y	12	1.1×10^{-10}	1.3×10^{-10}
Tc-C-08-3-12-433	7	Y	12	1.0×10^{-10}	3.3×10^{-10}
Tc-C-08-3-12-435	15	Y	12	4.4×10^{-10}	3.1×10^{-10}

4.0 Probit Analysis of Tc Cores

A set of diffusion experiments were initiated during FY 2007 using concrete-soil half-cells containing Tc. The concentration results were presented in the FY 2008 report. The preparation method, previously discussed, is found in section 2.1. Concrete half-cell specimens were spiked with Tc to achieve a measurable diffusion profile in the soil part of the half-cell. The characteristics of the specimens used are listed in Table 4.1. From the concentration data, probit plots were constructed.

Table 4.1. Characteristics of Cement Specimens Used in Fractured Concrete-Soil Half-Cell Tests

Core ID	Concrete Treatment	Tc Concentration (μg/g concrete)	Height of Concrete Half-Cell (cm)	Volume of Concrete Half-Cell (cm^3)	Density Concrete (g/cm^3)	Soil Moisture Content (%)
Tc-C-4-0-204	0% Fe	0.67	4.169	61.05	2.04	4
Tc-C-4-4-213	4% Fe	0.62	4.26	62.195	2.23	4
Tc-C-4-0-203	0% Fe	0.67	4.343	63.392	2.07	7
Tc-C-4-4-212	4% Fe	0.62	4.226	61.77	2.23	7
Tc-C-4-0-202	0% Fe	0.67	4.389	64.183	2.08	15
Tc-C-4-4-211	4% Fe	0.62	4.367	63.816	2.23	15

The diffusion profiles reported previously indicated, except for the low moisture soil cores, the diffusion of Tc had proceeded to near equilibrium conditions in that no concentration gradients from the concrete-soil interface were present. Comparatively, in the low moisture cores (Figure 4.1 and Figure 4.2), distinct Tc concentration gradients were observed from the interface. These data indicated that the time allowed for diffusion to take place (351days) was too long when the moisture conditions were higher (7% and 15%).

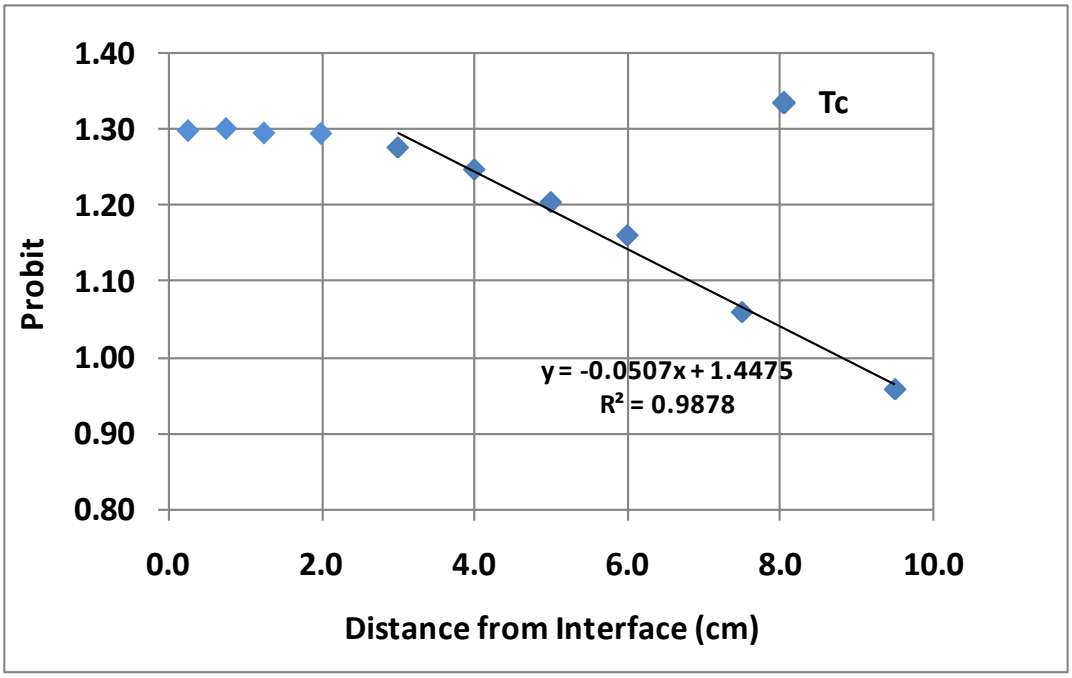

Figure 4.1. Probit Analysis for Core Tc-C-4-0-204

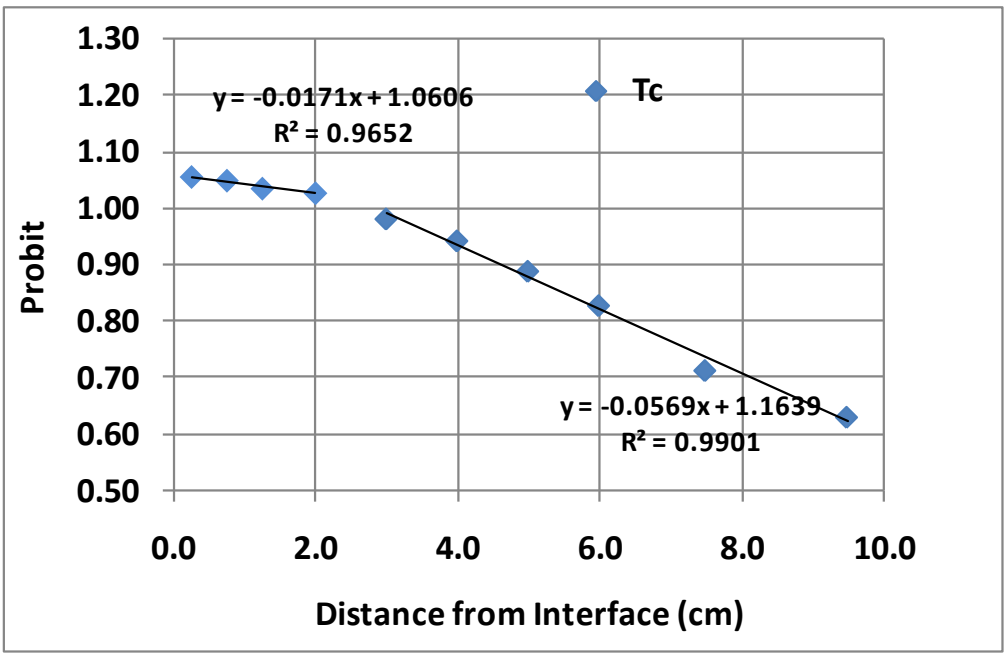

Figure 4.2. Probit Analysis for Core Tc-C-4-4-213

Therefore, the Tc diffusion calculations using probit analyses were conducted using data from the two soil cores containing 4% moisture content with and without 4% by mass iron particles. The resulting probit plots are shown in Figure 4.1 and Figure 4.2 and the data is also tabulated (Table 4.2). The Tc diffusion coefficient for core 204 without iron particles was 2.2×10^{-7} cm^2/s. Whereas, for the core 213 containing 4% by mass iron particles, the Tc diffusion coefficient was found to be 2.1×10^{-7} cm^2/s. These

data indicated the presence of iron particles (4% by mass) did not significantly affect Tc diffusivity in soils with ~4% moisture content. Similar comparisons in Tc diffusivities in soils with higher moisture contents (7% and 15%) could not be made to due to near equilibrium diffusion of Tc that resulted in lack of concentration gradients.

Table 4.2. Diffusivity Analysis of FY 2008 Tc Cores

Core ID	MC wt%	Carbonation	Fe wt%	Tc Diffusivity cm^2/s
Tc-C-4-0-204	4	N	0	2.20×10^{-7}
Tc-C-4-4-213	4	N	4	1.93×10^{-6}
				1.74×10^{-7}

5.0 Concrete-Soil Half-Cell Experiments to Determine the Diffusion of Iodine and Rhenium into Fractured Concrete

A set of diffusion experiments were initiated during FY 2007 using fractured concrete-soil half-cells. The preparation method, previously discussed, is found in section 2.1. Soil half-cell specimens were spiked with I and Re to achieve a measurable diffusion in the fractured concrete part of the half-cell. The characteristics of the specimens used are listed in Table 5.1. The diffusion tests were conducted under unsaturated conditions at 4%, 7%, and 15% (moisture content by weight). The concentration plots were reported previously. Presented below are diffusion plots from this set. The diffusion gradient data for this set of tests has been presented in a previous report (Wellman et al. 2008a). The results of the probit analysis of these data are shown in Figure 5.1 through Figure 5.3, and the diffusivity data is tabulated in Table 5.2.

Table 5.1. Characteristics of Cement Specimens Used in Fractured Concrete-Soil Half-Cell Tests

Specimen No.	Length (cm)	Diameter (cm)	Surface Area (cm^2)	Volume (cm^3)	Moisture Content			Treatment	
					4%	7%	15%	Fe	Carbonation
C-5-0-2	4.15	4.33	85.89	61.10	x			No	No
C-5-4-26	3.89	4.34	82.44	57.35	x			Yes	No
C-5-0-1	4.15	4.33	86.04	61.25	x			No	Yes
C-5-4-21	4.02	4.33	84.04	59.10	x			Yes	Yes
C-5-0-7	4.24	4.33	87.02	62.32		x		No	No
C-5-4-27	3.98	4.34	83.75	58.77		x		Yes	No
C-5-0-5	4.18	4.34	86.63	61.89		x		No	Yes
C-5-4-23	4.12	4.34	85.68	60.87		x		Yes	Yes

C-5-0-10	4.37	4.34	89.05	64.51	x	No	No
C-5-4-30	3.95	4.34	83.31	58.29	x	Yes	No
C-5-0-6	4.76	4.34	94.54	70.48	x	No	Yes
C-5-4-24	4.52	4.34	91.26	66.91	x	Yes	Yes

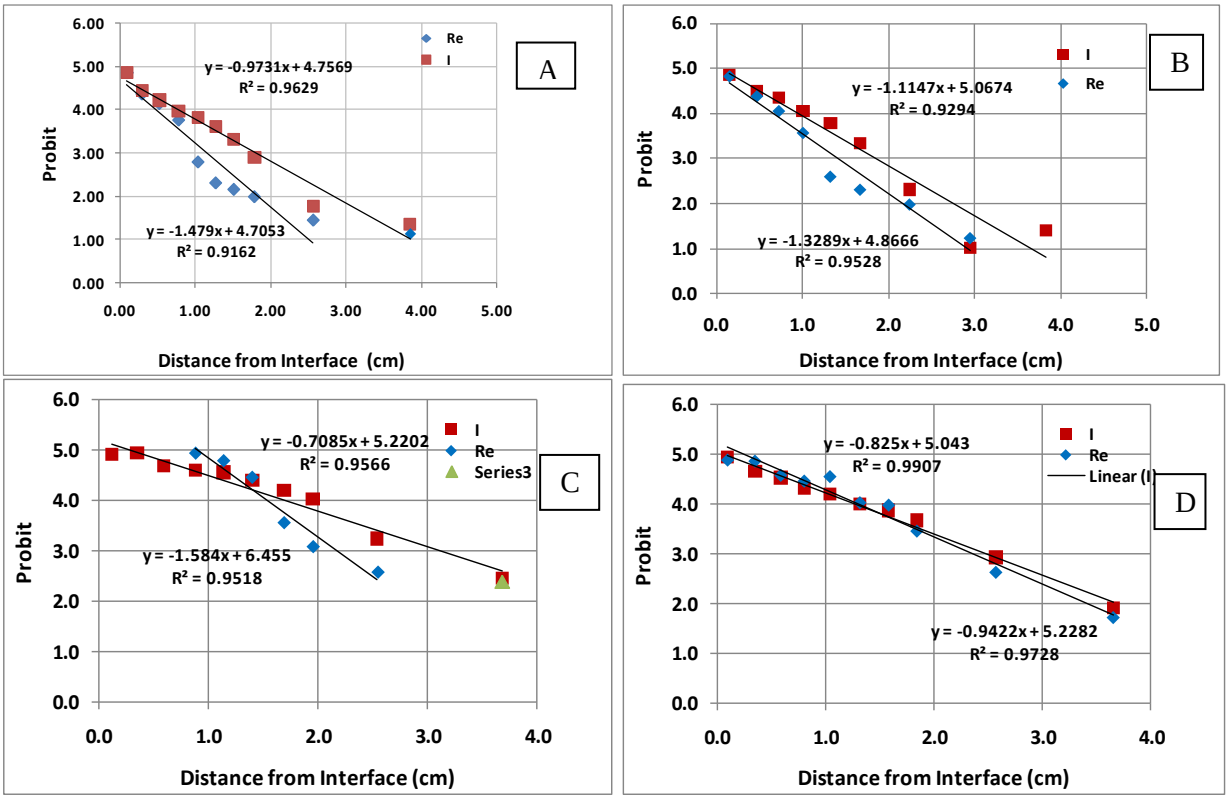

Figure 5.1. Probit Plots for (a) C-5-0-2 (b) C-5-4-26 (c) C-5-0-1 (d) C-5-4-21 Half-Cells

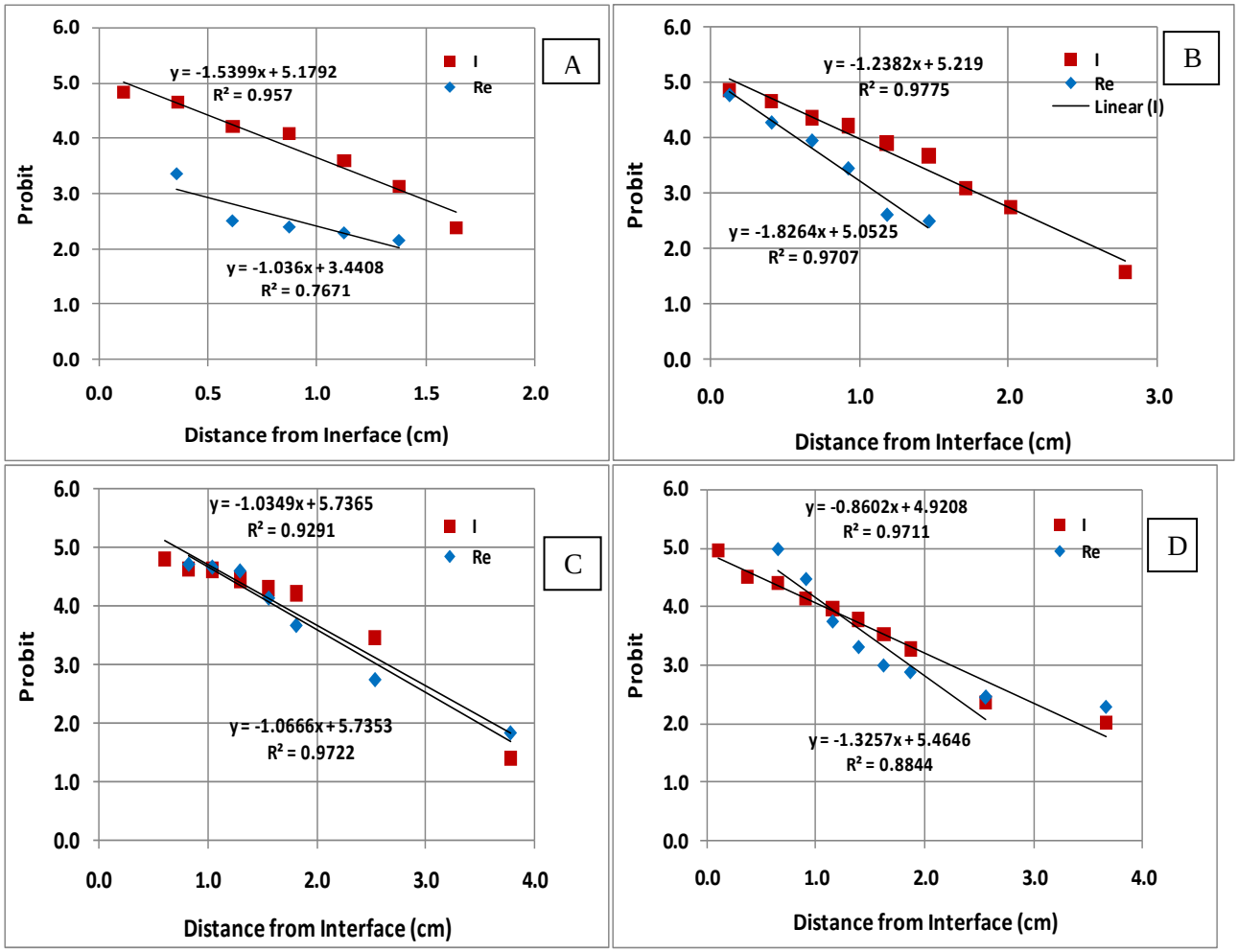

Figure 5.2. Diffusion Plots for (a) C-5-0-7 (b) C-5-4-27 (c) C-5-0-5 (d) C-5-4-23

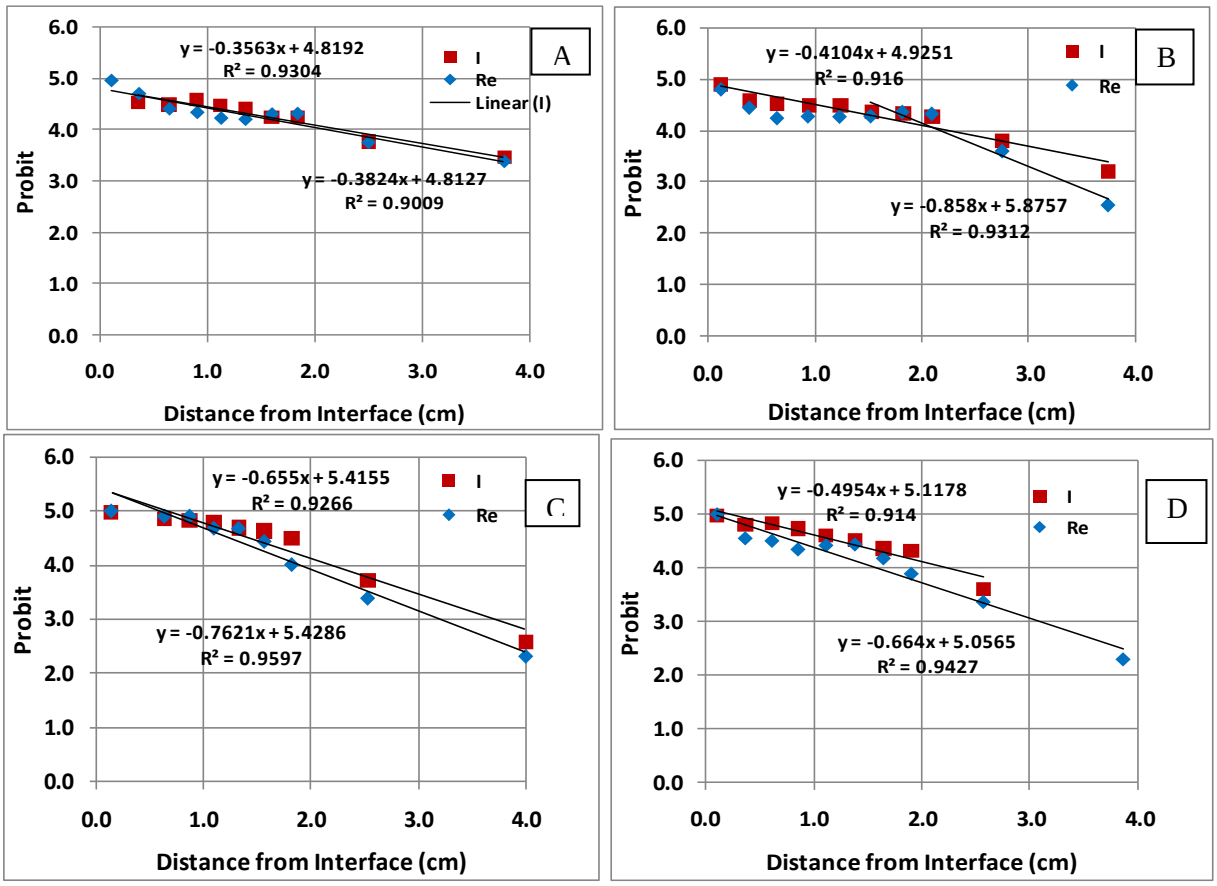

Figure 5.3. Diffusion Plots for (a) C-5-0-10 (b) C-5-4-30 (c) C-5-0-6 (d) C-5-4-24 Half-Cells

Overall, the calculated diffusivities for Re ranged from 3.8 x 10^{-12} to 2 x 10^{-9} cm^2/s, and I ranged from 1.3 x 10^{-10} to 2.3 x 10^{-9} cm^2/s in fractured concrete. The highest Re and I diffusivities were observed in fractured concrete cores that were in contact with spiked soils with 15% moisture content. Fe- free carbonated concrete cores had enhanced Re and I diffusivities when contacted with soil containing 4% and 7% moisture content. The diffusivities were significantly attenuated (66% and 78%) when in contact with soil containing 15% moisture content.

As compared to Fe-free, uncarbonated concrete half-cells, Re diffusivity in Fe-containing uncarbonated concrete half-cell in contact with soil half-cell with 4% moisture content was enhanced by about 24%. Whereas, I diffusivity was attenuated to the same extent. In uncarbonated, Fe-containing concrete half-cells contacting soil at 7% moisture content, Re and I diffusivities showed significant enhancement over Fe-free uncarbonated concrete samples. When the similar concrete half-cells were contacted with soils with 15% moisture content, diffusivities of both Re and I were attenuated by 80% and 24%, respectively.

In carbonated Fe-containing concrete half-cells in contact with Re, diffusivity increased significantly when contacted with soil at 4% moisture content, but decreased by 35% at 7% moisture content and by 3% at 15% moisture content. Comparatively, the I diffusivity in the same cores showed reduction at 4% soil moisture and increases of 44% and 137% at 7% and 15% soil moisture, respectively.

In summary, these data showed:

- Variations in Re or I diffusivities did not show any functional relationship with either concrete treatment (iron addition and carbonation) or soil moisture content.
- The presence of fractures and fracture geometry appears to exert significant influence on Re and I diffusivity.
- Because the random nature of the number of fractures and the fracture geometry in the cement cores were highly variable and not replicable because of the mode of fracture induction, the variations in Re and I diffusivities were unpredictable.

Table 5.2. Diffusion Data for Re-I Half-Cells

Core ID	MC wt%	Carbonation	Fe wt%	Re Diffusivity cm^2/s	I Diffusivity cm^2/s
C-5-0-2	4	N	0	1.4×10^{-10}	3.1×10^{-10}
C-5-4-26	4	N	4	1.7×10^{-10}	2.4×10^{-10}
C-5-0-1	4	Y	0	1.2×10^{-10}	5.9×10^{-10}
C-5-4-21	4	Y	4	3.3×10^{-10}	4.4×10^{-10}
C-5-0-7	7	N	0	3.8×10^{-12}	1.3×10^{-10}
C-5-4-27	7	N	4	8.9×10^{-11}	1.9×10^{-10}
C-5-0-5	7	Y	0	2.6×10^{-10}	2.8×10^{-10}
C-5-4-23	7	Y	4	1.7×10^{-10}	4.0×10^{-10}
C-5-0-10	15	N	0	2.0×10^{-09}	2.3×10^{-09}
C-5-4-30	15	N	4	4.0×10^{-10}	1.8×10^{-09}
C-5-0-6	15	Y	0	6.9×10^{-10}	5.1×10^{-10}
C-5-4-24	15	Y	4	6.7×10^{-10}	1.2×10^{-09}

6.0 Concrete-Soil Half-Cell Experiments to Determine the Diffusion of Iodine, Rhenium, and Technetium from Fractured Concrete into Soil

Two sets of diffusion experiments were initiated during FY 2008 using fractured concrete-soil half-cells. The preparation method, previously discussed, is found in section 2.1. Concrete half-cell specimens were spiked with I and Re (set 1) or Tc and I (set 2) to achieve a measurable diffusion profile in the soil part of the half-cell. The characteristics of the specimens used are listed in Table 6.1. Presented below is concentration data, probit plots, and the diffusion coefficients for the Re and I fractured cores. Sectioning and analyses of Tc-bearing half-cell tests was postponed due to the results of Re and I half-cells presented below.

Table 6.1. Characteristics of Concrete Specimens Used in Concrete-Soil Half-Cells

Core ID	Length (cm)	Diameter (cm)	r^2	Surface Area (cm^2)	Volume (cm^3)	Weight (g)	Density (g/cm^3)	Colloidal Iron (%)	Carbonated	Moisture Content (%)
Concrete Half-Cells Containing Iodine and Rhenium										
C-08-5-0-501	3.92	4.32	4.66	82.37	57.31	137.08	2.39	0	N	4
C-08-5-0-502	3.94	4.31	4.64	82.48	57.43	137.23	2.39	0	N	7
C-08-5-0-503	4.13	4.32	4.67	85.35	60.52	145.80	2.41	0	N	15
C-08-5-0-504	4.00	4.32	4.65	83.43	58.45	141.89	2.43	0	Y	4
C-08-5-0-505	3.86	4.32	4.66	81.68	56.55	138.20	2.44	0	Y	7
C-08-5-0-507	3.99	4.31	4.65	83.28	58.29	141.02	2.42	0	Y	15
C-08-5-4-526	3.86	4.32	4.67	81.77	56.65	136.50	2.41	4	N	4
C-08-5-4-527	4.14	4.32	4.66	85.43	60.61	145.87	2.41	4	N	7
C-08-5-4-528	3.80	4.32	4.67	81.02	55.83	134.05	2.40	4	N	15
C-08-5-4-530	3.96	4.33	4.68	83.27	58.26	139.27	2.39	4	Y	4
C-08-5-4-531	4.11	4.32	4.68	85.16	60.31	145.56	2.41	4	Y	7
C-08-5-4-532	3.85	4.32	4.66	81.45	56.31	134.81	2.39	4	Y	15
C-08-5-8-552	4.12	4.31	4.64	84.94	60.08	146.32	2.44	8	N	4
C-08-5-8-553	4.04	4.32	4.67	84.28	59.36	145.89	2.46	8	N	7
C-08-5-8-554	3.89	4.30	4.62	81.63	56.53	138.57	2.45	8	N	15
C-08-5-8-555	3.95	4.30	4.62	82.40	57.36	140.05	2.44	8	Y	4
C-08-5-8-556	3.92	4.30	4.63	82.12	57.05	140.48	2.46	8	Y	7
C-08-5-8-557	4.07	4.30	4.62	84.05	59.13	145.19	2.46	8	Y	15
C-08-5-12-576	4.05	4.31	4.65	84.03	59.10	144.99	2.45	12	N	4
C-08-5-12-577	4.08	4.31	4.64	84.36	59.46	144.82	2.44	12	N	7
C-08-5-12-578	3.84	4.31	4.64	81.11	55.96	137.24	2.45	12	N	15

Table 5.1. (contd)

Core ID	Length (cm)	Diameter (cm)	r^2	Surface Area (cm^2)	Volume (cm^3)	Weight (g)	Density (g/cm^3)	Colloidal Iron (%)	Carbonated	Moisture Content (%)
C-08-5-12-580	4.06	4.31	4.65	84.27	59.36	144.46	2.43	12	Y	4
C-08-5-12-581	4.29	4.31	4.64	87.17	62.49	153.33	2.45	12	Y	7
C-08-5-12-552	3.92	4.31	4.64	82.11	57.04	141.77	2.49	12	Y	15
Concrete Half-Cells Containing Technetium										
Tc-C-08-5-0-603	3.51	4.28	4.59	76.07	50.60	112.52	2.22	0	N	4
Tc-C-08-5-0-604	3.87	4.30	4.62	81.26	56.13	124.77	2.22	0	N	7
Tc-C-08-5-0-605	4.00	4.30	4.63	83.24	58.25	129.15	2.22	0	N	15
Tc-C-08-5-4-623	4.06	4.31	4.63	83.97	59.04	131.09	2.22	4	N	4
Tc-C-08-5-4-624	3.97	4.30	4.63	82.76	57.74	127.84	2.21	4	N	7
Tc-C-08-5-4-625	3.69	4.31	4.64	79.08	53.76	119.01	2.21	4	N	15
Tc-C-08-5-8-641	3.52	4.30	4.63	76.70	51.22	113.02	2.21	8	N	4
Tc-C-08-5-8-643	3.59	4.31	4.64	77.65	52.23	115.88	2.22	8	N	7
Tc-C-08-5-8-644	3.78	4.31	4.64	80.31	55.09	122.51	2.22	8	N	15
Tc-C-08-5-12-661	3.73	4.31	4.64	79.62	54.35	122.34	2.25	12	N	4
Tc-C-08-5-12-662	3.70	4.31	4.64	79.32	54.03	122.08	2.26	12	N	7
Tc-C-08-5-12-664	3.74	4.31	4.65	79.84	54.59	123.09	2.25	12	N	15

The diffusion profiles of soil half-cells are shown in Figures 5.1 through 5.3, and the Re and I spiked concrete half-cells are shown in Figures 5.4 through 5.6. Low moisture (4%) soil cores showed well defined diffusion gradient; however, the diffusivity of both Re and I was low due to lack of adequate moisture (Figure 6.1). The low moisture (4%) soils in contact with spiked carbonated concrete without Fe showed lower diffusivity as compared to soils in contact with uncarbonated, Fe-free concrete. Metallic Fe additions to the concrete also appeared to depress Re and I diffusivities into soils with 4% moisture (Figure 3.1)

Rhenium and I showed deeper penetration (increased diffusivity) into soils with 7% moisture content (Figure 6.2). Carbonation of concrete without iron also seemed to decrease Re and I diffusivities in soils contacting these half-cells. Addition of metallic Fe to spiked concrete also noticeably depressed Re and I diffusivities in soils.

In soils with the highest moisture content (15%), the diffusion progressed to the extent that there were no diffusion gradients (Figure 6.3). When the experiments were terminated, apparent diffusion equilibrium had been reached as indicated by relatively constant ionic concentrations throughout the soil half-cells. However, the influence of carbonation was very pronounced in that the concentrations of Re and I were significantly higher in soils in contact with uncarbonated concrete with or without Fe additions. Lack of distinct concentration gradients precluded computation of diffusion coefficients in these high moisture content (15%) soils.

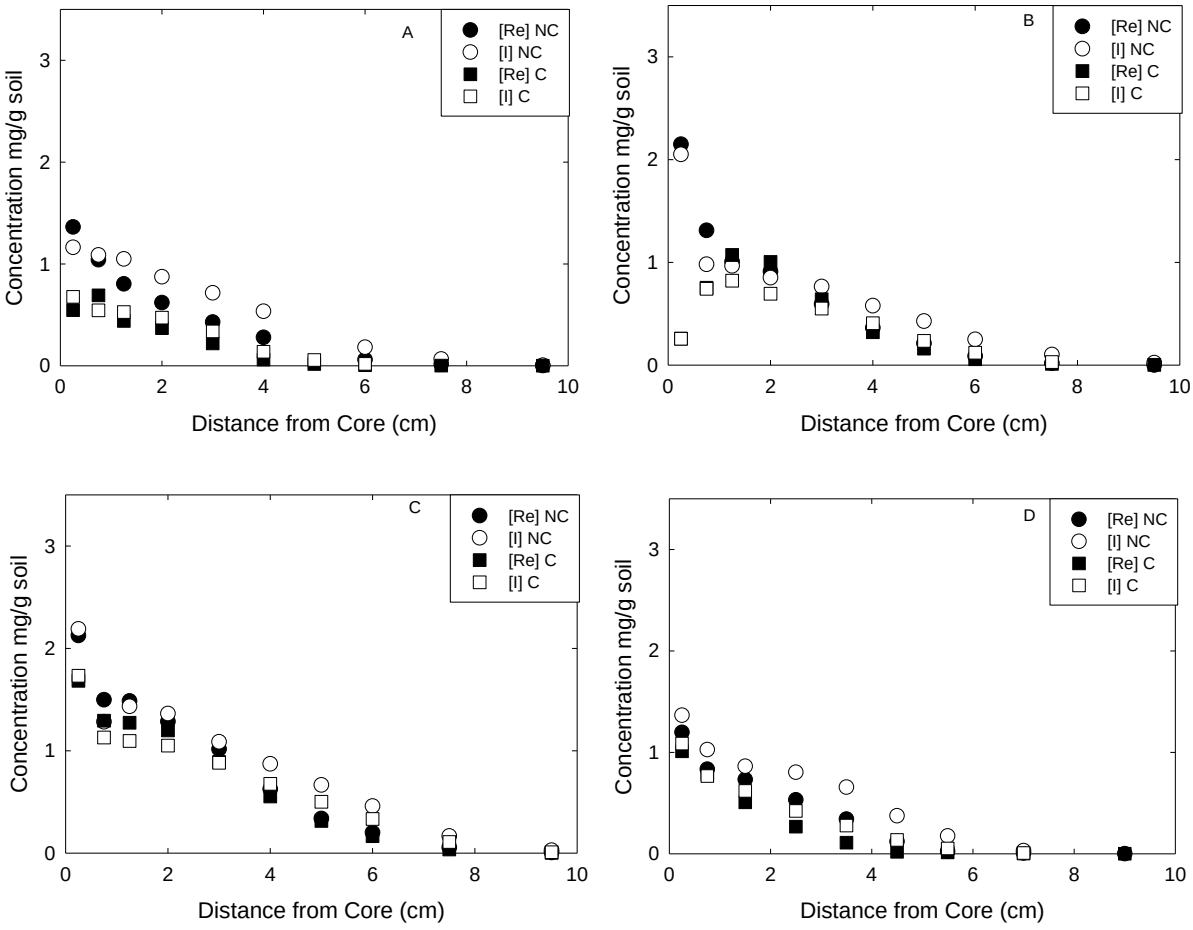

Figure 6.1. Concentration Profiles for Soil Half-Cell I and Re Profiles
A) 4% moisture with 0% Fe B) 4% moisture with 4% Fe
C) 4% moisture with 8% Fe, D) 4% moisture with 12% Fe

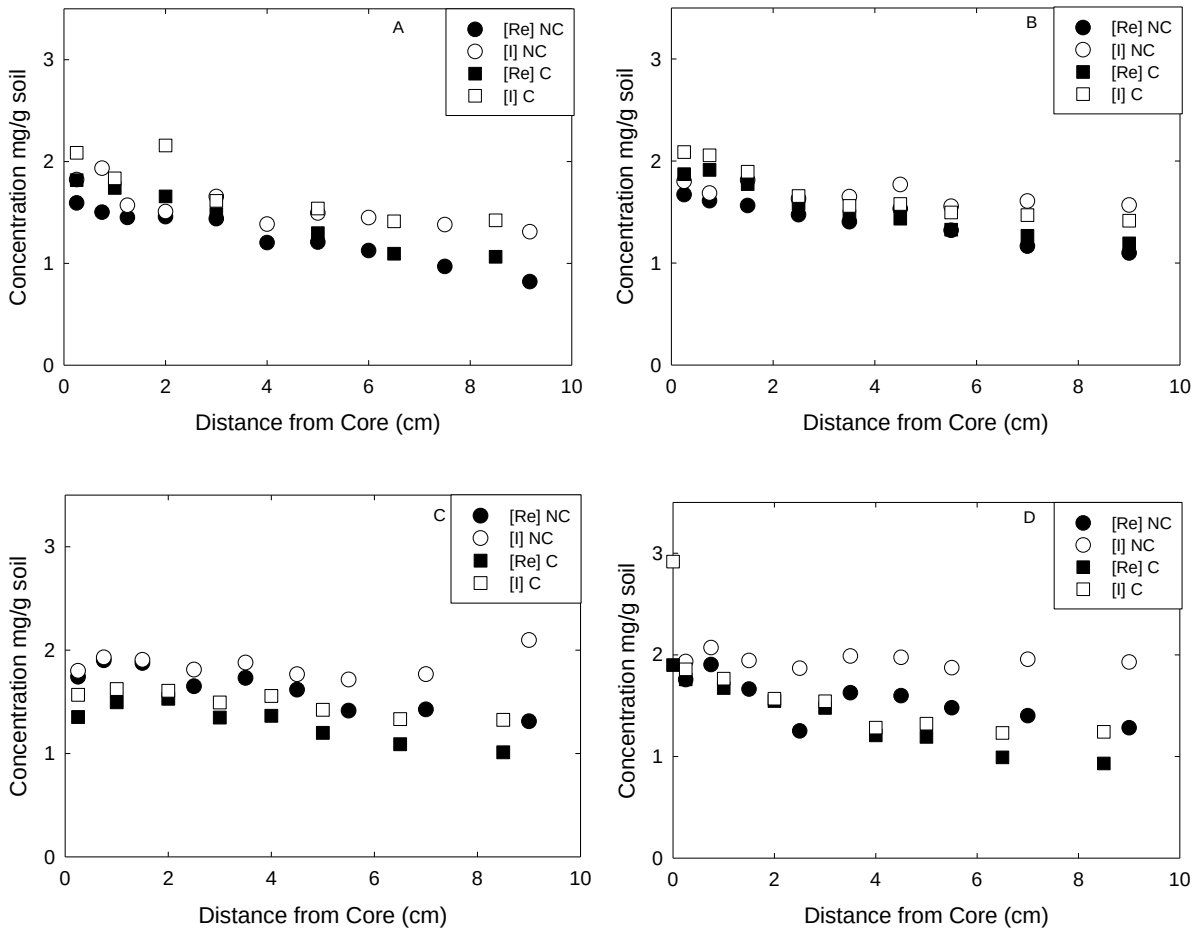

Figure 6.2. Concentration Profiles for Soil Half-Cell I and Re Profiles
A) 7% moisture with 0% Fe, B) 7% moisture with 4% Fe
C) 7% moisture with 8% Fe, D) 7% moisture with 12% Fe

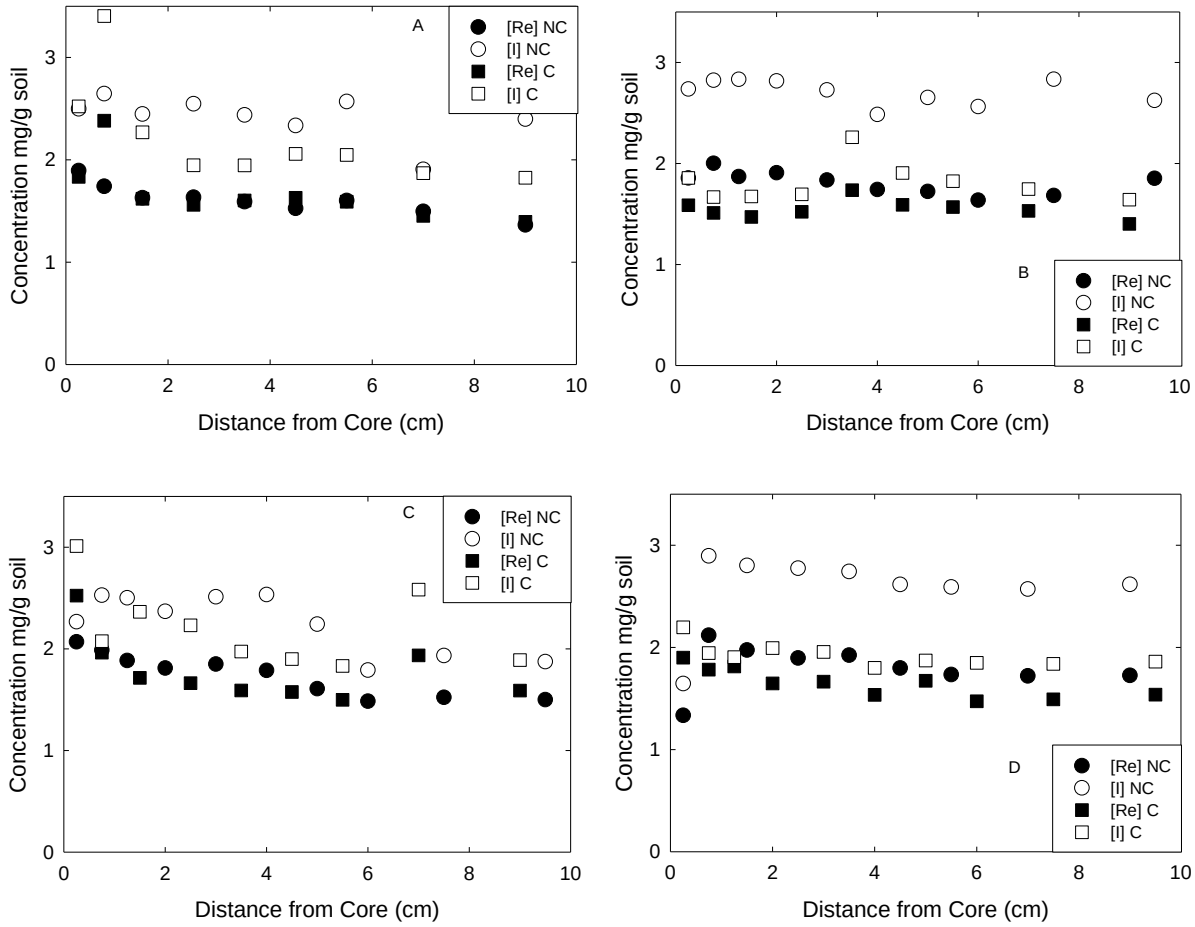

Figure 6.3. Profiles for Soil Half-Cell I and Re Profiles
A) 15% moisture with 0% Fe, B) 15% moisture with 4% Fe
C) 15% moisture with 8% Fe, D) 15% moisture with 12% Fe

Table 6.2. Concentration Profile for Re and I Soil Half-Cells

Distance From Core, cm	Re, mg/g	I, mg/g	Distance From Core, cm	Re, mg/g	I, mg/g	Distance From Core, cm	Re, mg/g	I, mg/g	Distance From Core, cm	Re, mg/g	I, mg/g
4% Soil--NC 0% Iron			4% Soil--NC 4% Iron			4% Soil--C 0% Iron			4% Soil--C-4% Iron		
9.50	0.001	0.003	9.50	0.001	0.02	9.50	0.001	ND	9.50	0.003	ND
7.50	0.02	0.07	7.50	0.02	0.10	7.50	0.001	ND	7.50	0.01	0.03
6.00	0.06	0.18	6.00	0.09	0.25	6.00	0.01	0.02	6.00	0.06	0.12
4.00	0.28	0.53	5.00	0.21	0.43	5.00	0.02	0.06	5.00	0.16	0.24
3.00	0.43	0.72	4.00	0.36	0.58	4.00	0.06	0.14	4.00	0.32	0.41
2.00	0.62	0.87	3.00	0.59	0.76	3.00	0.22	0.34	3.00	0.64	0.55
1.25	0.80	1.05	2.00	0.91	0.85	2.00	0.37	0.47	2.00	1.00	0.69
0.75	1.04	1.09	1.25	1.01	0.97	1.25	0.44	0.53	1.25	1.07	0.82
0.25	1.36	1.16	0.75	1.31	0.98	0.75	0.69	0.54	0.75	0.75	0.74
			0.25	2.15	2.05	0.25	0.55	0.68	0.25	0.26	0.26
4% Soil--NC 8% Iron			4% Soil--NC 12% Iron			4% Soil--C 8% Iron			4% Soil--C-12% Iron		
9.50	0.01	0.03	9.00	0.001	ND	9.50	0.002	0.01	9.00	0.001	ND
7.50	0.05	0.17	7.00	0.01	0.03	7.50	0.04	0.11	7.00	0.002	0.01
6.00	0.20	0.46	5.50	0.02	0.18	6.00	0.17	0.33	5.50	0.013	0.05
5.00	0.34	0.67	4.50	0.12	0.37	5.00	0.31	0.50	4.50	0.02	0.14
4.00	0.62	0.87	3.50	0.34	0.66	4.00	0.55	0.68	3.50	0.11	0.28
3.00	1.02	1.09	2.50	0.53	0.80	3.00	0.89	0.88	2.50	0.27	0.42
2.00	1.28	1.36	1.50	0.73	0.86	2.00	1.20	1.05	1.50	0.51	0.62
1.25	1.49	1.43	0.75	0.83	1.03	1.25	1.27	1.10	0.75	0.78	0.77
0.75	1.50	1.28	0.25	1.20	1.37	0.75	1.29	1.13	0.25	1.01	1.09
0.25	2.13	2.19				0.25	1.68	1.73			

Table 6.2. (contd)

Distance From Core, cm	Re, mg/g	I, mg/g	Distance From Core, cm	Re, mg/g	I, mg/g	Distance From Core, cm	Re, mg/g	I, mg/g	Distance From Core, cm	Re, mg/g	I, mg/g
7% Soil--NC 0% Iron			7% Soil--NC 4% Iron			7% Soil--C 0% Iron			7% Soil--C-4% Iron		
9.18	0.82	1.31	9.00	1.10	1.57	8.50	1.06	1.42	9.00	1.19	1.41
7.50	0.97	1.38	7.00	1.16	1.61	6.50	1.09	1.41	7.00	1.27	1.47
6.00	1.12	1.45	5.50	1.32	1.56	5.00	1.30	1.54	5.50	1.33	1.50
5.00	1.21	1.49	4.50	1.53	1.77	4.00	0.13	0.34	4.50	1.43	1.58
4.00	1.20	1.38	3.50	1.40	1.65	3.00	1.48	1.61	3.50	1.46	1.56
3.00	1.44	1.66	2.50	1.47	1.63	2.00	1.66	2.16	2.50	1.58	1.66
2.00	1.46	1.51	1.50	1.56	1.81	1.00	1.74	1.83	1.50	1.77	1.89
1.25	1.45	1.57	0.75	1.61	1.68	0.25	1.82	2.09	0.75	1.91	2.06
0.75	1.50	1.93	0.25	1.67	1.80				0.25	1.87	2.09
0.25	1.59	1.82									
7% Soil--NC 8% Iron			7% Soil--NC 12% Iron			7% Soil--C 8% Iron			7% Soil--C-12% Iron		
9.00	1.31	2.10	9.00	1.28	1.93	8.50	1.01	1.33	8.50	0.93	1.24
7.00	1.43	1.77	7.00	1.40	1.96	6.50	1.09	1.33	6.50	0.99	1.23
5.50	1.41	1.71	5.50	1.48	1.87	5.00	1.20	1.42	5.00	1.19	1.32
4.50	1.62	1.77	4.50	1.60	1.97	4.00	1.36	1.56	4.00	1.21	1.28
3.50	1.73	1.88	3.50	1.63	1.99	3.00	1.35	1.49	3.00	1.48	1.54
2.50	1.65	1.81	2.50	1.25	1.87	2.00	1.53	1.61	2.00	1.55	1.57
1.50	1.87	1.90	1.50	1.66	1.94	1.00	1.50	1.62	1.00	1.67	1.77
0.75	1.90	1.93	0.75	1.90	2.07	0.25	1.35	1.57	0.25	1.76	1.86
0.25	1.74	1.80	0.25	1.76	1.93						

Table 6.2. (contd)

Distance From Core, cm	Re, mg/g	I, mg/g	Distance From Core, cm	Re, mg/g	I, mg/g	Distance From Core, cm	Re, mg/g	I, mg/g	Distance From Core, cm	Re, mg/g	I, mg/g
15% Soil--NC 0% Iron			15% Soil--NC 4% Iron			15% Soil--C 0% Iron			15% Soil--C-4% Iron		
9.00	1.36	2.40	9.50	1.85	2.62	9.00	1.39	1.82	9.00	1.40	1.64
7.00	1.50	1.91	7.50	1.68	2.83	7.00	1.45	1.87	7.00	1.53	1.75
5.50	1.60	2.57	6.00	1.64	2.56	5.50	1.59	2.05	5.50	1.57	1.82
4.50	1.53	2.33	5.00	1.72	2.65	4.50	1.63	2.06	4.50	1.59	1.91
3.50	1.59	2.44	4.00	1.74	2.48	3.50	1.60	1.95	3.50	1.74	2.26
2.50	1.63	2.55	3.00	1.84	2.73	2.50	1.56	1.95	2.50	1.52	1.69
1.50	1.63	2.45	2.00	1.91	2.82	1.50	1.62	2.27	1.50	1.47	1.67
0.75	1.74	2.65	1.25	1.87	2.83	0.75	2.38	3.40	0.75	1.51	1.67
0.25	1.89	2.50	0.75	2.00	2.82	0.25	1.83	2.52	0.25	1.59	1.86
			0.25	1.86	2.74						
15% Soil--NC 8% Iron			15% Soil--NC 12% Iron			15% Soil--C 8% Iron			15% Soil--C-12% Iron		
9.50	1.50	1.87	9.00	1.73	2.62	9.00	1.59	1.89	9.50	1.54	1.86
7.50	1.52	1.93	7.00	1.72	2.57	7.00	1.94	2.58	7.50	1.49	1.84
6.00	1.48	1.79	5.50	1.73	2.59	5.50	1.50	1.83	6.00	1.47	1.85
5.00	1.61	2.24	4.50	1.80	2.62	4.50	1.58	1.90	5.00	1.67	1.87
4.00	1.79	2.53	3.50	1.92	2.74	3.50	1.59	1.97	4.00	1.54	1.80
3.00	1.85	2.51	2.50	1.90	2.77	2.50	1.66	2.23	3.00	1.66	1.96
2.00	1.81	2.37	1.50	1.97	2.80	1.50	1.71	2.36	2.00	1.65	1.99
1.25	1.88	2.50	0.75	2.12	2.90	0.75	1.96	2.08	1.25	1.81	1.90
0.75	1.99	2.53	0.25	1.33	1.65	0.25	2.52	3.01	0.75	1.78	1.94
0.25	2.07	2.27							0.25	1.90	2.20

The diffusion profiles of Re and I in spiked concrete half-cells are shown in Figures 5.4 through 5.6. One distinctive feature of these profiles is the apparent bidirectional nature of ion diffusion in the concrete cores. The reason for such anomaly was apparent at the end of the experiment when the half-cells were dismantled for sampling. During vertical storage of these half-cells, some of the soils from the soil half-cells at the top had worked down the gap between the concrete half-cells and the surrounding plastic tube. Therefore, the soils contacting both top and bottom of the concrete half- cells inadvertently seemed to have set up bidirectional diffusion in Re and I spiked half-cells.

Except very near the interfaces, no distinctive concentration gradients were observed in any of the soil half-cells. Therefore, on average, the relatively constant concentrations throughout the soil half-cells reflected the spike concentrations of I and Tc, respectively.

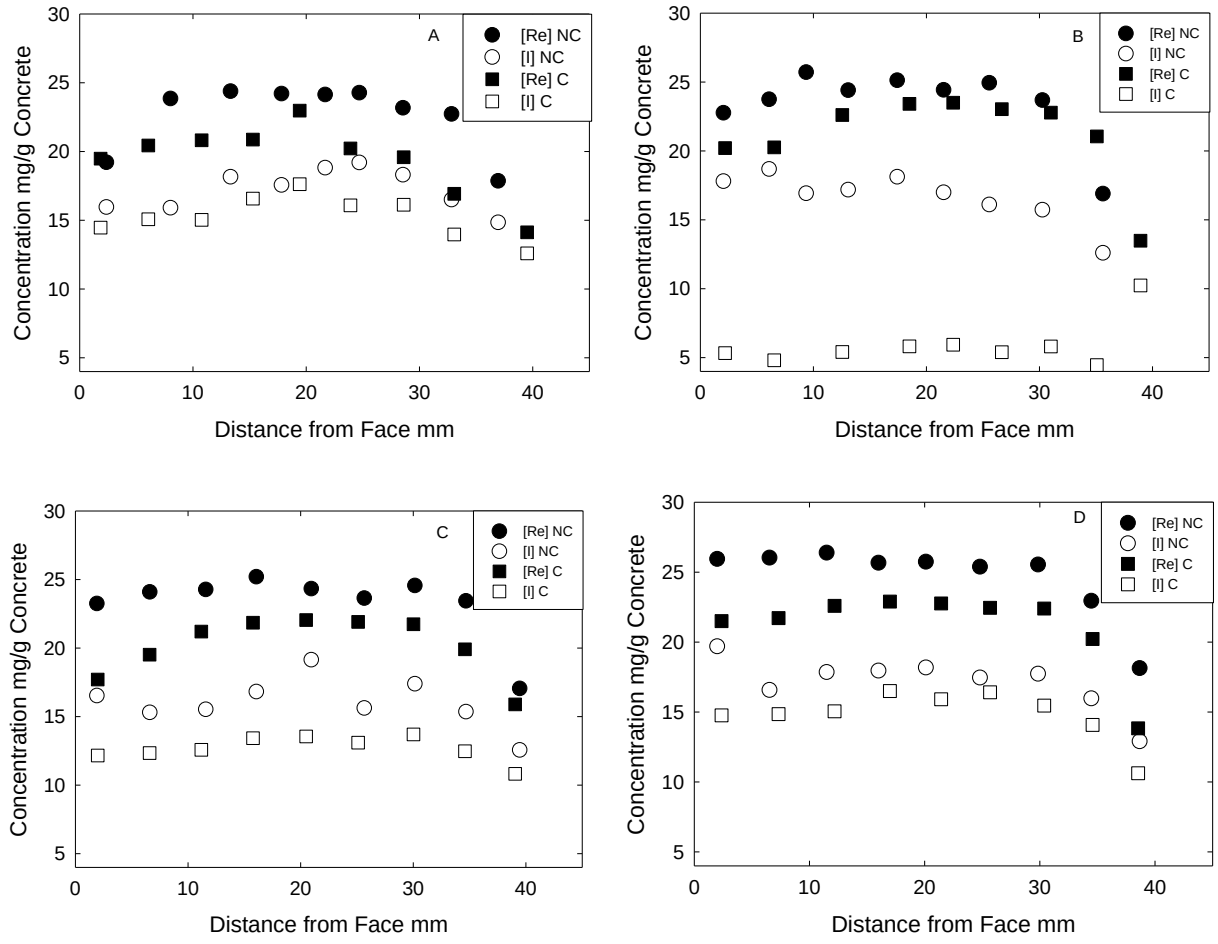

Figure 6.4. I and Re Concrete Half-Cell Concentration Profile
A) 4% soil moisture and 0% Fe, B) 4% soil moisture and 4% Fe,
C) 4% soil moisture and 8% Fe, D) 4% moisture and 12% Fe

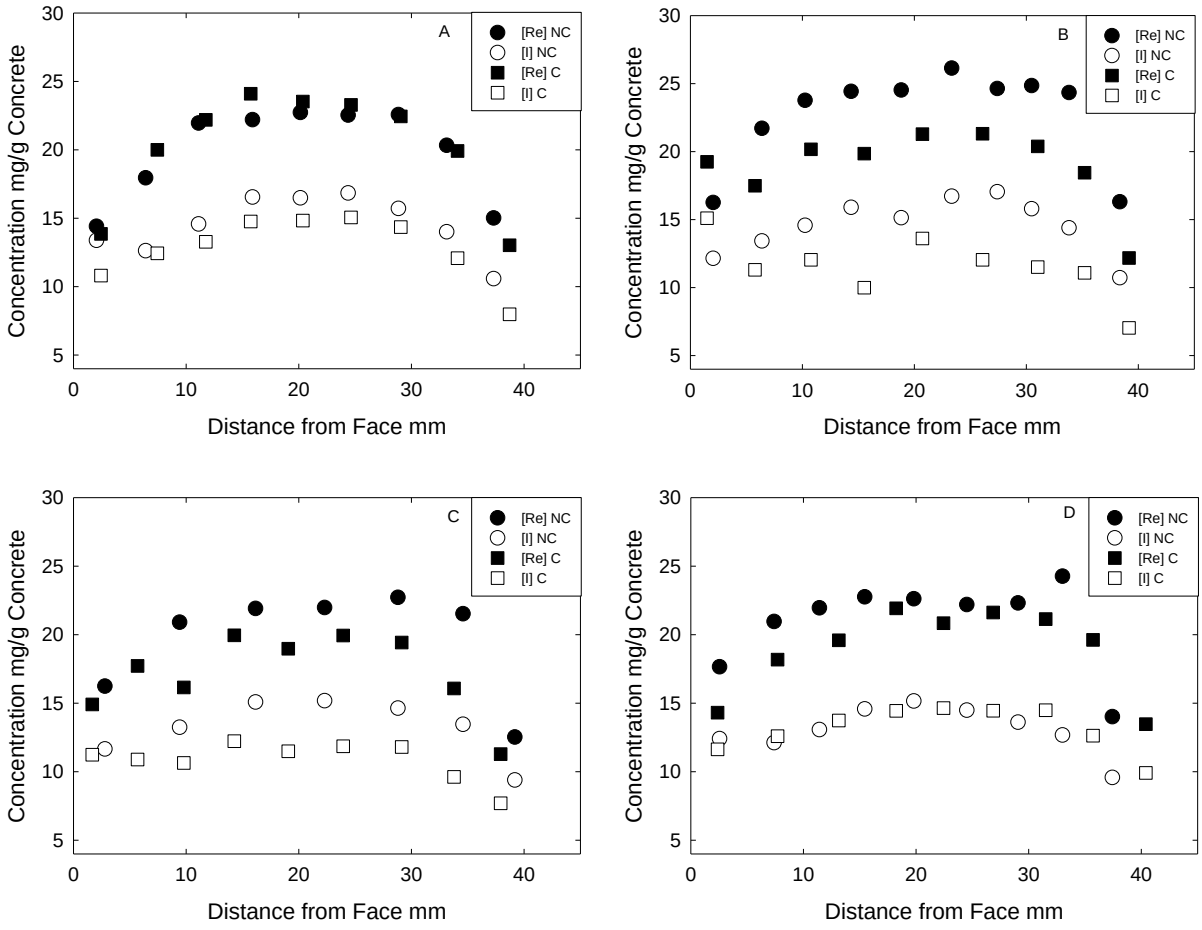

Figure 6.5. I and Re Concrete Half-Cell Concentration Profile
A) 7% soil moisture and 0% Fe, B) 7% soil moisture and 4% Fe,
C) 7% soil moisture and 8% Fe, D) 7% moisture and 12% Fe

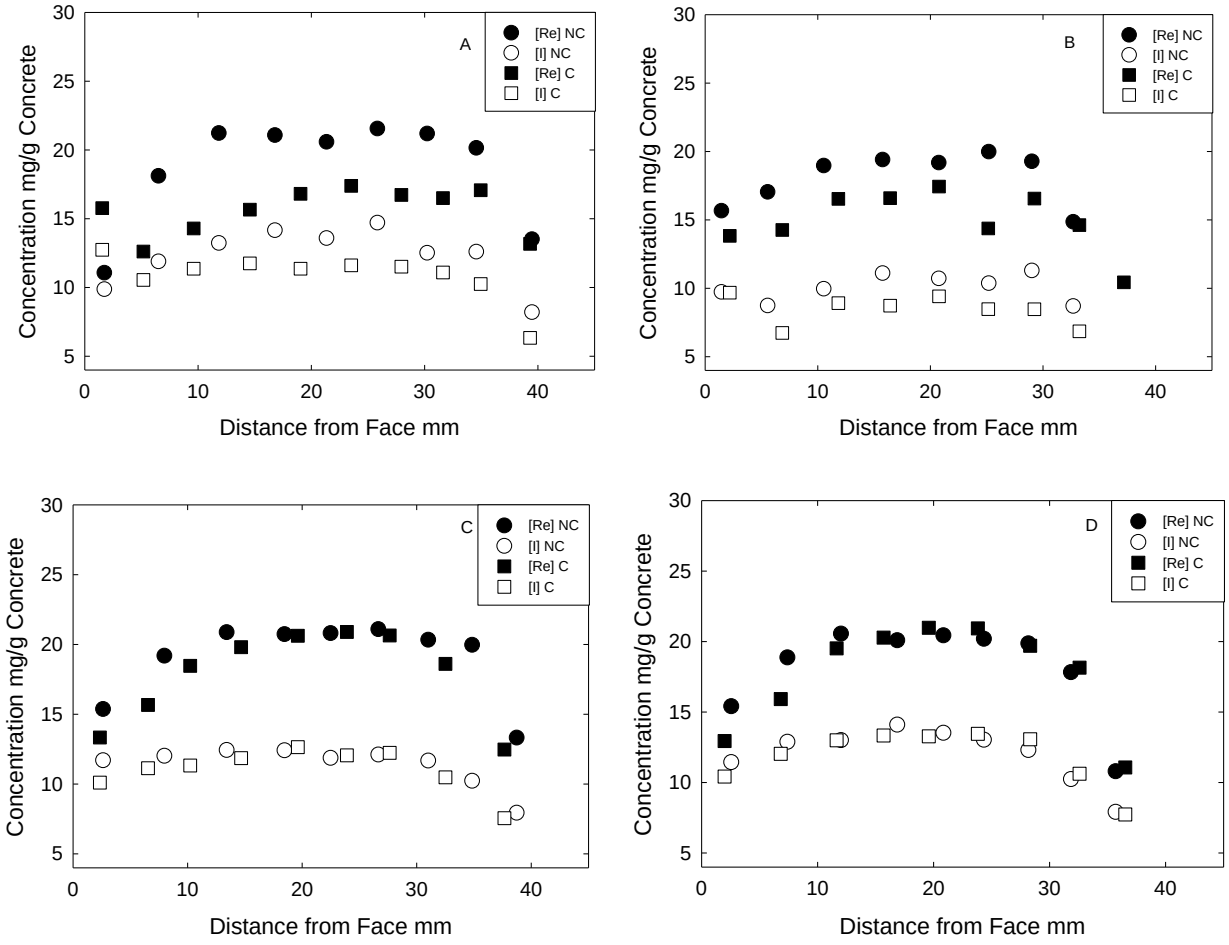

Figure 6.6. I and Re Concrete Half-Cell Concentration Profile
A) 15% soil moisture and 0% Fe, B) 15% soil moisture and 4% Fe,
C) 15% soil moisture and 8% Fe, D) 15% moisture and 12% Fe

Table 6.3. I and Re Concrete Half-Cell Concentration Profile

Center of slice to face, mm	I, mg/g	Re, mg/g	Center of slice to face, mm	I, mg/g	Re, mg/g	Center of slice to face, mm	I, mg/g	Re, mg/g	Center of slice to face, mm	I, mg/g	Re, mg/g
4% Soil--NC 0% Iron			4% Soil--NC 4% Iron			4% Soil--C 0% Iron			4% Soil--C-4% Iron		
2.37	15.96	19.21	2.05	17.80	22.76	1.85	14.46	19.48	2.19	5.32	20.21
8.03	15.90	23.84	6.09	18.68	23.74	6.06	15.07	20.44	6.54	4.81	20.26
13.32	18.15	24.38	9.37	16.92	25.71	10.77	15.03	20.82	12.56	5.41	22.61
17.83	17.56	24.20	13.08	17.18	24.41	15.30	16.57	20.87	18.50	5.81	23.42
21.68	18.81	24.13	17.42	18.12	25.12	19.43	17.62	22.97	22.37	5.94	23.50
24.70	19.20	24.27	21.52	16.99	24.43	23.91	16.08	20.22	26.67	5.39	23.03
28.55	18.30	23.17	25.57	16.10	24.94	28.61	16.13	19.58	31.01	5.81	22.77
32.84	16.50	22.72	30.26	15.73	23.68	33.07	13.96	16.92	35.08	4.45	21.05
36.95	14.84	17.86	35.62	12.60	16.89	39.51	12.59	14.12	38.94	10.23	13.48
4% Soil--NC 8% Iron			4% Soil--NC 12% Iron			4% Soil--C 8% Iron			4% Soil--C-12% Iron		
1.92	16.53	23.24	1.99	19.69	25.94	1.98	12.16	17.70	2.38	14.76	21.50
6.61	15.30	24.09	6.54	16.57	26.03	6.60	12.33	19.51	7.33	14.85	21.71
11.58	15.52	24.27	11.50	17.85	26.39	11.18	12.58	21.20	12.19	15.05	22.59
16.07	16.82	25.20	16.00	17.95	25.66	15.77	13.42	21.85	16.99	16.50	22.90
20.95	19.15	24.33	20.12	18.18	25.74	20.49	13.55	22.04	21.43	15.91	22.76
25.66	15.62	23.64	24.81	17.45	25.39	25.11	13.10	21.91	25.69	16.41	22.45
30.15	17.39	24.56	29.85	17.73	25.54	30.02	13.69	21.74	30.38	15.46	22.40
34.68	15.36	23.44	34.47	15.97	22.94	34.60	12.47	19.91	34.59	14.08	20.22
39.46	12.56	17.04	38.67	12.90	18.13	39.05	10.82	15.89	38.54	10.62	13.83

Table 6.3. (contd)

Center of slice to face, mm	I, mg/g	Re, mg/g	Center of slice to face, mm	I, mg/g	Re, mg/g	Center of slice to face, mm	I, mg/g	Re, mg/g	Center of slice to face, mm	I, mg/g	Re, mg/g
7% Soil--NC 0% Iron			7% Soil--NC 4% Iron			7% Soil--C 0% Iron			7% Soil--C-4% Iron		
2.05	13.38	14.40	2.04	12.14	16.25	2.44	10.81	13.85	1.49	15.10	19.25
6.42	12.62	17.95	6.39	13.43	21.71	7.45	12.44	20.00	5.78	11.31	17.48
11.11	14.57	21.95	10.25	14.58	23.76	11.75	13.27	22.19	10.77	12.04	20.17
15.90	16.54	22.19	14.36	15.90	24.43	15.74	14.76	24.10	15.53	9.99	19.85
20.15	16.49	22.72	18.84	15.13	24.52	20.37	14.82	23.53	20.72	13.61	21.29
24.39	16.84	22.53	23.35	16.72	26.13	24.64	15.05	23.28	26.10	12.04	21.31
28.85	15.71	22.57	27.41	17.04	24.63	29.06	14.35	22.44	31.02	11.51	20.39
33.13	14.00	20.33	30.48	15.79	24.85	34.10	12.08	19.92	35.20	11.08	18.45
37.30	10.58	15.01	33.82	14.39	24.33	38.72	7.98	13.02	39.18	7.03	12.18
			38.35	10.72	16.30						
7% Soil--NC 8% Iron			7% Soil--NC 12% Iron			7% Soil--C 8% Iron			7% Soil--C-12% Iron		
2.79	11.65	16.24	2.56	12.40	17.65	1.67	11.24	14.91	2.38	11.63	14.30
9.43	13.24	20.91	7.40	12.11	20.96	5.70	10.89	17.72	7.71	12.59	18.18
16.17	15.08	21.91	11.43	13.06	21.95	9.80	10.63	16.15	13.15	13.74	19.59
22.3	15.18	21.97	15.45	14.58	22.75	14.28	12.23	19.95	18.24	14.44	21.92
28.805	14.64	22.72	19.81	15.15	22.61	19.07	11.49	18.97	22.44	14.64	20.84
34.585	13.46	21.52	24.52	14.49	22.19	23.95	11.85	19.94	26.86	14.45	21.62
39.185	9.39	12.52	29.06	13.61	22.30	29.14	11.81	19.43	31.52	14.49	21.13
			33.01	12.67	24.26	33.78	9.62	16.08	35.72	12.63	19.62
			37.44	9.58	14.01	37.92	7.69	11.28	40.41	9.91	13.47

Table 6.3. (contd)

Center of slice to face, mm	I, mg/g	Re, mg/g	Center of slice to face, mm	I, mg/g	Re, mg/g	Center of slice to face, mm	I, mg/g	Re, mg/g	Center of slice to face, mm	I, mg/g	Re, mg/g
15% Soil--NC 0% Iron			15% Soil--NC 4% Iron			15% Soil--C 0% Iron			15% Soil--C-4% Iron		
1.74	9.87	11.07	1.46	9.73	15.67	1.55	12.74	15.77	2.20	9.68	13.83
6.52	11.89	18.11	5.56	8.74	17.04	5.18	10.55	12.62	6.86	6.74	14.26
11.84	13.23	21.22	10.53	9.96	18.97	9.62	11.37	14.29	11.83	8.91	16.54
16.79	14.16	21.08	15.77	11.11	19.41	14.58	11.75	15.66	16.43	8.73	16.59
21.35	13.58	20.58	20.75	10.72	19.18	19.05	11.36	16.81	20.77	9.41	17.43
25.83	14.71	21.55	25.19	10.37	19.98	23.52	11.61	17.39	25.14	8.48	14.38
30.23	12.52	21.19	29.02	11.30	19.27	27.95	11.51	16.73	29.24	8.47	16.56
34.57	12.60	20.14	32.68	8.70	14.86	31.63	11.09	16.50	33.23	6.86	14.62
39.48	8.20	13.50				34.96	10.25	17.07	37.18	3.88	10.43
						39.31	6.34	13.17			
15% Soil--NC 8% Iron			15% Soil--NC 12% Iron			15% Soil--C 8% Iron			15% Soil--C-12% Iron		
2.63	11.70	15.37	2.56	11.44	15.40	2.34	10.10	13.34	1.99	10.42	12.94
7.98	12.02	19.19	7.40	12.88	18.87	6.55	11.14	15.67	6.83	12.03	15.92
13.41	12.44	20.88	12.02	13.00	20.56	10.23	11.33	18.46	11.65	12.99	19.52
18.46	12.41	20.73	16.87	14.10	20.09	14.67	11.86	19.81	15.69	13.33	20.28
22.49	11.87	20.80	20.85	13.52	20.44	19.62	12.65	20.62	19.59	13.28	20.98
26.66	12.11	21.09	24.35	13.03	20.19	23.91	12.06	20.89	23.82	13.45	20.93
31.01	11.67	20.33	28.18	12.30	19.86	27.65	12.23	20.65	28.33	13.06	19.70
34.85	10.23	19.96	31.85	10.24	17.82	32.52	10.48	18.61	32.59	10.62	18.15
38.74	7.94	13.32	35.70	7.91	10.80	37.66	7.55	12.47	36.53	7.73	11.07

6.1 Probit Analysis

The probit analytical plots for these set of diffusion data are shown in Figure 6.7 through Figure 6.9, and the resulting Re and I diffusion coefficient values are tabulated (Table 6.3). The calculations showed that at 4 % moisture content with no iron present, carbonation reduced the diffusivities of both Re and I in soils roughly in half. Addition of 4% by mass Fe in to uncarbonated concrete did not significantly affect Re and I diffusivities in soil. In carbonated specimens, adding 4% Fe seemed to increase only I diffusivity without significantly affecting Re diffusivity. When the concentrations of Fe in concrete cores were increased to 8%, significantly enhanced diffusivities in soils were observed. For instance, in soils in contact with uncarbonated concrete cores, presence of 8% Fe in concrete increased Re and I diffusivities by ~17% and 36%, respectively. With carbonation, however, the diffusivities of both Re and I more than doubled as compared to carbonated specimen s with no Fe. Similarly, increasing the Fe content to 12% by mass in both uncarbonated and carbonated concrete increased Re diffusivities soils by about a third as compared to soils contacting cores with no added Fe. In soils contacting similarly treated concrete cores, the I diffusivities did not change significantly (carbonation) or decreased by ~20% (no carbonation).

In soil cores with higher moisture content (7%) and in contact with carbonated concrete cores containing no iron, the diffusivity of Re was ~20% lower than in soils in contact with uncarbonated concrete cores. Addition of 4% Fe by mass to carbonated concrete cores increased Re and I soil diffusivities by ~1.5 and ~3 times as compared to diffusivities in soil cores contacting concrete half-cell with no Fe content. Rhenium diffusivity in soil core in contact with uncarbonated concrete half-cell with 12% Fe was about an order of magnitude lower than in soil core in contact with similar concrete half-cell containing no Fe. In soil cores (7% moisture content) contacting Fe-free concrete with and without carbonation, the Re and I diffusivities were more than an order of magnitude higher than in soils containing 4% moisture content.

At the end of the experiment lasting more than a year, Re and I diffusion in soil cores with 15% moisture content had proceeded to the degree that no distinct concentration gradients were present. Therefore, diffusivity values could not be ascertained.

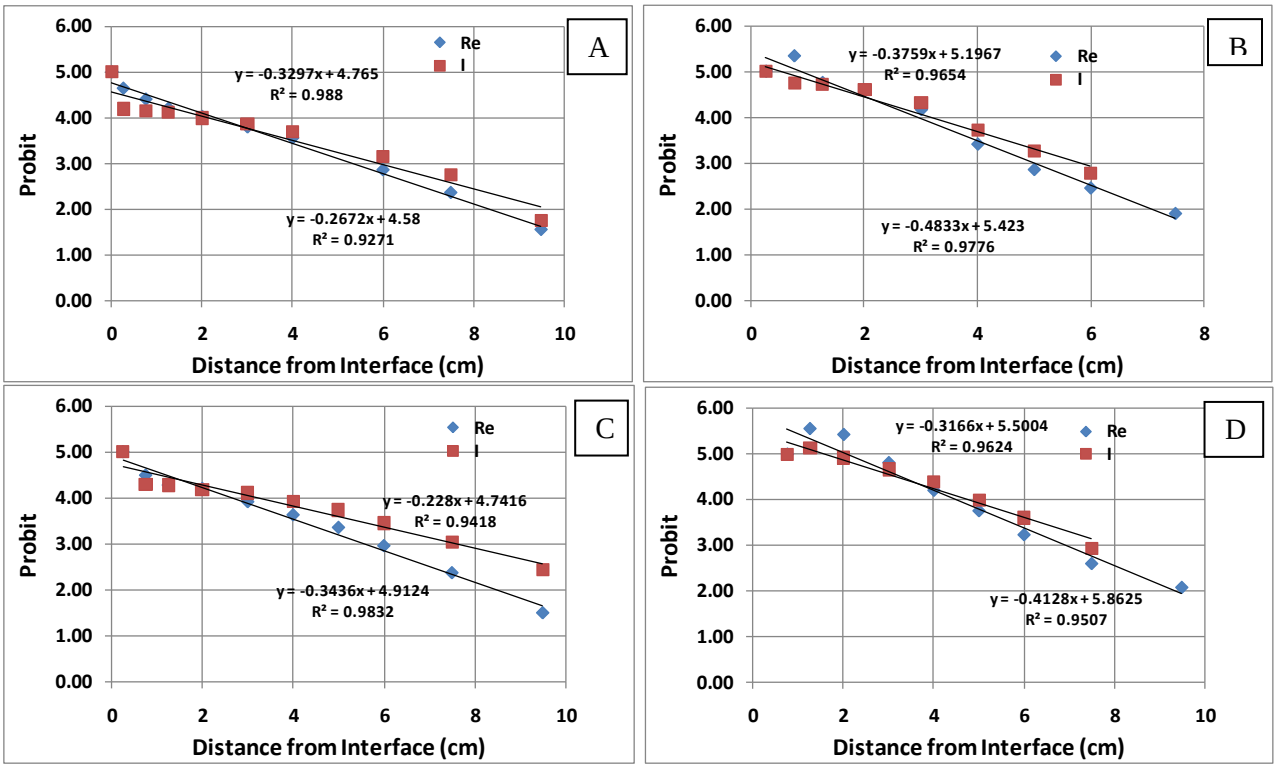

Figure 6.7. Probit Analysis for FY 2008 Re and I Cores
A) C-08-5-0-501, B) C-08-5-0-504, C) C-08-5-4-526, D) C-08-5-4-530

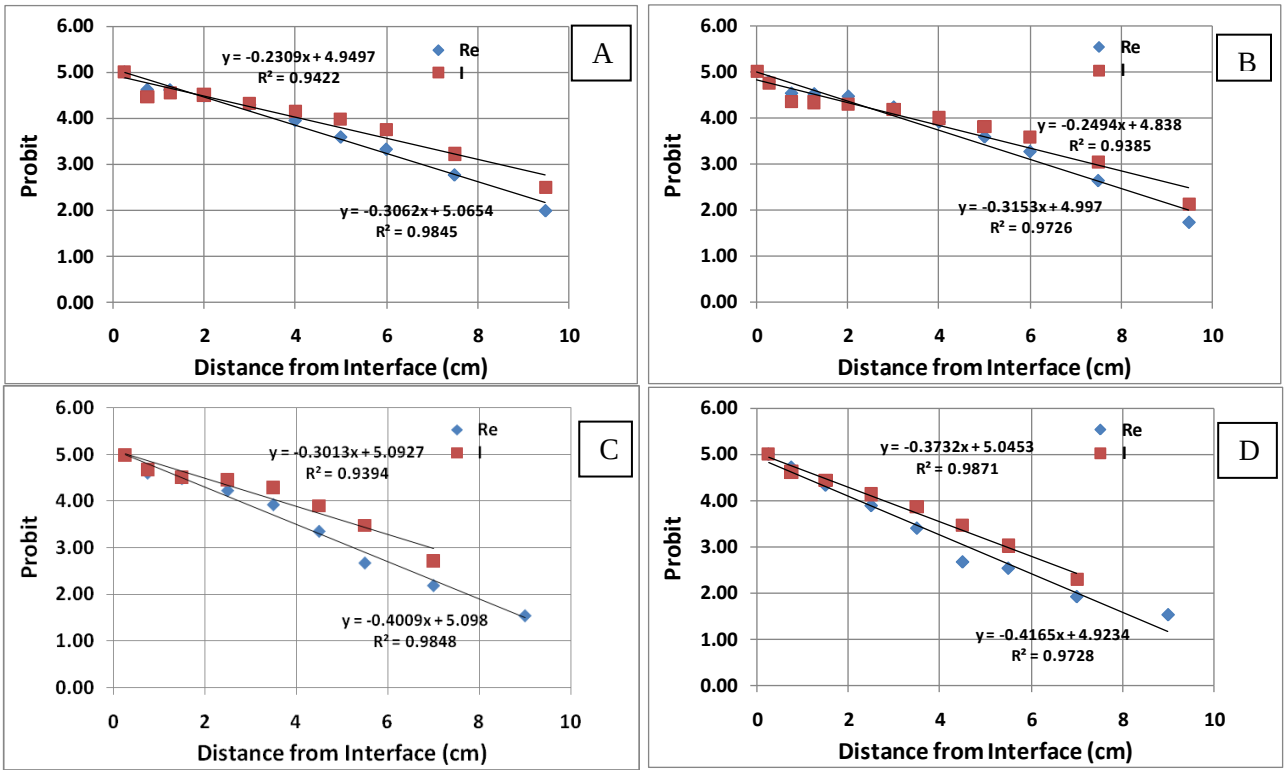

Figure 6.8. Probit Analysis for FY 2008 Re and I Cores
A) C-08-5-8-552, B) C-08-5-8-555, C) C-08-5-12-576, D) C-08-5-12-580

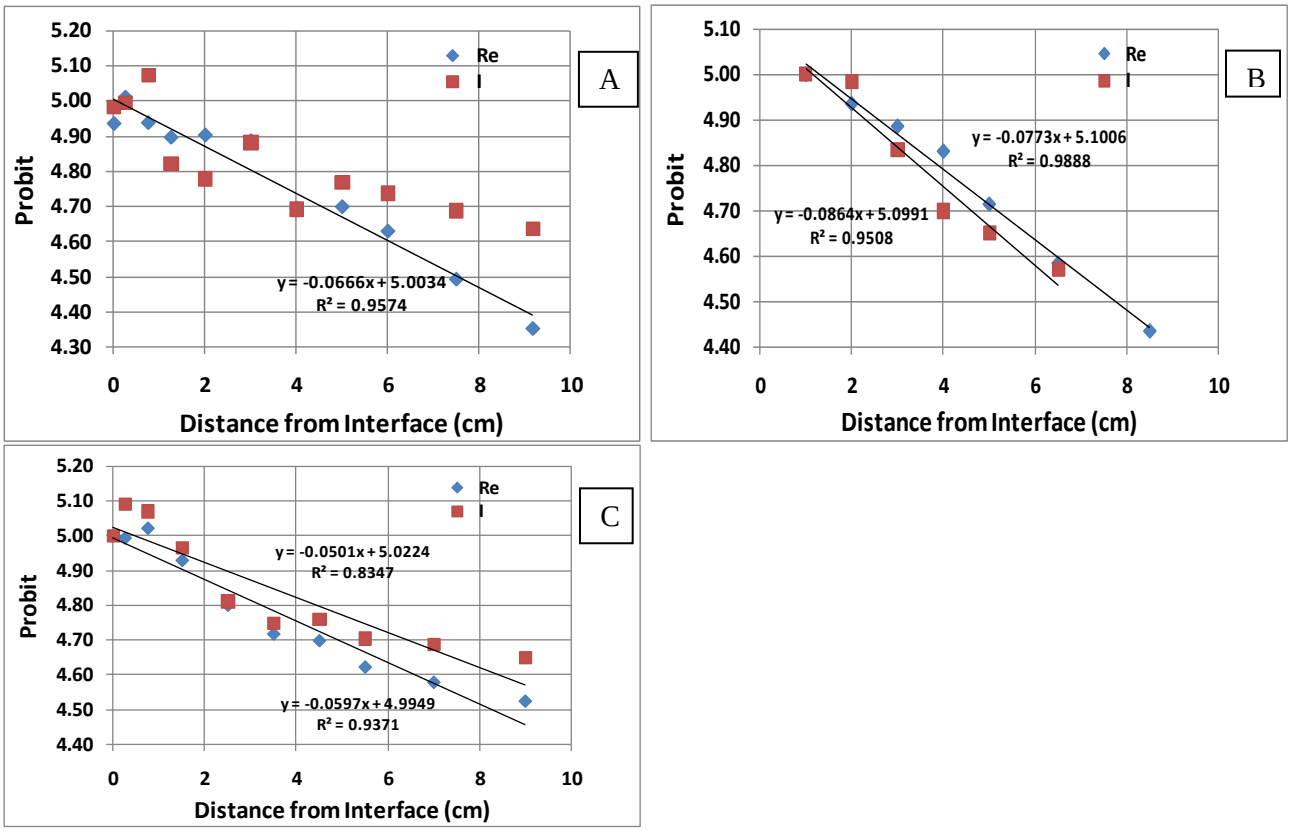

Figure 6.9. Probit Analysis for FY 2008 Re and I Cores
A) C-08-5-0-502, B) C-08-5-0-505, C) C-08-5-4-531

Table 6.4. Diffusivity Analysis FY 2009 Re and I Cores

Core ID	MC (wt %)	Carbonation	Fe (wt %)	Re Diffusivity (cm^2/s)	I Diffusivity (cm^2/s)
C-08-5-0-501	4	N	0	9.4×10^{-09}	1.4×10^{-08}
C-08-5-0-502	7	N	0	4.0×10^{-07}	NA
C-08-5-0-503	15	N	0	NA	NA
C-08-5-0-504	4	Y	0	4.4×10^{-09}	7.2×10^{-09}
C-08-5-0-505	7	Y	0	3.3×10^{-07}	2.4×10^{-07}
C-08-5-0-507	15	Y	0	NA	NA
C-08-5-4-526	4	N	4	8.7×10^{-09}	2.0×10^{-08}
C-08-5-4-527	7	N	4	NA	NA
C-08-5-4-528	15	N	4	NA	NA
C-08-5-4-530	4	Y	4	6.0×10^{-09}	1.0×10^{-08}
C-08-5-4-531	7	Y	4	5.0×10^{-07}	7.1×10^{-07}
C-08-5-4-532	15	Y	4	NA	NA
C-08-5-8-552	4	N	8	1.1×10^{-08}	1.9×10^{-08}
C-08-5-8-553	7	N	8	1.0×10^{-08}	1.6×10^{-08}
C-08-5-8-554	15	N	8	NA	NA
C-08-5-8-555	4	Y	8	1.0×10^{-08}	1.6×10^{-08}
C-08-5-8-556	7	Y	8	NA	NA
C-08-5-8-557	15	Y	8	NA	NA
C-08-5-12-576	4	N	12	6.4×10^{-09}	1.1×10^{-08}
C-08-5-12-577	7	N	12	NA	NA
C-08-5-12-578	15	N	12	NA	NA
C-08-5-12-580	4	Y	12	5.9×10^{-09}	7.3×10^{-09}
C-08-5-12-581	7	Y	12	NA	NA
C-08-5-12-582	15	Y	12	NA	NA

The summary observations from these tests are:

- Carbonation of concrete containing no Fe decreases Re and I diffusivity in soils at both 4% and 7% moisture content.
- Generally, Fe additions to untreated and carbonated concrete half-cells enhances Re and I diffusivities in soils irrespective of soil moisture content.
- Rhenium and I diffusivities in soil cores (7% moisture content) contacting Fe-free concrete with and without carbonation were more than an order of magnitude higher than in soils with 4% moisture content.

7.0 Moisture Gradient within Concrete-Soil Half-Cell Tests

A set of concrete-soil half-cell experiments were initiated during FY 2008. The preparation method, previously discussed, is found in section 2.1. The characteristics of the specimens used are listed in Table 7.1. In FY 2009, the soil half-cell was sectioned. The moisture content throughout the sediment half-cell profile was determined by sectioning the soil half-cell as described in section 2.3. The sectioned soil samples were weighed, placed in a 105 ºC oven for 24 hours, and reweighed. The difference between initial and final weight was assumed to be water weight.

Table 7.1. Characteristics of Cement Specimens Used in Fractured Concrete-Soil Half-Cell Tests

Core ID	Length (cm)	Diameter (cm)	r^2	Surface Area (cm^2)	Volume (cm^3)	Weight (g)	Density (g/cm^3)	Initial Moisture Content (%)
C-08-6-0-302	4.222	4.322	4.670	86.668	61.941	135.997	2.20	4
C-08-6-0-305	4.170	4.329	4.685	86.149	61.376	135.730	2.21	7
C-08-6-0-314	4.033	4.327	4.681	84.233	59.305	130.768	2.21	15

The resulting moisture profiles for the three soil half-cells are shown in Table 7.2. These data indicated there was no significant moisture movement within each core and the moisture content variations in all soil cores were similar. The average moisture content values for soil cores 302, 305, and 314 were 1.0% ± 0.3%, 4.0% ± 0.4% and 10.5% ± 1.5%, respectively. These measured moisture contents were lower than the target values of 4%, 7%, and 15%, respectively and these differences to some extent are attributable to the loss of moisture from the samples following dismantling of the cores. However, these results confirmed that under isothermal test conditions, there would be no significant moisture movement and redistribution within soil cores during the duration of the half-cell diffusion tests.

Table 7.2. Moisture Content Depth Profile

4% Core		7% Core		15% Core	
Distance from Core (cm)	Moisture Content (%)	Distance from Core (cm)	Moisture Content (%)	Distance from Core (cm)	Moisture Content (%)
9.5	1.67	10.5	3.23	10	9.26
8	0.93	9.5	4.29	9	9.93
7	1.12	8.5	3.96	8	10.64
6	0.73	7.5	3.59	7	10.65
5	1.23	6.5	3.41	6	14.64
4	0.89	5.5	3.80	5	6.85
3	1.07	4.5	3.99	4	10.13
2	0.55	3.5	4.23	3	10.21
1	0.80	2.5	0.70	2	11.50
0.25	1.15	1.5	4.37	1	11.28
		0.5	4.34	0.25	11.95

8.0 Reactivity of Limited Solubility U(VI)-Bearing Compounds in Concrete

A study was initiated during FY 2004 to better understand the reactivity of limited solubility uranium(VI)-bearing compounds in Portland cement grout specimens. The U(VI) nitrate-spiked specimens were aged for various time spans ranging from 2 weeks to 1 year. Scanning electron microscopy/energy dispersive spectrometer (SEM-EDS) was used to identify the uranium-bearing compounds that formed in the specimens. The uranium phases were identified to be those of soddyite, becquerelite, uranophane, and autunite. A literature search conducted in FY 2004 revealed that reliable thermochemical data are not available for these phases under conditions present in concrete waste forms. In FY 2006, we developed synthetic routes for the precipitation of pure uranium soddyite, becquerelite, and uranophane. In FY 2007 and FY 2008, we conducted solubility tests for these uranium-solid phases by conducting equilibrium solubility measurements under concrete porewater conditions. Preliminary confirmation of secondary phases was conducted using SEM-EDS in FY 2008. Results suggested the formation of 1) a calcium-uranium oxide from the reaction of becquerelite, 2) uranophane group minerals from the reaction of soddyite, and 3) mixed sodium-calcium uranium phosphate secondary phases from the reaction of autunite in simulated Portland cement-equilibrated porewater. In FY 2009, detailed Extended Absorption X-ray Fine Structure (EXAFS) spectroscopic analyses and thermodynamic geochemical modeling of porewater compositions in equilibrium with the uranium phases were completed to further understand the stability and long-term control of uranium provided by concrete waste forms.

8.1 Modeling

Geochemical models MINTEQA2 (Allison et al. 1991) and EQ3NR (Wolery 1992) were applied to element concentrations under steady state conditions to evaluate the aqueous speciation and saturation state of the effluent solutions with respect to key minerals, solids, and aqueous phases. Thermodynamic databases from numerous literature sources were used to update the computer codes (Alwan and Williams 1980, Chen et al. 1999, Finch 1997, Grenthe et al. 1992, Kalmykov and Choppin 2000, Langmuir 1978, Nguyen et al. 1992, O'Hare et al. 1976, Sergeyeva et al. 1972, and Vochten and Haverbeke 1990). It is important to note that because of the complex chemistry of U, there is significant debate within the literature regarding the stoichiometry and the thermodynamic values assigned to aqueous U species and secondary mineral phases. As such, the solubility calculations are based on current knowledge, but may have significant uncertainty associated with them.

Table 8.1. Thermodynamic Geochemical Modeling Results for Simulated Concrete Porefluids in Equilibrium with Uranium Phases Identified as Primary Controls on Uranium Mobility in Concrete Waste Forms

Autunite			
Phase/End-member	Log moles	Aqueous Species	% Total
9:1 BFS/OPC			
Autunite-Ca: $Ca(UO_2)_2(PO4)_2$•10-12(H_2O)	-1.95	$UO_2(HPO_4)_2^{2-}$	99.40
Autunite-Na: $Na_2(UO_2)_2(PO4)_2$•8(H_2O)	-2.80		
Schoepite-JZ: $(UO_2)_8O_2(OH)_{12}$•12(H_2O)	-3.04		
Soddyite: $(UO_2)_2(SiO_4)$•2(H_2O)	-4.64		
OPC/BFS/L			
Autunite-Ca: $Ca(UO_2)_2(PO4)_2$•10-12(H_2O)	-1.85	$UO_2(HPO_4)_2^{2-}$	76.01
Autunite-Na: $Na_2(UO_2)_2(PO4)_2$•8(H_2O)	-2.80	$UO_2(OH)_2$(aq)	10.82
Schoepite-JZ: $(UO_2)_8O_2(OH)_{12}$•12(H_2O)	-4.55	$Ca_2UO_2(CO_3)_3$(aq)	4.28
Soddyite: $(UO_2)_2(SiO_4)$•2(H_2O)	-3.15	$UO_2(CO_3)_2^{2-}$	2.24
		$(UO_2)_2CO_3(OH)_3^-$	4.06
		UO_2CO_3(aq)	1.49
		$UO_2PO_4^-$	0.29
Harwell			
Autunite-Ca: $Ca(UO_2)_2(PO4)_2$•10-12(H_2O)	-1.87	$UO_2(HPO_4)_2^{2-}$	87.98
Schoepite-JZ: $(UO_2)_8O_2(OH)_{12}$•12(H_2O)	-3.19	$UO_2(OH)_2$(aq)	10.43
Soddyite : $(UO_2)_2(SiO_4)$•2(H_2O)	-7.25	$UO_2PO_4^-$	0.31
		$UO_2(OH)$+	0.23
		UO_2OH^+	0.23
OPC/L			
Autunite-Ca: $Ca(UO_2)_2(PO4)_2$•10-12(H_2O)	-2.16	$UO_2(HPO_4)_2^{2-}$	99.50
Autunite-Na: $Na_2(UO_2)_2(PO4)_2$•8(H_2O)	-3.51		
Schoepite-JZ: $(UO_2)_8O_2(OH)_{12}$•12(H_2O)	-2.66		
Soddyite: $(UO_2)_2(SiO_4)$•2(H_2O)	-6.02		
SRPC/L			
Autunite-Ca: $Ca(UO_2)_2(PO4)_2$•10-12(H_2O)	-1.86	$UO_2(HPO_4)^{2-}$	99.29
Schoepite-JZ: $(UO_2)_8O_2(OH)_{12}$•12(H_2O)	-3.14		
Soddyite: $(UO_2)_2(SiO_4)$•2(H_2O)	-5.28		
Soddyite			
Phase/End-member	Log moles	Aqueous Species	% Total
9:1 BFS/OPC			
Boltwoodite-Na $(H_3O)(Na,K)(UO_2)SiO_4$•(H_2O)	-2.65	$UO_2(OH)_3^-$	99.00
$CaUO_4$	-2.19	$UO_2(OH)_2$(aq)	0.83
Haiweeite: $Ca[(UO_2)_2Si_5O_{12}(OH)_2]$•3($H_2O$)	-3.50		

Table 8.1. (contd)

Autunite			
Phase/End-member	Log moles	Aqueous Species	% Total
Soddyite: $(UO_2)_2(SiO_4)•2(H_2O)$	-1.93		
OPC/BFS/L			
$CaUO_4$	-2.81	$UO_2(OH)_3^-$	94.14
Haiweeite: $Ca[(UO_2)_2Si_5O_{12}(OH)_2]•3(H_2O)$	-3.60	$UO_2(OH)_2(aq)$	5.81
Soddyite: $(UO_2)_2(SiO_4)•2(H_2O)$	-1.82		
Harwell			
$CaUO_4$	-2.26	$UO_2(OH)_3^-$	94.00
Haiweeite: $Ca[(UO_2)_2Si_5O_{12}(OH)_2]•3(H_2O)$	-3.27	$UO_2(OH)_2(aq)$	5.96
Soddyite: $(UO_2)_2(SiO_4)•2(H_2O)$	-1.89		
OPC/L			
CaUO4	-1.74	$UO_2(OH)_3^-$	98.29
Haiweeite: $Ca[(UO_2)_2Si_5O_{12}(OH)_2]•3(H_2O)$	-2.76	$UO_2(OH)_4^{2-}$	1.62
Soddyite $(UO_2)_2(SiO_4)•2(H_2O)$	-2.28		
SRPC/L			
CaUO4	-2.22	$UO_2(OH)_3^-$	98.03
Haiweeite $Ca[(UO_2)_2Si_5O_{12}(OH)_2]•3(H_2O)$	-3.34	$UO_2(OH)_2(aq)$	1.89
Soddyite $(UO_2)_2(SiO_4)•2(H_2O)$	-1.88		
Becquerelite			
Phase/End-member	Log moles	Aqueous Species	% Total
9:1 BFS/OPC			
CaUO4	-2.06	$UO_2(OH)_3^-$	97.17
Clarkeite-JZ: $(Na,Ca,Pb)(UO_2)O(OH)•0\text{-}1(H_2O)$	-2.87	$UO_2(OH)_4^{2-}$	2.77
Becquerelite-JZ: $Ca(UO_2)_6O_4(OH)_6•8(H_2O)$	-1.83		
Soddyite: $(UO_2)_2(SiO_4)•2(H_2O)$	-4.64		
OPC/BFS/L			
CaUO4	-2.61	$UO_2(OH)_3^-$	99.07
Becquerelite-JZ: $Ca(UO_2)_6O_4(OH)_6•8(H_2O)$	-1.80		
Soddyite: $(UO_2)_2(SiO_4)•2(H_2O)$	-3.15		
Harwell			
CaUO4	-2.14	$UO_2(OH)_3^-$	97.59
Becquerelite-JZ: $Ca(UO_2)_6O_4(OH)_6•8(H_2O)$	-1.83	$UO_2(OH)_4^{2-}$	2.34
Soddyite: $(UO_2)_2(SiO_4)•2(H_2O)$	-7.33		
OPC/L			
$CaUO_4$	-1.62	$UO_2(OH)_3^-$	93.91
Clarkeite-JZ: $(Na,Ca,Pb)(UO_2)O(OH)•0\text{-}1(H_2O)$	-4.04		
Becquerelite-JZ: $Ca(UO_2)_6O_4(OH)_6•8(H_2O)$	-1.92		
Soddyite $(UO_2)_2(SiO_4)•2(H_2O)$	-6.18		
SRPC/L			

$CaUO_4$	-2.10	$UO_2(OH)_3^-$	97.65
Becquerelite-JZ: $Ca(UO_2)_6O_4(OH)_6•8(H_2O)$	-1.81	$UO_2(OH)_4^{2-}$	2.28
Soddyite: $(UO_2)_2(SiO_4)•2(H_2O)$	-5.28		
Uranophane			
Phase/End-member	Log moles	Aqueous Species	% Total
9:1 BFS/OPC			
Boltwoodite-Na-JZ: $(H_3O)(Na,K)(UO_2)SiO_4•(H_2O)$	-2.65	$UO_2(OH)_3^-$	98.28
$CaUO_4$	-1.73	$UO_2(OH)_4^{2-}$	1.62
Haiweeite: $Ca[(UO_2)_2Si_5O_{12}(OH)_2]•3(H_2O)$	-2.31		
Soddyite: $(UO_2)_2(SiO_4)•2(H_2O)$	-2.86		
OPC/BFS/L			
$CaUO_4$	-1.87	$UO_2(OH)_3^-$	99.18
Haiweeite: $Ca[(UO_2)_2Si_5O_{12}(OH)_2]•3(H_2O)$	-2.32		
Soddyite: $(UO_2)_2(SiO_4)•2(H_2O)$	-2.30		
Harwell			
$CaUO_4$	-1.76	$UO_2(OH)_3^-$	98.44
Haiweeite: $Ca[(UO_2)_2Si_5O_{12}(OH)_2]•3(H_2O)$	-2.31	$UO_2(OH)_4^{2-}$	1.44
Soddyite: $(UO_2)_2(SiO_4)•2(H_2O)$	-2.59		
OPC/L			
$CaUO_4$	-1.49	$UO_2(OH)_3^-$	98.29
		$UO_2(OH)_4^{2-}$	1.62
SRPC/L			
$CaUO_4$	-1.74	$UO_2(OH)_3^-$	98.31
Haiweeite: $Ca[(UO_2)_2Si_5O_{12}(OH)_2]•3(H_2O)$	-2.30	$UO_2(OH)_4^{2-}$	1.59
Soddyite: $(UO_2)_2(SiO_4)•2(H_2O)$	-2.58		

8.2 Discussion and Conclusions

The aqueous concentration of uranium released from all potential U(VI)-bearing solid phases in the simulated Portland cement-equilibrate porewaters ranged from $\log_{10}[U(VI)]_{aq}$ = -5 to -9, suggesting that porewater cations and anions may be influencing the solubility of uranium through complexation (Table 7.1). The significance of porewater cation and anions on the uranium mineral solubility is also suggested by the formation of secondary phases.

Complexation of aqueous uranium can increase the solubility of uranium minerals (Langmuir 1997b; a). Two mechanisms may contribute to the increase in aqueous uranium: 1) a chelating effect, whereby oxygen-containing ligands (i.e., carbonate, phosphate, and hydroxide) bind to uranium in the mineral structure and subsequently release uranium complexes into solution, or 2) release of uranium from the mineral structure is followed by complexation by aqueous ligand. Thereby, the latter would reduce the activity of uranium in solution allowing further release of uranium from the mineral structure. The composition of the porewaters contains numerous ligands that form stable complexes with uranyl in solution and can significantly increase the aqueous concentration of uranium. Uranyl cations will form strong complexes with hydroxide (Cordfunke 1964 and 1969, Grenthe et al. 1992, and Langmuir 1978 and 1997b), carbonate (Clark et al. 1995 and Langmuir 1978), sulfate (Langmuir 1978 and 1997b), silicate (Cordfunke 1964 and1969, Grenthe et al. 1992, and Langmuir 1978 and 1997b), and phosphate (Sandino and Bruno 1992, Langmuir 1978 and 1997b, and Grenthe et al. 1992).

System pH can strongly influence the solubility, hydrolysis, sorption, complexation, and colloid formation of uranium. Hydrolysis reactions are highly sensitive to the activity and concentration of hydrogen ions in solution (Baes et al. 1953, Cordfunke 1969, Langmuir 1978, and Sylva and Davidson 1979). For example, Figure 8.1 is a chart, generated using MINTEQA2, displaying uranium speciation at 25 °C in the absence of all ligands except hydroxide. The plot shows that stepwise monomeric species dominate the distribution of uranium across the pH range.

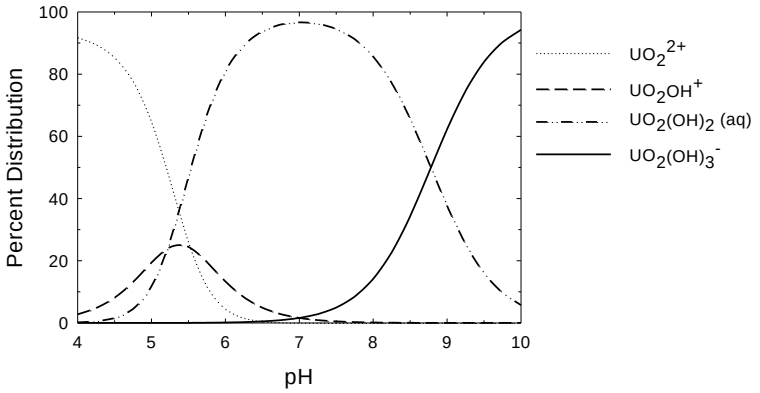

Figure 8.1. Percent Distribution of U^{6+}-H_2O System at 25 ºC, Ionic Strength = 0.1 M, pCO_2 = 0 bar, and $\Sigma U^{6+} = 10^{-6}$ M in the Absence of Complexing Ligands Other than Hydroxide

Figure 8.1 demonstrates the significance of pH and ligand identity on the speciation of uranium. The extent to which carbonate competes for uranium over hydroxyl complexes, especially above pH 6, is evident. Uranyl-carbonate species are significant in the uranium geochemical cycle. They increase the solubility of uranium minerals, facilitate uranium (IV) oxidation, and because these species are anionic in nature, they limit the extent of sorption in oxidized waters, thereby increasing the mobility of uranium (Langmuir 1997b, a).

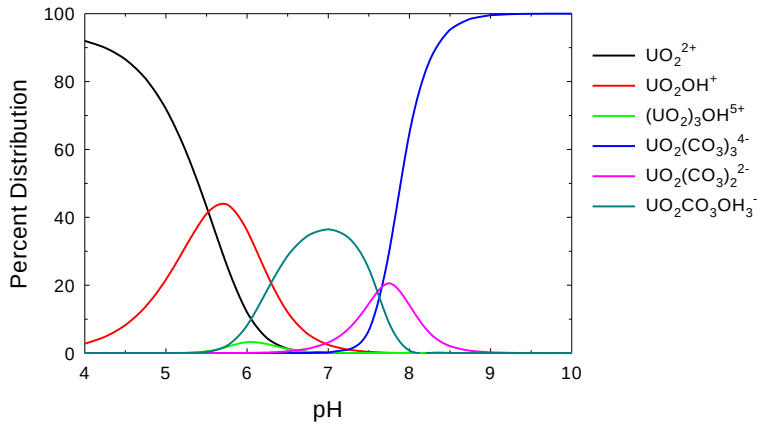

Figure 8.2. Percent Distribution of U^{6+} Species Calculated Using MINTEQA2 at 25 °C, Ionic Strength = 0.1 M, and $pCO_2 = 10^{-3.5}$ bar for $\sum U^{6+} = 10^{-6}$ M

Uranyl-sulfate complexes are important in aqueous environments where pH < 6, the evaporation rate is high, sulfides are being oxidized, and carbonate is absent (Garrels and Christ 1965 and Ondrus et al. 2003). There are few aqueous uranyl-silicate complexes which are moderately insoluble and readily

precipitate to form uranyl-silicate minerals. As such, uranyl-silicate minerals are of relatively low solubility and do not rapidly dissolve upon exposure to fresh water. In the pH range of 6-9, phosphate complexes dominant the system when $[PO_4]/[CO_3] > 0.1$. Uranyl forms more stable complexes with phosphate than with any other ligand (Langmuir 1978). Figure 8.3 illustrates the significance of the ligand species and concentration in determining the dominate uranium species at a given pH value.

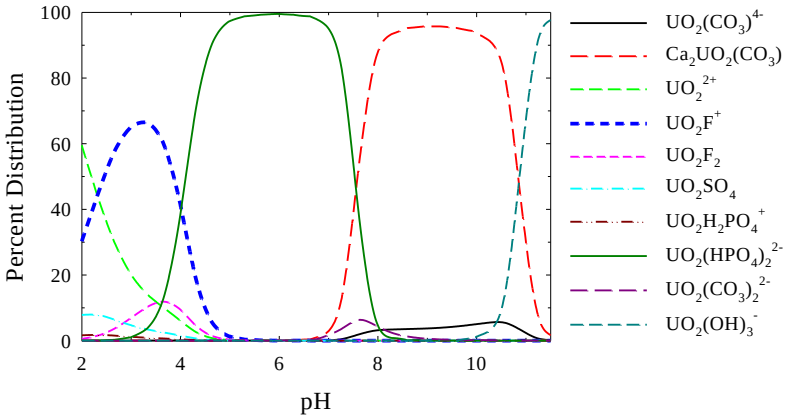

Figure 8.3. Percent Distribution of U^{6+} Aqueous Species Calculated Using MINTEQA2 in Hanford Groundwater Well-699-S3-25

There was no observed effect of carbonate or sulfate within the porewaters on the stability of the uranyl minerals or on the formation of secondary phases. However, there was a clear effect of calcium and silicon in the porewaters on the stability of all uranium minerals, as well as on the formation of secondary phases. Geochemical modeling results support preliminary spectroscopic results which suggested the formation of 1) a calcium-uranium oxide from the reaction of becquerelite, 2) uranophane/becquerelite group minerals from the reaction of soddyite, and 3) mixed sodium-calcium uranium phosphate secondary phases from the reaction of autunite in simulated Portland cement-equilibrated porewater. It is further suggested that 1) the release of uranium from the degradation of uranium oxyhydroxides will be controlled by the formation of secondary uranium oxides; 2) regardless of the replacement of soddyite by uranophane, uranyl-silicate phases will persist within concrete waste forms; and 3) the release of uranium from the degradation of uranium-phosphate phases will be controlled by the formation of secondary uranyl-phosphate phases.

8.3 Extended X-Ray Absorption Fine Structure Spectroscopy

Although SEM-EDS and X-ray diffraction (XRD) provide preliminary information regarding the possible secondary phases that form and may control uranium mobility in concrete porefluids, they provide limited structural and speciation information on phases present at < 5 wt%. Therefore, in order to precisely understand the mechanisms of transformation and identity of uranium phases controlling the long-term mobility of uranium in concrete waste forms, EXAFS analysis was conducted on pristine uranium phases, and the uranium phases reacted with simulated concrete porefluids. Uranium L_{III}-EXAFS measurements of the samples were conducted at room temperature on the Molecular Environmental Sciences Beamline 11-2 (Bargar et al. 2002) at the Stanford Synchrotron Radiation Laboratory (SSRL) using a cryogenically cooled Si (220), $\phi = 0°$, double-crystal monochromator. Fluorescence-yield data were collected using an argon-filled Stern-Heald-type detector (Lytle et al. 1984).

A collimating mirror before the monochromator was used for harmonic rejection, with a cutoff of 19.6 keV. Yttrium metal foil was mounted between two ionization chambers downstream of the sample for energy calibration; the first inflection point in the yttrium K-edge was set to 17038 eV. Background-subtracted k^3-weighted EXAFS data were analyzed using the SixPACK (Webb 2005) interface to IFEFFIT (Newville 2001). Data analysis is currently in progress, the data are being fit as linear combinations of the χ data from k = 3-12, k^3 weighted; results are forthcoming and will be available in a mid-FY 2010 interim progress report.

9.0 Single-Pass Flow-Through Tests on Cementitious Waste Forms

9.1 Characterization of Concrete Coupons

9.1.1 Microwave Digestion

Determination of the composition of the concrete waste form monoliths was determined though microwave digestion using a CEM Microwave Accelerated Reaction System 5 (MARS 5) under EPA method 3052X. The concrete was crushed into a fine powder using a mortar and pestle, and 0.25g of the concrete powder was placed into each reaction vessel, with 9 mL of concentrated HNO_3, 3 mL of concentrated HF, and 2 mL of concentrated HCL. After microwaving, the samples were analyzed with ICP-OES. The results are presented in Table 9.1 listed as the major oxide species.

Table 9.1. Concrete Core Composition (% oxide)

% Oxide (mol)	3-0-331	3-0-336	5-4-529	3-4-358	3-8-413	3-8-414	3-12-431	3-12-438
Sb_2O_3	0.17	0.13	0.18	0.12	0.15	0.19	0.13	0.09
CaO	1.35	1.50	1.43	1.59	1.67	1.58	1.74	3.03
Fe_2O_3	0.63	0.43	1.98	5.89	7.09	5.76	6.09	9.19
P_2O_5	0.18	0.16	0.24	0.19	0.21	0.18	0.21	0.15
K_2O	0.53	0.51	0.59	0.55	0.51	0.38	0.58	0.45
Re_2O_7	0.00	0.00	6.78	0.01	0.01	0.01	0.00	0.00
SiO_2	94.65	95.02	85.23	88.08	87.25	88.65	88.02	84.23
Na_2O	0.77	0.31	1.51	1.20	0.93	0.94	0.80	0.74
SO_3	0.90	1.08	1.07	1.24	1.07	1.38	1.44	1.03
TiO_2	0.37	0.37	0.38	0.43	0.38	0.38	0.42	0.37

9.1.2 Scanning Election Microscopy

Scanning electron microscopy (SEM) was performed using a SEM JEOL 840 equipped with a Robinson 6.0 backscatter detector. The beam conditions were 20 KeV acceleration and a 1 nA beam current. The samples were mounted on an aluminum plate using double-sided tape and were carbon-coated under a vacuum. The carbon coat provides a conductive path for the electrons and helps secure the particles. Images were acquired using GATAN DM software version 3.2, 1996. SEM was used to analyze unreacted and reacted concrete coupons. The SEM images in Figure 9.1 are of unreacted concrete coupons at different magnification. In both pictures, evidence of microcracking is present, which is a common effect with age, weathering, and carbonation of concrete (Wellman et al. 2008b). The SEM images of concrete coupons after a SPFT test are presented in section 9.3.

9.2 Single-Pass Flow-Through Test Methods

Evaluation of the dissolution of concrete waste forms was performed with the single-pass flow-through (SPFT) test method. The SPFT apparatus provides experimental flexibility, allowing each of the kinetic test parameters to be isolated and quantified. Temperature, flow rate, solution composition, and sample mass and size can be manipulated to assure accurate rate determinations. Results of this testing protocol provide critical insight into the mechanism of concrete waste form stability and radionuclide immobilization.

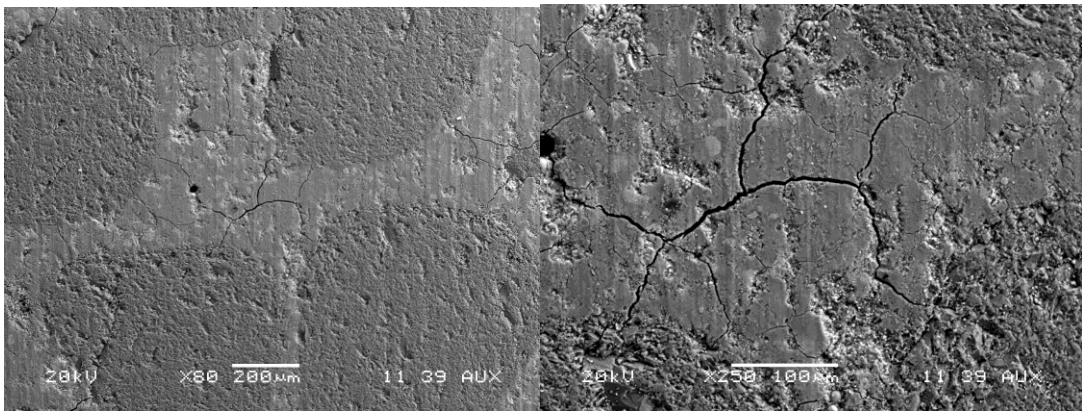

Figure 9.1. SEM Images of Unreacted Concrete Coupons Image at 80x Magnification (left) and Image at 250x Magnification (right)

The SPFT method has been described in detail elsewhere (McGrail et al. 1997 and Wellman et al. 2005 and 2006); therefore, only a brief description will be provided here. Interested readers should consult the noted references for additional information. In general, the SPFT system (Figure 9.2) consists of a programmable pump (Kloehn model 50300) that transports solutions from an influent reservoir via Teflon lines. Solution is transferred into 60-mL capacity *perfluoroalkoxide* (PFA) reactors (Savillex). The reactors are situated within constant temperature ovens (VWR Scientific Products), whose temperature is controlled to ±2 °C by tested and calibrated thermocouples (Glas-Col model TC105). The powdered specimen rests at the bottom of the reactor, and influent and effluent solutions enter and exit, respectively, from fluid transfer lines that protrude through two separate ports at the top of the reactor. The residence time of aqueous solutions in the reactor varies with the flow rate, which is adjusted in accordance with the needs of the experiment. The effluent line carries solution to collection vials that are positioned outside the oven.

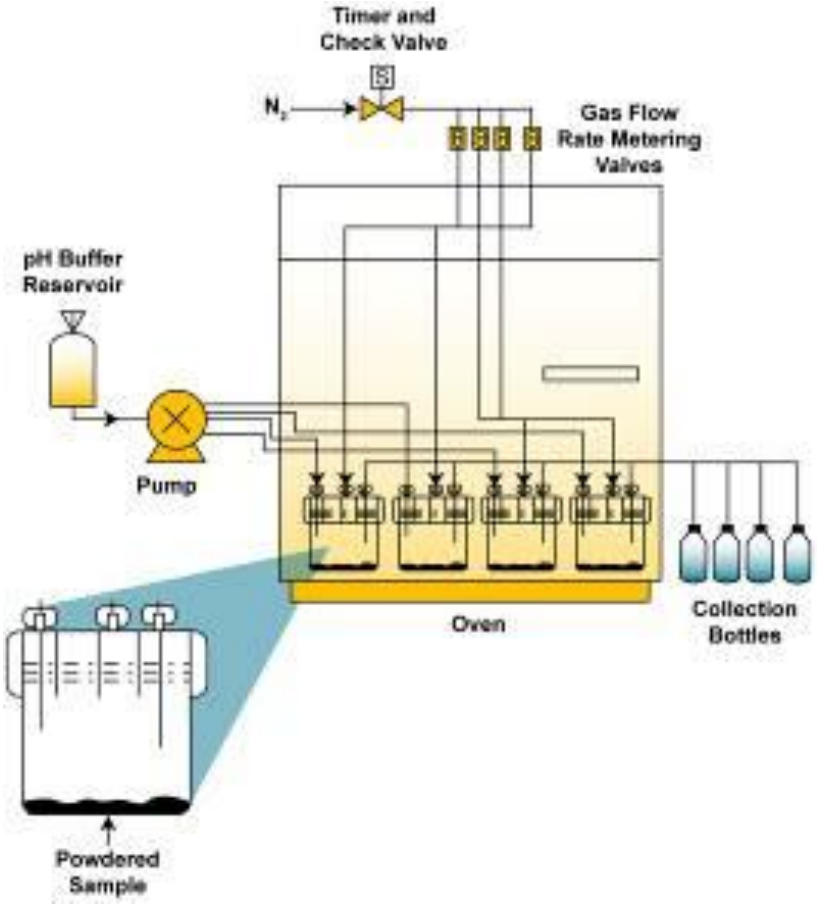

Figure 9.2. Schematic of the Single-Pass Flow-Through Dissolution Test System

Effluent solution was collected continuously and aliquots of the fluid sample were retained for both pH measurement and analysis of dissolved element concentrations by ICP-OES and ICP-MS. Solutions earmarked for analysis by ICP-OES and ICP-MS methods were preserved in Optima™ nitric acid. Concentrations of aqueous calcium and phosphorus were used to quantify the dissolution rates as a function of pH and temperature. Before the sample specimens were added to the reactor, blank solution samples were collected and used to establish the concentration of background analytes. The blank samples were treated in exactly the same manner as the samples.

The solutions used to control the pH during the SPFT experiments are summarized in Table 9.2. Table 9.2 also lists the *in situ* pH values computed at each test temperature using EQ3NR (Wolery 1992). It is important to take into account the change in pH that occurs at different temperatures when computing dissolution rates from SPFT data because the *in situ* pH can vary by as much as 1.5 pH units over the temperature range from 23 ºC to 90 ºC. By quantifying temperature and pH-dependent rate parameters, the dissolution rate of relevant minerals can be extrapolated to conditions representative of the subsurface. Buffer solutions were prepared by adding small amounts of the organic tris hydroxymethyl aminomethane (THAM) buffer to distilled deionized water (DDI) water and adjusting the solution to the desired pH value using 15.8M HNO_3 or 1 M LiOH.

Table 9.2. Composition of Solutions used in Single-Pass Flow-Through Experiments (Solution pH values above 23 ºC were calculated using EQ3NR code V7.2b database.)

		pH @			
Solution	Composition	23ºC	40ºC	70ºC	90ºC
1	0.05 M THAM + 0.0375 M HNO_3	5.91	5.99	6.06	5.99
2	0.05 M THAM + 0.047 M HNO_3	7.01	6.57	5.91	5.55
3	0.05 M THAM + 0.02 M HNO_3	8.32	7.9	7.25	6.89
4	0.05 M THAM + 0.0041 M HNO_3	8.99	8.67	8.08	7.72
5	0.05 M THAM + 0.003 M LiOH	9.99	9.55	8.88	8.52

THAM = tris hydroxymethyl aminomethane buffer.

The physical characteristics of the concrete cores used in the SPFT experiments are summarized in Table 9.3. Each core was sliced into several ~0.75g concrete coupons. SPFT experiments were run in two sets. The first set was run at conditions of pH 8, 90 ºC, and a flow rate of 0.25 L/day. The results from the first data set are presented below. The coupon ID and physical characteristics are found in Table 9.4. The second set of SPFT experiments were a q/S sweep run at pH 8, 60 ºC, with flow rates between 0.005 and 0.5 L/day. The second set of SPFTs is in progress and results will be presented in the next report available in FY 2010.

Table 9.3. Concrete Core Data for SPFTs

				Dia top	Dia bottom	Dia	height		SA	Volume	weight	density
Core ID	Carbonated	Re/I	Fe	cm	cm	Average	cm	r^2	cm^2	cm^3	g	g/ cm^3
C-08-3-0-331	no	no	no	4.38	4.29	4.33	4.52	4.69	90.94	66.56	148.35	2.23
C-08-3-0-336	yes	no	no	4.37	4.29	4.33	4.24	4.68	86.99	62.29	138.89	2.23
C-08-3-4-358	yes	no	yes	4.37	4.28	4.33	4.19	4.68	86.37	61.61	139.94	2.27
C-08-5-4-529	no	yes	yes	4.35	4.28	4.32	3.97	4.65	2298.98	1606.38	139.86	0.09
C-08-3-8-413	no	no	yes	4.36	4.28	4.32	3.86	4.67	71.75	56.63	131.03	2.31
C-08-3-8-414	yes	no	yes	4.36	4.28	4.32	4.23	4.66	86.62	51.89	138.14	2.23
C-08-3-12-431	no	no	yes	4.37	4.28	4.33	3.97	4.68	83.31	58.31	135.34	2.32
C-08-3-12-438	yes	no	yes	4.37	4.29	4.33	4.28	4.68	87.63	62.98	143.91	2.28

Table 9.4. Concrete Coupon Data Set 1

Core ID	Carbonated	Re/I	Fe	SA cm^2	Volume cm^3	Weight g	density g/cc
C-08-3-0-331	no	no	no	313.92	0.30	0.616	2.07
C-08-3-0-336	yes	no	no	309.92	0.34	0.712	2.10
C-08-3-4-358	yes	no	yes	364.29	0.38	0.827	2.17
C-08-5-4-529	no	yes	yes	364.19	0.44	0.962	2.21
C-08-3-8-413	no	no	yes	324.02	0.36	0.766	2.15
C-08-3-8-414	yes	no	yes	300.08	0.26	0.548	2.08
C-08-3-12-431	no	no	yes	364.96	0.42	0.947	2.24
C-08-3-12-438	yes	no	yes	286.13	0.28	0.582	2.08

9.2.1 Rate Calculations and Uncertainty

Dissolution rates, based on steady-state concentrations of elements in the effluent, are normalized to the amount of the element present in the sample by the following formula:

$$r_i = \frac{\left(C_i - \bar{C}_{i,b}\right) q}{f_i S} \tag{4}$$

where r_i = the normalized dissolution rate for element *i* (g m^{-2} d^{-1})

C_i = the concentration of the element *i* in the effluent (g L^{-1})

$\bar{C}_{i,b}$ = the average background concentration of the element of interest (g L^{-1})

q = the flow rate (L d^{-1})

f_i = the mass fraction of the element in the metal (dimensionless)

S = the surface area of the sample (m^2).

The value of f_i was calculated from the chemical composition of the sample. The chemical composition of each concrete monolith was determined by complete chemical digestion followed by ICP-OES analysis. Flow rates are determined by gravimetric analysis of the fluid collected in each effluent collection vessel upon sampling. The background concentration of the element of interest is determined, as previously discussed, by analyses of the starting input solution and three blank solutions. Typically, background concentrations of elements are below their respective detection threshold. The detection threshold of any element is defined here as the lowest calibration standard that can be determined reproducibly during an analytical run within 10%. In cases where the analyte is below the detection threshold, the background concentration of the element is set at the value of the detection threshold.

Determining the experimental uncertainty of the dissolution rate takes into account uncertainties of each parameter in Equation 4. For uncorrelated random errors, the standard deviation of a function $f(x_1, x_2, \ldots x_n)$ is given by:

$$\sigma_f = \sqrt{\sum_{i=1}^{n} \left(\frac{\partial f}{\partial x_i} \right)^2 \sigma_i^2} \tag{5}$$

where σ_f = the standard deviation of the function f

x_i = parameter i

σ_I = the standard deviation of parameter i.

Substituting Equations 4 into 5 results in the following:

$$\sigma_{r_i} = \sqrt{\left(\frac{q}{f_i S} \right)^2 (\sigma_{C_i}^2 + \sigma_{\bar{C}_{i,b}}^2) + \left(\frac{C_i - \bar{C}_{i,b}}{f_i S} \right)^2 \sigma_q^2 + \left(\frac{(C_i - \bar{C}_{i,b})q}{f_i^2 S} \right)^2 \sigma_{f_i}^2 + \left(\frac{(C_i - \bar{C}_{i,b})q}{f_i S^2} \right)^2 \sigma_S^2} \tag{6}$$

Equation 6 can also be expressed in terms of the relative error, $\hat{\sigma}_{r_i} = \sigma_{r_i} / r_i$, and is given by:

$$\hat{\sigma}_{r_i} = \sqrt{\frac{\left(\hat{\sigma}_{C_i} C_i \right)^2 + \left(\hat{\sigma}_{\bar{C}_{i,b}} \bar{C}_{i,b} \right)^2}{\left(C_i - \bar{C}_{i,b} \right)^2} + \hat{\sigma}_q^2 + \hat{\sigma}_{f_i}^2 + \hat{\sigma}_S^2} \tag{7}$$

Relative errors of 10%, 10%, 5%, 3%, and 15% for C_i, $\bar{C}_{i,b}$, q, f_i, and S, respectively, are typical for measurements conducted at PNNL. However, to reduce the error associated with mass fraction (f_i), the samples to be used in these experiments will be ground, homogenized, sub-sampled, and analyzed at least three times to obtain a more accurate composition with a better estimate of the uncertainty. The conservative appraisal of errors assigned to the parameters in Equation 7, in addition to the practice of imputing detection threshold values to background concentrations, results in typical uncertainties of approximately ±35% on the dissolution rate.

9.3 Results and Discussion

Figure 9.3 displays the $\log_{10}$ dissolution rate for the eight different concrete waste form compositions presented in Table 9.2. The dissolution rates are plotted as a function of each concrete waste form corresponding to Table 9.2. The rate of dissolution was indexed by the primary elements within the concrete composition, Ca, Al, Mg, Si, and P.

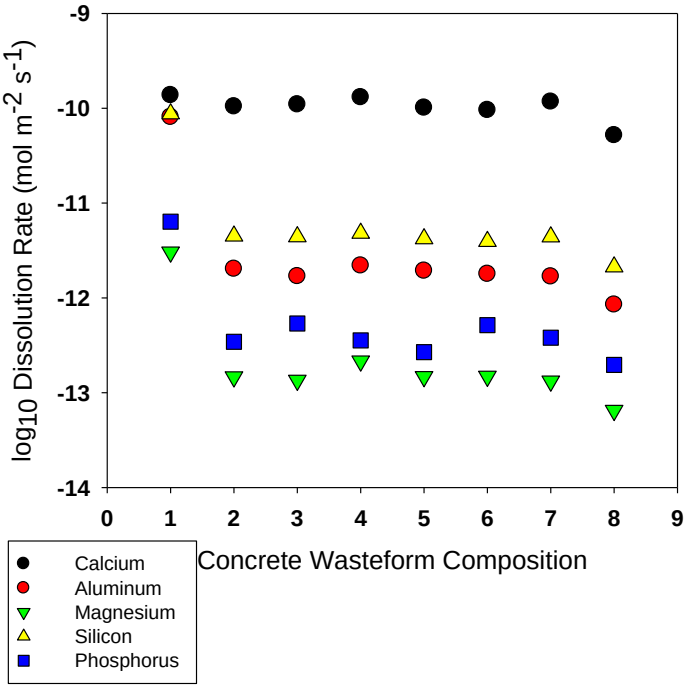

Figure 9.3. $\log_{10}$ Dissolution Rate Indexed by Ca, Al, Mg, Si, and P for Concrete Waste Form Samples

The rate of Ca release for all concrete waste form compositions is within analytical error. Additionally, the differences in concrete composition and treatment for waste forms 2 through 8 have no apparent effect on the rate of dissolution. Concrete waste form 1, C-08-3-0-331 released Al, Mg, Si, and P at a rate ~15x greater than the other seven compositions. This suggests that 1) the release of calcium within the composition of concrete waste forms may be controlled by a different mechanism than for that of Al, Mg, Si, and P, and 2) there may be additional structural difference afforded by the composition and/or treatment of C-08-3-0-331 that resulted in decreased stability relative to the other monolith.

Figure 9.4 presents SEM images of concrete coupons before (left) and after (right) SPFT testing. The large, dark circles in both images are sand particles within the sample. Prior to SPFT testing microcracks are clearly visible within the concrete waste form monoliths. These are a result of the inclusion of iron particles and carbonation of the concrete monolith (Wellman et al., 2008). The impact of microcracks subsequent to dissolution test is evident in the SEM image acquired post-SPFT testing. The presence of microcracks in concrete monoliths provides highly reactive surfaces which can lead to accelerated dissolution and overall degradation of the waste form material. The previous microcracks have undergone significant expansion and deepening within the waste form structure resulting in rapid dissolution.

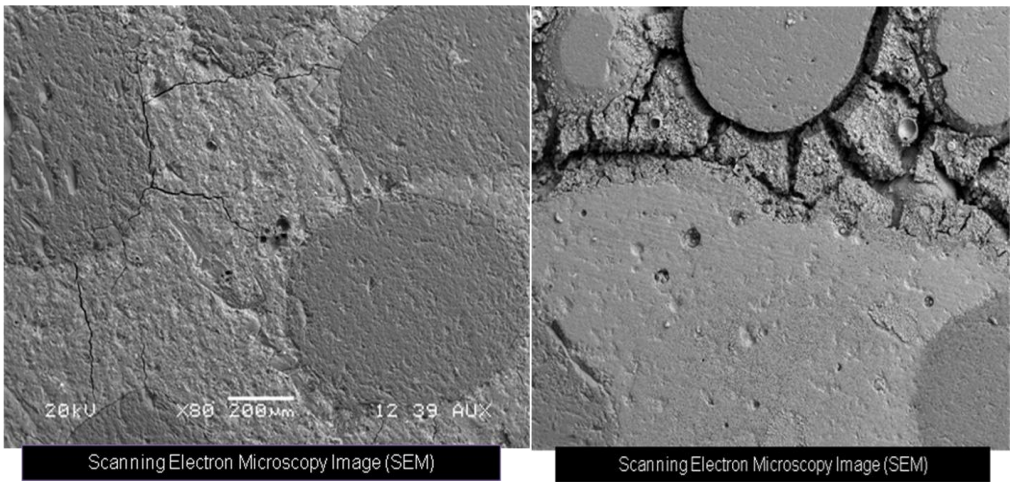

Figure 9.4. SEM Images of Unreacted (left) and Reacted (right) Concrete Monoliths

The SEM images do not suggest the formation of secondary phases, which would impact the apparent dissolution rate. Thus, there is no indication that elemental release is being influenced by the solution saturation state during dissolution testing. Rather, it is postulated that Ca is released through ion exchange, as well as matrix dissolution. Ion exchange (IEX) is a process by which aqueous cations exchanges for the ions contained in the waste form matrix. The mechanism ion exchange has been demonstrated to be an important process in mineral (Wellman, 2006and 2007) and glass waste form (McGrail et al. 2001b). The IEX rate typically decreases with increasing solution pH or temperature, resulting in matrix dissolution as the dominant mechanism. Consequently, as the activity of matrix elements increases in solution, the divergence between the rate of matrix dissolution and IEX increases. Under these conditions, the IEX rate becomes more pronounced because as the ion activity product (Q) approaches saturation with respect to some secondary phase(s), the rate of matrix dissolution slows. The addition of this mechanism may affect concrete waste form performance because of the significant CaO content, about 3%.

The section in the bottom left quadrant of Figure 9.5 is of the concrete under the silicon mask. The mask prevented the influent solution from contacting the surface of the coupon, allowing an unreacted section to be placed alongside the reacted concrete. The reacted portions of the SEM image show significant weathering of the coupon. The large ovals in the picture are sand grains. The weathering of the monolith occurs in the cement matrix not associated with the sand grains. This is clearly evident in the photograph in Figure 9.6, which is a coupon after testing. The silicon mask (red spot) is placed in the lower right quadrant of the monolith. The white particles are sand grains, which have been exposed by the weathering of the cement matrix.

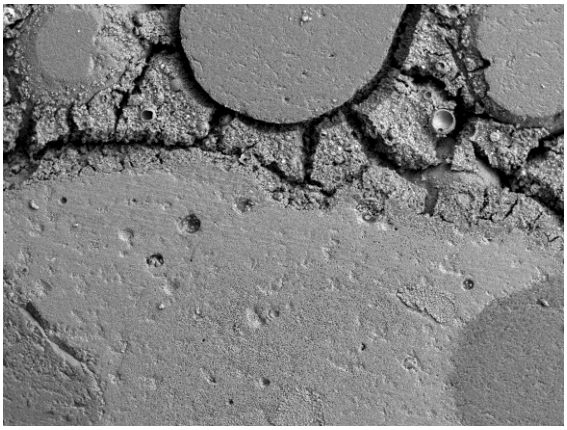

Figure 9.5. Reacted Concrete Coupon at 60x Magnification

Figure 9.6. Photograph of Concrete Coupon after SPFT Experiment

The results presented here provide critical initial information highlighting the significance of certain environmental variables and concrete waste form properties (e.g., pH, temperature, degree of waste form carbonation, and the inclusion of additives within concrete waste forms) that are the key to understanding the long-term performance and efficacy of concrete waste forms. The quantitative effects of these parameters are the subject of an ongoing comprehensive investigation.

10.0 Simulated Tank Waste-Concrete Half-Cell Test

10.1 Simulated Tank Waste Composition

In FY 2006, four concrete half-cells were prepared with simulated tank waste instead of soil. The composition of the tank waste used is an average composition of previously published tank waste analyses. In FY 2008, four additional tank waste-concrete half-cells were prepared with the addition of Tc to the simulated tank waste. The composition of both simulated tank wastes is listed in Table 10.1. The packing data for both sets of half-cells is listed in Table 10.2. The half-cells presented below will be sectioned in FY 2010. Results of these half-cell tests will provide a unique data set on the diffusion of simulated tank waste sludge into concrete and the stability of concrete in contact with tank waste.

Table 10.1. Elemental Composition of Simulated Tank Wastes

Tank Waste 1		Tank Waste 2	
Analyte	Concentration, µg/g	Analyte	Concentration, µg/g
Al	131,500	Al	131,500
Ca	46,500	Ca	46,500
Cr	24,000	Cr	24,000
Cu	4,000	Cu	4,000
Fe	125,000	Fe	125,000
I	100 pCi/g	I	100 pCi/g
Mg	3,000	Mg	3,000
Mn	108,000	Mn	108,000
Na	170,000	Na	170,000
Ni	5,000	Ni	5,000
P	9,000	P	9,000
Pb	8,000	Pb	8,000
Re	5	Re	5
Si	20,000	Si	20,000
Sr	500	Sr	500
U	50,000	Tc	100 ppm
Zn	1,000	U	50,000
Cl^-	1,500	Zn	1,000
CO_3^{2-}	171,000	Cl^-	1,500
NO_2^-	19,000	CO_3^{2-}	171,000
NO_3^-	163,000	NO_2^-	19,000
PO_4^{3-}	5,500	NO_3^-	163,000
SO_4^{2-}	5,000	PO_4^{3-}	5,500
		SO_4^{2-}	5,000

Table 10.2. Packing Data for Tank Waste-Concrete Half-Cells

Column ID	Tank Waste	% Fe	Carbonation	Core and Column Weight (g)	Final Weight (g)	Sludge Weight (g)
C-4-0-13	1	0	N	238.72	324.07	85.35
C-4-0-14	1	0	Y	242.65	325.94	83.29
C-4-4-33	1	4	N	243.55	327.98	84.43
C-4-4-34	1	4	Y	243.64	328.24	84.60
C-08-0-1	2	0	N	248.20	334.19	85.99
C-08-0-4	2	0	Y	246.10	334.23	88.14
C-08-4-6	2	4	N	245.64	332.24	86.61
C-08-4-7	2	4	Y	248.90	332.15	83.26

11.0 Works Cited

National Research Council. 2009. *National Advice on the Department of Energy's Cleanup Technology Roadmap: Gaps and Bridges*. Academies Press, Washington, D.C.

Al-Khayat H, MN Haque, and NI Fattuhi. 2002. "Concrete Carbonation in Arid Climate." *Materials and Structures* 35:421-426.

Allison JD, DS Brown, and KJ Novo-Gradac. 1991. *Minteqa2/Prodefa2, a Geochemical Assessment Model for Environmental Systems: Version 3 User's Manual*, EPA/600/3-91/021, Environmental Research Laboratory, Office of Research and Development, U.S. EPA, Athens, Georgia.

Alwan AK and PA Williams. 1980. "The Aqueous Chemistry of Uranium Minerals. Part 2. Minerals of the Liebigite Group." *Mineralogical Magazine* 43:665-667.

ANSI. 1986. *Measurement of the Leachability of Solidified Low-Level Radioactive Wastes Short-Term Test Procedure*, American Nuclear Society, Chicago.

Baes CF, JM Schreyer, and JM Lesser. 1953. *The Chemistry of Uranium (VI) Orthophosphate Solutions: Part I. A Spectrophotometric Investigation of Uranyl Phosphate Complex Formation in Perchloric Acid Solution*, ORNL-Y-12/ORNL-1577, Oak Ridge National Laboratory, Oak Ridge, Tennessee.

Bargar JR, GEB Jr., I Evans, T Rabedeau, M Rowen, and J Rogers. 2002. "A New Hard X-Ray XAFS Spectroscopy Facility for Environmental Samples, Including Actinides, at the Stanford Synchrotron Radiation Laboratory." *Proceedings of the Euroconference and NEA Workshop on Speciation, Techniques,and Facilities for Radioactive Materials at Synchrotron Light Sources,Grenoble, France, Sept. 10-12, 2000, NEA/OECD, Paris*, p. 57-68.

Brown DA, BE Fulton, and RE Phillips. 1964. "Ion Diffusion: I. A Quick-Freeze Method for the Measurement of Ion Diffusion in Soil and Clay Systems." *Soil Science Society of America Journal* 28:628-632.

Chen F, RC Ewing, and SB Clark. 1999. "The Gibbs Free Energies and Enthalpies of Formation of U^{6+} Phases: An Empirical Method of Prediction." *American Mineralogist* 84:650-664.

Clark DL, DE Hobart, and MP Neu. 1995. "Actinide Carbonate Complexes and Their Importance in Actinide Environmental Chemistry." *Chemical Reviews* 95:25-48.

Cordfunke EHP. 1964. "Heats of Formation of Some Hexavalent Uranium Compounds." *Journal of Physical Chemistry* 68(11):3353-3356.

Cordfunke EHP. 1969. *The Chemistry of Uranium*. Elsevier Publishing Company, Amsterdam, the Netherlands.

Crane PJ, HL Benny, and MI Wood. 1992. *Physical Modeling of Contaminant Diffusion from a Cementitious Waste Form*, WHC-SA-1345, Westinghouse Hanford Company, Richland, Washington.

Crank J. 1975. *The Mathematics of Diffusion*. Clarendon Press, Oxford, England.

Finch RJ. 1997. "Thermodynamic Stabilities of U(VI) Minerals: Estimated and Observed Relationships." *Material Research Society Symposium Proceedings* 465:1185-1192.

Finney DJ. 1971. *Probit Analysis*. Bambridge University Press, Cambridge.

Garrabrants AC, and DS Kosson. 2003. "Modeling Moisture Transport from a Portland Cement-Based Material During Storage in Reactive and Inert Atmospheres." *Drying Technology* 21(5):775-805.

Garrabrants AC, F Sanchez, C Gervais, P Moszkowicz, and DS Kosson. 2002. "The Effect of Storage in an Inert Atmosphere on the Release of Inorganic Constituents During Intermittent Wetting of a Cement-Based Material." *Journal of Hazardous Materials* B91:159-185.

Garrabrants AC, F Sanchez, and DS Kosson. 2004. "Changes in Constituent Equilibrium Leaching and Pore Water Characteristics of a Portland Cement Mortar as a Result of Carbonation." *Waste Management* 24:19-36.

Garrels RM and CL Christ. 1965. *Solutions, Minerals and Equilibria*. Harper and Row Publishing Co., New York.

Gervais C, AC Garrabrants, F Sanchez, R Barna, P Moszkowicz, and DS Kosson. 2004. "The Effects of Carbonation and Drying During Intermittent Leaching on the Release of Inorganic Constituents from a Cement-Based Matrix." *Cement and Concrete Research* 34:119-131.

Grenthe I, J Fuger, RJM Konings, RJ Lemire, AB Muller, C Nguyen-Trung, and H Wanner. 1992. *Chemical Thermodynamics of Uranium*. OECD Nuclear Energy Agency, Amsterdam, the Netherlands.

Kalmykov SN and GR Choppin. 2000. "Mixed $Ca^{2+}/Uo_2^{2+}/Co_3^{2-}$ Complex Formation at Different Ionic Strengths." *Radiochimica Acta* 88:603-606.

Lamar DW. 1989. *Measurement of Nitrate Diffusivity in Hanford Sediments via the Half-Cell Method*, Letter Report to Westinghouse Hanford Company, Pacific Northwest National Laboratory, Richland, Washington.

Langmuir D. 1978. "Uranium Solution-Mineral Equilbria at Low Temperatures with Applications to Sedimentary Ore Deposits." *Geochimica et Cosmochimica Acta* 42:547-569.

Langmuir D. 1997a. Aqueous *Environmental Chemistry*. Prentice-Hall, Upper Saddle River, New Jersey.

Langmuir D. 1997b. "Aqueous Geochemistry of Uranium." In *Aqueous Environmental Chemistry*, ed. R McConnin. Prentice-Hall, Upper Saddle River, New Jersey.

Lytle FW, RB Greegor, DR Sandstrom, EC Marques, J Wong, CL Spiro, GP Huffman, and FE Huggins. 1984. "Measurement of Soft X-Ray Absorption Spectra with a Fluorescent Ion Chamber Detector." *Nuclear Instruments & Methods in Physics Research, Section A: Accelerators, Spectrometers, Detectors, and Associated Equipment* 226:542-548.

Mann FM, RJ Puigh II, SH Finfrock, EJ Freeman, R Khaleel, DH Bacon, MP Bergeron, PB McGrail, and SK Wurstner. 2001. *Hanford Immobilized Low-Activity Waste Performance Assessment: 2001 Version*, DOE/ORP-2000-24, Rev. B, Pacific Northwest National Laboratory, Richland, Washington.

Martin PF, RJ Serne, VL Legore, and CW Lindenmeier. 1994. *Status Report on Ionic Diffusion through Asphalt*, HGTP-93-0602-01, Pacific Northwest National Laboratory, Richland, Washington.

Mattigod SV, GA Whyatt, RJ Serne, PF Martin, KE Schwab, and MI Wood. 2001. *Diffusion and Leaching of Selected Radionuclides (Iodine-129, Technetium-99, and Uranium) through Category 3 Waste Encasement Concrete and Soil Fill Material*, PNNL-13639, Pacific Northwest National Laboratory, Richland, Washington.

McGrail PB, WL Ebert, AJ Bakel, and DK Peeler. 1997. "Measurement of Kinetic Rate Law Parameters on a Na-Ca-Al Borosilicate Glass for Low-Activity Waste." *Journal of Nuclear Materials* 249:175-189.

Newville M. 2001. "IFEFFIT: Interactive XAFS Analysis and FEFF Fitting." *Journal of Synchrotron Radiation* 8:322-324.

Nguyen SN, RJ Silva, HC Weed, and JE Andrews. 1992. "Standard Gibbs Free Energies of Formation at the Temperature 303.15k of Four Uranyl Silicates: Soddyite, Uranophane, Sodium Boltwoodite, and Sodium Weeksite." *Journal of Chemical Thermodynamics* 25:359-376.

O'Hare PAG, HR Hoekstra, and DR Frederickson. 1976. "Thermochemistry of Uranium Compounds: Vii. Solution Calorimetry of Alpha and Beta-Na_2uo_4, Standard Enthalpy of Formation of Beta-Na_2uo_4 and the Enthalpy of the Alpha to Beta Transition at 298.15 K." *Journal of Chemical Thermodynamics* 8:255-258.

Ondrus P, R Skala, F Veselovsky, J Sejkora, and C Vitti. 2003. "Cejkaite, the Triclinic Polymorph of $Na_4(Uo_2)(Co_3)_3$ - a New Mineral from Jachymov, Czech Republic." *American Mineralogist* 88:686-693.

Sanchez F, AC Garrabrants, and DS Kosson. 2003. "Effects of Intermittent Wetting on Concentration Profiles and Release from a Cement-Based Waste Matrix." *Environmental Engineering Science* 20(2):135-153.

Sanchez F, C Gervais, AC Garrabrants, R Barna, and DS Kosson. 2002. "Leaching of Inorganic Contaminants from Cement-Based Waste Materials as a Result of Carbonation During Intermittent Wetting." *Waste Management* 22:249-260.

Sandino A and J Bruno. 1992. "The Solubility of $(Uo_2)_3(Po_4)_2 \cdot 4h_2o$(S) and the Formation of U (Vi) Phosphate Complexes: Their Influence Speciation in Natural Waters." *Geochimica et Cosmochimica Acta* 56:4135-4145.

Sergeyeva EI, AA Nikitin, IL Khodakovkiy, and GB Naumov. 1972. "Experimental Investigation of Equilibria in the System Uo_3-Co_2h_2o in 25 - 200°C Temperature Interval." *Geochemistry International* 9:900-910.

Serne RJ, JL Conca, VL LeGore, KJ Cantrell, CW Lindenmeier, JA Campbell, JE Amonette, and MI Wood. 1993. *Solid-Waste Leach Characterization and Contaminant-Sediment Interactions*, PNL-8889, Vol. 1, Pacific Northwest National Laboratory, Richland, Washington.

Serne RJ, RO Lokken, and LJ Criscenti. 1992. "Characterization of Grouted LLW to Support Performance Assessment." *Waste Management* 12:271-287.

Serne RJ, WJ Martin, and VL LeGore. 1995. *Leach Test of Cladding Removal Waste Grout Using Hanford Groundwater*, PNL-10745, Pacific Northwest National Laboratory, Richland, Washington.

Serne RJ, WJ Martin, VL LeGore, CW Lindenmeier, SB McLaurine, PFC Martin, and RO Lokken. 1989. *Leach Tests on Grouts Made with Actual and Trace Metal-Spiked Synthetic Phosphate/Sulfate Waste*, PNL-7121, Pacific Northwest National Laboratory, Richland, Washington.

Specification for Concrete Encasement for Contact-Handled Category 3 Waste. 1998." In: *Waste Management*, Unpublished Report.

Sylva RN and MR Davidson. 1979. "The Hydrolysis of Metal Ions. Part 2. Dioxouranium (VI)." *Dalton Transactions* 8:465-471.

Vochten R and LV Haverbeke. 1990. "Transformation of Schoepite into the Uranyl Oxide Hydrates: Becquerelite, Billietite, and Wolsendorfite." *Contributions to Mineralogy and Petrology* 43:65-72.

Webb SM. 2005. "SixPACK: A Graphical User Interface for XAS Analysis Using IFEFFIT." *Physica Scripta* T115:1011-1014.

Wellman DM, CC Bovaird, SV Mattigod, KE Parker, RM Ermi, and MI Wood. 2008a. *Effect of Concrete Wasteform Properties on Radionuclide Migration*, Pacific Northwest National Laboratory, Richland, Washington.

Wellman DM, JP Icenhower, AP Gamerdinger, and SW Forrester. 2006. "Effects of Ph, Temperature, and Aqueous Organic Material on the Dissolution Kinetics of Meta-Autunite Minerals, $(Na,Ca)_{2-1}[(UO_2)(PO_4)]_2 \cdot 3H_2O$." *American Mineralogist* 91:143-158.

Wellman DM, JP Icenhower, and WJ Weber. 2005. "Elemental Dissolution Study of Pu-Bearing Borosilicate." *Journal of Nuclear Materials* 340:149-162.

Wellman DM, SV Mattigod, GA Whyatt, L Powers, KE Parker, LN Clayton, and MI Wood. 2008b. "Effect of Iron and Carbonation on the Diffusion of Iodine and Rhenium in Waste Encasement Concrete and Soil Fill Material under Hydraulically Unsaturated Conditions." *Applied Geochemistry* 23:2256-2271.

Wolery TJ. 1992. *Eq3nr, a Computer Program for Geochemical Aqueous Speciation-Solubility Calculations: Theoretical Manual, User's Guide, and Related Documentation (Version 7.0)*, UCRL-MA-110662, Lawrence Livermore National Laboratory, Livermore, California.

Wood MI, R Khaleel, PD Rittman, AH Lu, S Finfrock, RJ Serne, and KJ Cantrell. 1995. *Performance Assessment for the Disposal of Low-Level Waste in the 218-W-5 Burial Ground*, WHC-EP-0645, Westinghouse Hanford Company, Richland, Washington.

Pacific Northwest
NATIONAL LABORATORY

U.S. DEPARTMENT OF
ENERGY

Proudly Operated by Battelle *Since 1965*

902 Battelle Boulevard
P.O. Box 999
Richland, WA 99352
1-888-375-PNNL (7665)
www.pnl.gov